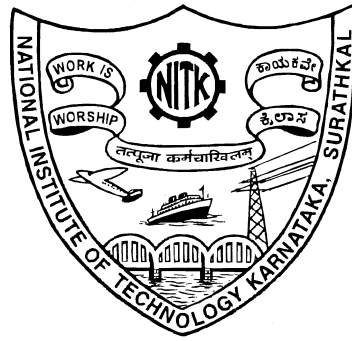


# SEGMENTATION AND FEATURE EXTRACTION OF HAND RADIOGRAPHS FOR BONE AGE ASSESSMENT

Thesis

Submitted in partial fulfillment of the requirements for the degree of  
DOCTOR OF PHILOSOPHY

by  
SHREYAS A. SIMU



DEPARTMENT OF ELECTRONICS AND COMMUNICATION ENGINEERING,  
NATIONAL INSTITUTE OF TECHNOLOGY KARNATAKA,  
SURATHKAL, MANGALURU -575025

MAY, 2018

# DECLARATION

I hereby *declare* that the Research Thesis entitled **Segmentation and Feature Extraction of Hand Radiographs for Bone Age Assessment** which is being submitted to the *National Institute of Technology Karnataka, Surathkal* in partial fulfillment of the requirements for the award of the Degree of *Doctor of Philosophy* in **Electronics and Communication Engineering** is a *bona fide report of the research work carried out by me*. The material contained in this thesis has not been submitted to any University or Institution for the award of any degree.

**Shreyas A. Simu**

Register No.: EC14F09

Department of Electronics and Communication Engineering

Place: NITK-Surathkal.

Date:

# CERTIFICATE

This is to *certify* that the Research Thesis entitled **Segmentation and Feature Extraction of Hand Radiographs for Bone Age Assessment**, submitted by **Shreyas A. Simu** (Register Number: EC14F09) as the record of the research work carried out by him, is *accepted* as the *Research Thesis submission* in partial fulfillment of the requirements for the award of degree of *Doctor of Philosophy*.

**Prof. Shyam Lal.**

Research Guide

Assistant Professor

Dept. Electronics and Communication Engg.

NITK Surathkal - 575025

**Chairman - DRPC**

(Signature with Date and Seal)

*Asato mā sad gamaya  
Tamaso mā jyotir gamaya  
Mṛtyor mā amṛtaṃ gamaya*

*To Aai, Pappa, Rucha and Geeta*

## Acknowledgements

I would like to express sincere and heartfelt gratitude to my research supervisor Dr. Shyam Lal. I thank him for his constant support and guidance that he has provided me throughout my research work. I would also like to thank him for the time he spent in putting this thesis in the present form. I am truly indebted to him, for all the kindness and encouragement that helped me in confronting different challenges in life.

I would like to thank Prof. M. S. Bhat, the former Head and Prof. U. Sri-pati Acharya, the present Head, Department of Electronics and Communication Engineering for their invaluable advice and administrative support. My heartfelt thanks to Dr. A. V. Narsimadhan and Dr. Jidesh P., RPAC members, for their assessment and useful guidance. I am grateful to Dr. Ashwini Chaturvedi for helping me in writing of this thesis. I also take this opportunity to thank all the other faculty and non-teaching staff of E&C department, NITK-Surathkal.

I am very grateful to Dr. Kunal Fadte and Dr. Pranav Nagarsekar from Goa Medical College, Goa, India, for their immense help in the creation of ground truth images and validating the segmentation results. I would also like to thank Dr. Ateeque Harlapur from Belgaum Institute of Medical Sciences, Belgaum, Karnataka, India along with Dr. Amrish Naik from Directorate of Health Services, Goa, India for validating the segmentation results. Special thanks to Professor Roberto A. Lotufo from the University of Campinas for helping out with the license of morphology toolbox, which has been an immense help.

I thank all my fellow research scholars at NITK for their support. Special thanks to my colleagues Shilpa Suresh, Asha C. S. and Anu Shaju for their technical support. I would also like to mention Vasudev Reddy and Princy Paul for their moral support and unconditional friendship which will be cherished forever.

My deepest gratitude goes to my parents Shri Ajitkumar Simu and Smt. Teja Simu who have been a constant source of encouragement, guidance, and support to me throughout my research work. Without them, it would not have been possible to achieve greater heights. I am without words to express my gratitude for their efforts and sacrifices which made me strong enough to face any difficulties in life. I thank my mother for always being benevolent towards me. I thank my father for being a beacon of light and guiding me on this journey.

# Abstract

The Bone Age is a fairly reliable measure of persons growth and maturation of skeleton. Bone age assessment (BAA) has been a standard procedure to predict the age of a person from hand radiograph. The difference between chronological age and bone age indicates the presence of endocrinological problems. The automated bone age assessment system (ABAA) based on Tanner and Whitehouse method (TW3) requires monitoring the growth of radius-ulna and short bones (phalanges) of a left hand. The Tanner and Whitehouse - 3 (TW3) method involves assigning scores to the bones of interest of left hand and assessing the age of a person using the aggregate of scores. Due to the complexity and involved processing time, it is difficult for pediatricians to use the TW3 method in clinics. Hence, automating the whole procedure avoids human error at the same time reduces the processing time.

This thesis investigates design and development of ABAA system to predict bone age of a person from hand radiograph. Fully ABAA system consists of 5 main stages which are (1)Pre-processing, (2)ROI extraction, (3)Segmentation, (4)Feature extraction and (5)Classification. In this context, two fully automatic extraction methods are proposed for the region of interest of phalanges (PROI) and radius-ulna bones (RUROI) using the left-hand radiograph. Experimental results demonstrate that fully automated PROI and RUROI extraction methods are simple, accurate and fast because underlying mechanism is free from complex mathematical procedure.

Segmentation of hand bones plays a vital role in process of ABAA, though it is a challenging task to segment bones from the soft tissue. The problem arises because of overlapping pixel intensities between the bone region and soft tissue region and also overlapping pixels between soft tissue region and background. Hence, there is a need for a robust segmentation technique. In this context, two segmentation techniques are proposed, one for extracted PROI images and other for RUROI images. Quantitative

and qualitative results of proposed segmentation techniques are evaluated and compared with other state-of-the-art segmentation techniques. The segmentation accuracy achieved by proposed segmentation techniques is 94 percent and is 97 percent on PROI and RUROI extracted images respectively. Medical experts have also validated the qualitative results of proposed segmentation techniques. Experimental results reveal that proposed techniques provide higher segmentation accuracy as compared to the other state-of-the-art segmentation techniques.

Further, the development of an ABAA system requires robust feature extraction and efficient classification methods. In this context, this thesis implements and analyzes three different feature extraction methods namely texture feature analysis, Histogram of Oriented Gradients (HOG) and Bag of Features (BoF) methods on segmented PROI images. Also, three different classifiers namely Artificial Neural Networks (ANN), Support Vector Machines (SVM), and Random Forest classifier are implemented to evaluate the performance of extracted features. Further, experimental results of BoF with random forest classifier yields a mean error (Merr) of 0.58 years and root mean square error (RMSE) of 0.77 years for the bone age range of 0-18 years and outperforms other existing BAA methods. Finally, experimental results have also proved that the use of gender bias improves the classification performance. The best performance is obtained from ring, middle and index fingers. Hence, the proposed fully automated technique can be used for bone age assessment of a person with enhanced accuracy.

**Keywords:** Automated Bone Age Assessment, Hand Bone Segmentation, Extraction of phalanges, radius and ulna bones, Edge-based Segmentation, Feature extraction and Classification.



# Contents

Dedication . . . . .	i
Acknowledgements . . . . .	ii
Abstract . . . . .	iv
List of figures . . . . .	viii
List of tables . . . . .	x
Nomenclature . . . . .	xii
Abbreviations . . . . .	xii
<b>1 INTRODUCTION</b>	<b>1</b>
1.1 Overview . . . . .	1
1.2 Motivation . . . . .	3
1.3 Background . . . . .	4
1.4 Bone Age Assessment System . . . . .	7
1.5 Problem Formulation . . . . .	8
1.6 Objectives of the thesis . . . . .	9
1.7 Contributions of the thesis . . . . .	9
1.8 Organization of the thesis . . . . .	10
<b>2 LITERATURE REVIEW</b>	<b>12</b>
2.1 Literature review on pre-processing and ROI extraction techniques . . . . .	12
2.2 Literature review on hand bone segmentation techniques . . . . .	14
2.3 Literature review on feature extraction methods and classification techniques . . . . .	17
2.4 Research gap analysis . . . . .	21
<b>3 PRE-PROCESSING AND ROI EXTRACTION</b>	<b>22</b>
3.1 Introduction . . . . .	22

3.2	Pre-processing and extraction of PROI and RUROI . . . . .	23
3.2.1	Pre-processing and PROI extraction technique . . . . .	23
3.2.2	Pre-processing and RUROI extraction technique . . . . .	25
3.3	Experimental results and discussion . . . . .	25
3.3.1	Image database . . . . .	26
3.3.2	Implementation of PROI extraction technique . . . . .	27
3.3.3	Implementation of RUROI extraction technique . . . . .	27
3.3.4	PROI and RUROI extraction results . . . . .	28
3.3.5	Discussion . . . . .	28
3.4	Summary . . . . .	32
<b>4</b>	<b>SEGMENTATION OF HAND BONES</b>	<b>33</b>
4.1	Introduction . . . . .	33
4.2	Edge preservation for PROI . . . . .	34
4.3	Edge enhancement for RUROI . . . . .	35
4.4	Segmentation using Level Set Method . . . . .	36
4.5	Post-processing . . . . .	39
4.6	Implementation and illustrations . . . . .	40
4.6.1	Implementation of phalangeal segmentation technique . . . . .	40
4.6.2	Illustration of phalangeal segmentation technique . . . . .	40
4.6.3	Implementation of radius and ulna segmentation . . . . .	41
4.6.4	Illustration of radius and ulna segmentation technique . . . . .	42
4.7	Experimental results and discussion . . . . .	47
4.7.1	Performance metrics . . . . .	47
4.7.2	Experimental settings for segmentation of phalanges . . . . .	49
4.7.3	Quantitative and qualitative analysis of phalangeal segmentation	51
4.7.4	Experimental settings for segmentation of Radius-Ulna . . . . .	64
4.7.5	Quantitative and qualitative analysis of radius and ulna seg- mentation . . . . .	64
4.7.6	Segmentation accuracy and its validation . . . . .	67
4.8	Discussion . . . . .	70
4.9	Summary . . . . .	72
<b>5</b>	<b>FEATURE EXTRACTION AND CLASSIFICATION</b>	<b>73</b>
5.1	Introduction . . . . .	73

5.2	Feature extraction methods . . . . .	75
5.2.1	Texture feature analysis . . . . .	75
5.2.2	Histogram of oriented gradients . . . . .	75
5.2.3	Bag of features . . . . .	77
5.3	Classification techniques . . . . .	79
5.3.1	Artificial Neural Networks . . . . .	79
5.3.2	Support Vector Machines . . . . .	79
5.3.3	Random Forest Classifier . . . . .	80
5.4	Implementation . . . . .	81
5.5	Experimental results and discussion . . . . .	81
5.5.1	Results . . . . .	82
5.5.2	Selection of number of clusters for BoF method . . . . .	84
5.5.3	Result comparision with other existing BAA methods . . . . .	85
5.6	Summary . . . . .	86
<b>6</b>	<b>CONCLUSION AND FUTURE WORK</b>	<b>87</b>
	<b>BIBLIOGRAPHY</b>	<b>96</b>
	<b>PUBLICATIONS</b>	<b>97</b>

# List of Figures

1.1	Development of bone. . . . .	2
1.2	Bones of hand and wrist. . . . .	5
1.3	Bones of hand and wrist. . . . .	7
1.4	Block diagram of Automated Bone Age Assessment system. . . . .	8
2.1	Different types of segmentation techniques. . . . .	15
3.1	Block diagram of the proposed ROI extraction technique. . . . .	23
3.2	Test hand radiograph images used for ROI extraction and segmentation. . . . .	26
3.3	PROI images extracted from the hand radiographs. . . . .	29
3.4	PROI images extracted from the hand radiographs. . . . .	30
3.5	RUROI images extracted from the hand radiographs. . . . .	31
4.1	Schematic block diagram of the proposed segmentation technique. . . . .	34
4.2	Output images from each stage of the proposed technique on extracted PROI image of 1 year old person [5173.jpg]. . . . .	43
4.3	Output images from each stage of the proposed technique on extracted PROI image of 10 year old person [5113.jpg]. . . . .	44
4.4	Output images from each stage of the proposed technique on extracted PROI image of 16 year old person [5257.jpg]. . . . .	45
4.5	Output images from each stage of the proposed technique on extracted RUROI image of 1 year old [5173.jpg]. . . . .	46
4.6	Output images from each stage of the proposed technique on extracted RUROI image of 7 year old [5154.jpg]. . . . .	47
4.7	Output images from each stage of the proposed technique on extracted RUROI image of 18 year old [6145.jpg]. . . . .	47

4.8	Boxplots of segmentation techniques against various quality metrics for segmented PROI images. . . . .	53
4.9	Segmentation results of different algorithms on hand radiograph taken from 1 year old person [5173.jpg]. . . . .	55
4.10	Segmentation results of different algorithms on hand radiograph taken from 3 year old person [6102.jpg]. . . . .	56
4.11	Segmentation results of different algorithms on hand radiograph taken from 5 year old person [7143.jpg]. . . . .	57
4.12	Segmentation results of different algorithms on hand radiograph taken from 7 year old person [5154.jpg]. . . . .	58
4.13	Segmentation results of different algorithms on hand radiograph taken from 10 year old person [5113.jpg]. . . . .	59
4.14	Segmentation results of different algorithms on hand radiograph taken from 12 year old person [5322.jpg]. . . . .	60
4.15	Segmentation results of different algorithms on hand radiograph taken from 14 year old person [5237.jpg]. . . . .	61
4.16	Segmentation results of different algorithms on hand radiograph taken from 16 year old person [5257.jpg]. . . . .	62
4.17	Segmentation results of different algorithms on hand radiograph taken from 18 year old person [6145.jpg]. . . . .	63
4.18	Boxplots of segmentation techniques against various quality metrics for segmented RUROI images. . . . .	66
4.19	Segmentation results of different techniques on RUROI of different ages.	68
5.1	Block diagram of Feature extraction and Classification stages of ABAA system. . . . .	74
5.2	Overview of Bag of Features method . . . . .	77
5.3	Steps for building a Random Forest Classifier . . . . .	80
5.4	Graph of error values versus number of clusters in bag of features . . . .	84

# List of Tables

1.1	Comparison between GP method and TW Method. . . . .	5
1.2	Difference between TW2 method and TW3 Method. . . . .	7
2.1	Summary of different pre-processing techniques used for bone age assessment on hand radiographs. . . . .	14
2.2	Summary of different segmentation techniques for bone age assessment of hand radiographs. . . . .	18
2.3	Summary of various feature extraction techniques and classification methods . . . . .	20
4.1	PSNR, MSE, and SSIM performance comparison of results after each stage of the proposed technique on hand radiographs of ages 1, 10 and 16 year old person. . . . .	42
4.2	Performance results after each stage of the proposed technique . . . . .	46
4.3	Simulation parameters and their values used for various segmentation techniques of PROI images . . . . .	50
4.4	Performance comparison of different segmentation techniques on PROI . . . . .	52
4.5	Statistical values of various quality metrics against segmentation techniques . . . . .	54
4.6	Simulation parameters and their values used for various segmentation techniques of RUROI images . . . . .	64
4.7	Performance comparison between different segmentation techniques on RUROI based on various quality metrics . . . . .	65
4.8	Statistical values of various quality metrics against segmentation techniques . . . . .	67
4.9	Ratings given by medical experts to the PROI segmentation results of proposed technique. . . . .	69

4.10	Ratings given by medical experts to the RUROI segmentation results of proposed technique. . . . .	70
5.1	Age group and corresponding number of segmented PROI images . . .	82
5.2	Classification results for different feature extraction methods on combined dataset . . . . .	83
5.3	Classification results for different feature extraction methods on male dataset . . . . .	83
5.4	Classification results for different feature extraction methods on female dataset . . . . .	83
5.5	Random Forest classifier results for BoF with k=500 and with reduced dataset (2-17 years) . . . . .	85
5.6	Comparison between our results and various other existing methods from literature . . . . .	85

# Nomenclature

SYMBOL	MEANING
$k$	Number of clusters in k-means algorithm
$*$	Convolution
$\sigma$	Standard Deviation
$\ominus$	Morphological Erosion
$\subset$	Subset
$\cup$	Union
$\nabla(B)$	Image Gradient
$\ \nabla(B)\ $	Magnitude of Image Gradient
$\bullet$	Morphological Closing
$\circ$	Morphological Opening
$\oplus$	Morphological Dilation
$b$	Bias Field
$n$	Additive Noise
$u_i$	Membership Function
$H$	Heaviside Function
$R(\phi)$	Regularization term
$S^c$	180 rotation of S
$I'$	Compliment of image I
$\lambda$	Constant used to control diffusion
$\varpi$	Weight of regularization term
$\mu$	Statistical Mean
$t_p$	True Positive
$t_n$	True Negative
$f_p$	False Positive
$f_n$	False Negative
$\epsilon$	Constant
$\eta$	Unnormalised Descriptor Vector
$\tilde{H}$	Hessian Matrix
$c$	Coefficient of diffusion
$\nu$	Constant



## Abbreviations - I

Abbreviation	Expansion
BAA	Bone Age Assessment
ABAA	Automated Bone Age Assessment
GP	Greulich and Pyle
TW	Tanner and Whitehouse
UNICEF	United Nations Childrens Fund
SMS	Skeletal Maturity Score
RUS	Radius Ulna and Short bones
ROI	Region Of Interest
EMROI	Epiphyseal-Metaphyseal ROI
CROI	Carpal Region of Interest
PROI	Phalangeal Region of Interest
RUROI	Radius-Ulna Region of Interest
DoG	Derivative of Gaussian
GVF	Gradient Vector Flow
GRF	Gibb's Random Fields
PSO	Particle Swarm Optimisation
ACM	Active Contour Model
ASM	Active Shape Model
AAM	Active Appearance Model
CASAS	Computer based Skeletal Age Scoring System
GSP	Generalized Softmax Perceptron
LDA	Linear Discriminant Analysis
PCA	Principal Component Analysis
SVM	Support Vector Machines
SIFT	Scale Invariant Feature Transform
Acc	Classification Accuracy
ME	Mean Error
Std	Standard deviation of ME

## Abbreviations - II

Abbreviation	Expansion
kNN	k-Nearest Neighbour
ANN	Artificial Neural Network
CNN	Convolutional Neural Network
NA	Not Available
GUI	Graphical User Interface
E-M	Epiphysis-Metaphysis
GLCM	Gray Level Co-occurrence Matrix
CHLA	Children's Hospital Los Angeles
GMC	Goa Medical College
CV	Chan-Vese
Pre	Edge-Enhancement/Preservation stage
Seg	Segmentation stage
Post	Post-processing stage
QM	Quality Metric
PSNR	Peak Signal to Noise Ratio
MSE	Mean Squared Error
SSIM	Structural Similarity Index
KMS	k-means
KGRF	k-means with Gibb's Random Fields
DPSO	Darwinian PSO
AKFM	Adaptively Regularized Kernel-Based Fuzzy C-Means Clustering
BFV	Biconvex Fuzzy Variational
JSI	Jaccard Similarity Index
ACC	Segmentation Accuracy
GM	Geometric Mean
MCC	Matthew's Correlation Coefficient
PT	Proposed Technique
GT	Ground Truth

# Chapter 1

## INTRODUCTION

This chapter gives a brief introduction to the field of bone age assessment (BAA). An overview of BAA and the underlying system are discussed. A short background information is also presented in this chapter. In closing, problem formulation, contribution of the thesis and its organisation are discussed.

X-ray radiography was the first non-invasive method used to study the internal structure of the human body and to diagnose an illness. Owing to its simplicity in acquiring an image, it is one of the most widely used imaging methods for diagnosis and research. The advent of digital image processing methods have boosted the field of diagnostic medicine and increased the accuracy of results obtained. In past few decades, there has been a growing interest in bone age determination by applying digital image processing techniques on hand radiographs.

### 1.1 Overview

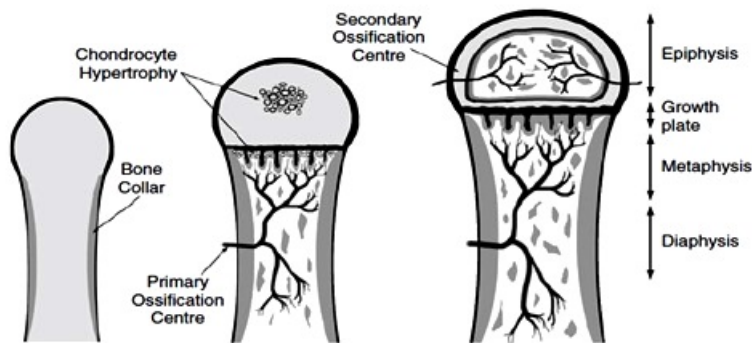
Bone age assessment is one of the most important procedures for the evaluation of biological maturity of children whose age is ambiguous. It is defined as a clinical method for evaluating the stage of skeletal maturation of a child, hence it is also called as skeletal age assessment. Skeletal maturity gives the measure of the development of a bone incorporating its shape, size, and degree of mineralization (Gilsanz and Ratib (2005)).

Bone age assessment is often used to determine the difference between the skeletal

bone age and the chronological age (age from the date a person is born). Normally, the bone age should be approximately within 10 percent of chronological age (Gilsanz and Ratib (2005)). The discrepancies between the two, (i.e. chronological age and bone age), shows that there are abnormalities in the skeletal growth of children or there is a hormonal imbalance. BAA is based on occurrences of the three major events as follows

1. Appearance of primary and secondary centres of ossification,
2. Growth of the ossification centers,
3. The time when fusion of the primary and secondary center occurs.

Primary ossification center is a region in the long shaft of bone, where initial calcification begins as shown in the Figure 1.1, which is obtained from the book on hand bones by Gilsanz and Ratib (2005). Many flat bones, like carpal bones (wrist bones), completely ossify from a primary center; but all long bones develop a secondary center that appears at the cartilage of extremities of a bone.



**Figure 1.1:** Development of bone.

It is still unclear, which factors exactly affect the maturity and growth; but it is certain that hormones, genetics, diet and environmental factors play an important role (Gilsanz and Ratib (2005)). The judgment about the age is based on the identification of the time at which ossification centers appear and epiphyseal fusion happens. BAA is performed usually by comparing an X-ray of a left-hand wrist with an atlas of known sample bones which is the most commonly used method in clinical practice known as Greulich and Pyle (1959) (GP) method which contains a reference set of normal standard images.

Another procedure is the Tanner and Whitehouse-3 (TW3) method, which is more flexible and has been derived from a solid mathematical base (Tanner *et al.* (2001)). In the TW3 method, a detailed analysis of every bone of left hand is done, which further leads to assigning scores to each bone and the sum of all scores assesses the bone age. GP method is outdated and based on human judgment, but preferred by pediatricians due to ease of use over the complexity and time-consumed by the TW3 bone assessment process. Automating the TW3 procedure would reduce the complexity and give a second opinion to radiologists and pediatricians while reducing the overall execution time.

However, automation of assessment process is obstructed by the presence of non-uniformities in X-ray exposure on the hand bones. This non-uniform exposure is inherent to the radiography which is largely credited to the ‘heel effect’. The intensity inhomogeneity is a smoothly varying function of spatial location. The relative brightness of an object placed for X-ray image acquisition is position dependent. According to Behiels *et al.* (2002) this is due to the fact that image acquisition parameters that affect intensity inhomogeneity differ due to the position of hand from the recording device. It poses a major challenge to the automation of BAA along with the problem of pixel intensity overlapping between bone and soft tissue region.

## 1.2 Motivation

An open document of United Nations Children’s Fund (UNICEF), says that “In India, an estimated 27 million births take place every year. The current level of birth registration in the country is 70 percent (UNICEF (2011)). Thus, around 30 percent (approx. 8 million) newly born children are not registered even within one year of birth. This leads to difficulty in getting them access to basic services and protection, including prevention of child labor, trafficking, countering child marriage, and providing appropriate care and protection.”

According to the Census of India (2011), the birth registration is less than 80 percent in 8 states (viz. Andhra Pradesh, Bihar, Chhattisgarh, Jammu and Kashmir, Jharkhand, Sikkim, Uttarakhand and Uttar Pradesh) and 2 union territories (viz. Dadra and Nagar Haveli, Lakshadweep). Statistics of birth registration is approxi-

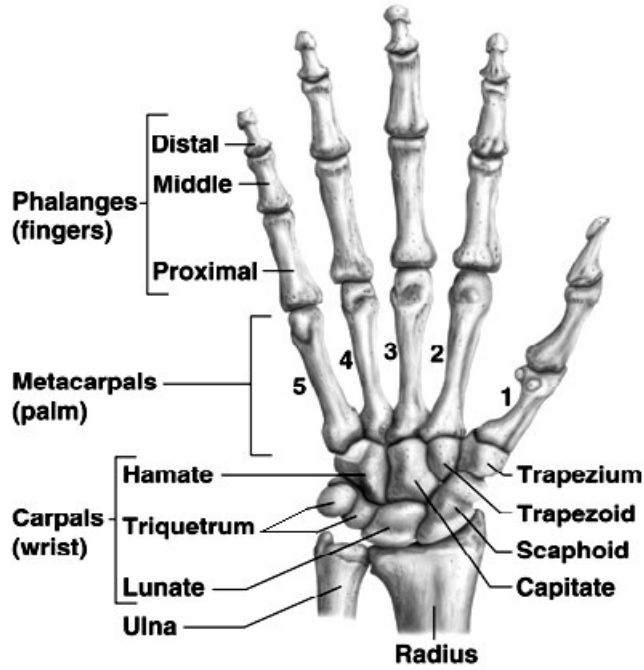
mately 50-60 percent in other developing countries. Without evidence, the children are at risk of underage recruitment into armed forces or early marriage. There also exists unaccounted child labour which thrives because it is unchecked. There is a major problem of early marriage in India before the legal age of 18 years. Children without an identity proof are vulnerable to judgment as an adult rather than child or juvenile in criminal courts.

The endocrinological problems in youngsters are already evident in many countries, varying in scale and intensity for different age groups and sex. Also, change in lifestyle and eating habits of people are the modern factors that lead to endocrine disorders. Thus, BAA plays a significant role because of its reliability and practicability in diagnosing hereditary diseases and growth disorders.

### 1.3 Background

Angerer in 1886, was the first person who stated that the carpal bones (wrist bones) can be used for the estimation of age in young people (Van Lenthe *et al.* (1998)). Soon after Roentgen discovered x-ray radiography, Franz Boas came up with a phrase tempo of growth and predicted that by the end of the century, there will be differences in the rate of maturity in children (Van Lenthe *et al.* (1998)). Events that occur during puberty and throughout adolescence such as the eruption of a certain tooth, occurrence of the first menstrual period, the degree of testicular activity and appearance of pubic hair were used as indicators for the maturity. But all these are coarsely spaced event sequences that lead to incomplete and uneven coverage of developmental age span (Tanner *et al.* (2001)). This motivates the usage of hand and wrist bones for BAA which contains sufficient number of sequences that could cover the age span. The Figure 1.2 shows bones of hand and wrist which is procured from an online source ([www.pinterest.com](http://www.pinterest.com)).

In 1959 and 1975, the most important methods for the estimation of age based on radiological analysis were defined by Greulich and Pyle (1959) (GP method) and Tanner *et al.* (1975) (TW1 method) respectively. GP method which is an atlas matching method is still the most commonly used technique because the evaluation is very simple and less time-consuming. The TW1 method is more flexible and has been derived



**Figure 1.2:** Bones of hand and wrist.

from a solid mathematical base. The TW1 method calculates maturity score which is known as Skeletal maturity score(SMS). It takes one bone at a time, in the order radius, ulna, metacarpals I, III, V, proximal phalanges I, III, V, middle phalanges III, V, distal phalanges I, III, V, capitates, hamate, triquetral, lunate, scaphoid, trapezium, trapezoid, and assigns score to each bone by reference to the text. The scores are then aggregated to give the final skeletal maturity score (SMS). The SMS is then mapped to bone age with the help of charts and tables given in the TW reference book by Tanner *et al.* (1975). The major differences in these two methods are summarised in the Table 1.1.

**Table 1.1:** Comparison between GP method and TW Method.

Sr. No.	GP Method	TW Method
1	Atlas matching method.	Score assigning method.
2	Faster and easier to use.	Complex and time consuming.
3	Not easily reproducible.	Easily reproducible.
4	Error margin is more.	Error margin is less.

The TW2 method Tanner *et al.* (1975) was a revised version of TW1 in terms of scores associated to each stage and also the differences between both sexes. In the TW2 method, the regions of interest (ROIs), considered for the bone age evaluation are as follows:

1. Epiphysis/metaphysis ROI (EMROI) of Radius, Ulna and Short bones (phalanges) which is aggregated to give the RUS score.
2. Carpal bones (CROI), which give the carpal score.

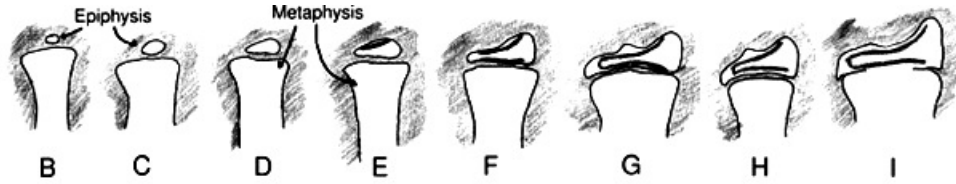
The bone development in each ROI is divided into nine discrete stages, and each stage is given a letter (A to I). RUS score spans the development of bones from 0-18 years, but carpal score can only predict from 1-14 years. In EMROI, there are two important parts: Epiphysis and Metaphysis. The stages of Epiphysis and Metaphysis are roughly described as follows:

1. Stage A - Epiphysis is absent
2. Stage B - Single deposit of calcium
3. Stage C - Epiphyseal center is visible
4. Stage D - Maximum diameter of epiphysis is half or more than the width of the metaphysis.
5. Stage E - Border of epiphysis is concave.
6. Stage F - Epiphysis is as wide as the metaphysis.
7. Stage G - Epiphysis forms a sharp articulation and has distinct C- shape.
8. Stage H - Epiphysis caps the metaphysis.
9. Stage I - Epiphysis is fused to metaphysis.

A numerical score is further associated with each stage of every bone in ROI. Aggregating the scores of all ROIs, an overall maturity score is obtained. The Figure 1.3 shows stages of radius which is procured from the literature (Aja-Fernández *et al.* (2004)).

The TW2 method has been modified throughout the years, evolving to TW3 method (Tanner *et al.* (2001)) which maintains the description for the bone stages but calibrates the scoring method on the North American and European children. Other difference between the two methods is that TW2 collects the maturity evidence





**Figure 1.3:** Bones of hand and wrist.

**Table 1.2:** Difference between TW2 method and TW3 Method.

Sr. No.	TW2 Method	TW3 Method
1	British population.	American & European population.
2	20 bone score.	RUS score & Carpal score.
3	TW2 & TW3 scores are different.	A year ahead from age 10 upwards.

from twenty bones consisting of the combination of radius, ulna and short bones (RUS) and carpals. Whereas, TW3 collects maturity evidence separately from RUS or Carpal scores. Scores of TW2 and TW3 are different for a few bones. Thus, the conversion of SMS to bone age is changed; TW3 bone ages are a year ahead of TW2 ages from age 10 upwards. The TW3 method is seldom used because of its high complexity, yet its modular structure makes it suitable for automation. Table 1.2 summarizes the differences between TW2 and TW3.

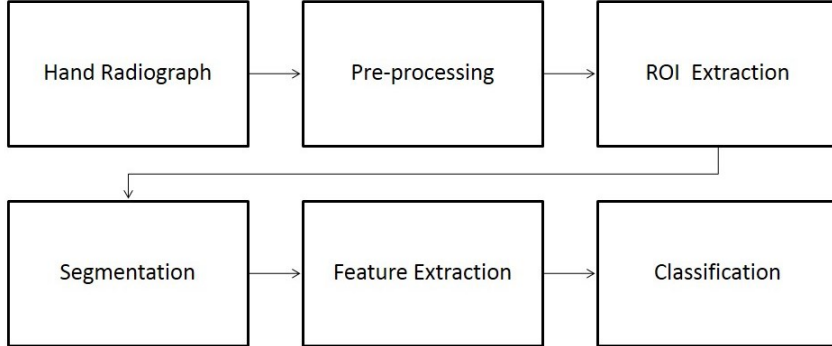
## 1.4 Bone Age Assessment System

The automation of bone age assessment is categorised into five main stages:

1. Pre-processing of the left hand X-ray image
2. Extraction of the Region of Interest (ROI).
3. Segmentation of bones in the extracted ROI.
4. Feature Extraction from segmented bones.
5. Classification.

The pre-processing stage involves noise removal and enhancement of the X-ray image. The next process is the extraction of ROI for further analysis namely phalangeal region of interest (PROI) and radius-ulna region of interest (RUROI). The pre-processing stage renders a better segmentation of bone which is the next stage.

In feature extraction stage, various types of feature are extracted from the segmented bone structures which will guide the system into proper classification and estimation of the bone age. The generalized block diagram of Automated Bone Age Assessment (ABAA) system is shown in Figure 1.4.



**Figure 1.4:** Block diagram of Automated Bone Age Assessment system.

## 1.5 Problem Formulation

Poor accuracy in extraction of the region of interest (ROI) and further segmentation of bones may be caused by an absence of robust pre-processing technique. The existence of high variations in background luminance, low contrast or excessively enhanced contrast in a hand bone radiograph causes a discrepancy in the bone age assessment. The existing BAA systems are not yet fully developed due to the inherent problems in hand radiograph processing especially incase of low contrast in ossification area. The contrast variation of bone texture in ossification regions are of critical importance in the TW3 bone age assessment. If both, the structure and texture of ossification bones are well defined, then the important features are distinguishable.

Inhomogeneity in pixel intensities poses a major challenge in the segmentation process because of the overlapping pixels between bone and soft tissue, identifying the tissue region also as an object of interest. The segmentation technique should not track the cancellous bone region along with the cortical bone region. Cancellous bone is also known as the trabecular bone which is a soft osseous tissue that forms the internal bone; whereas cortical/compact bone forms the exterior part of the bone.

Finally, the segmentation stage should make feature extraction easier for interpretation and accurate classification.

Feature extraction stage mainly relies on the precision of previous stages. Different kinds of feature can be extracted from segmented bones such as morphological, statistical, texture based etc. The ability of automated bone age assessment (ABAA) system to correctly classify the test image depends on the type of feature extracted and the classification method used. Most of the current classification methods are highly conducive and productive. Hence, the focus mainly relies on finding the best possible feature extraction method for getting a higher accuracy from the BAA system.

## **1.6 Objectives of the thesis**

The objectives envisaged for bone age assessment (BAA) are listed as follows:

1. To propose a novel ROI extraction method and realize a suitable pre-processing technique for application on hand radiographs.
2. To propose a novel segmentation technique and evaluate its performance on hand radiographs for bone age assessment.
3. To frame an efficient feature extraction mechanism for classification of segmented hand radiographs for bone age assessment.

## **1.7 Contributions of the thesis**

The main contributions of research work are summarized as follows:

1. A fully automated ROI extraction methods are developed for hand radiographs. Two ROI regions have been extracted which are phalangeal region (PROI) and radius-ulna region (RUROI). The PROI extraction method is fast, accurate and extracts all 5 phalangeal regions at the same time. The RUROI extraction method is also fast, accurate and extracts radius and ulna bones. The process of extraction for both ROI's is quite simple because it was devoid of on any complex mathematical framework and follows a simple hierarchical bone localization technique.

2. A fully automated segmentation techniques are proposed for extracted ROI's from hand radiograph. The phalangeal bones and radius-ulna bones are segmented with moderately high segmentation accuracy. The proposed segmentation techniques are based on morphological tools, active contours, and post-processing. The proposed techniques successfully tackle the heel effect problem or the bias field that is present in hand radiographs while segmenting the required bones which was not tackled for bone segmentation by researchers.
3. The segmentation results of proposed techniques are evaluated and compared with many other state-of-the-art segmentation techniques which only a few researchers had done before. Further, a quantitative analysis of the segmentation results is done using various quality metrics such as peak signal-to-noise ratio (PSNR), mean square error (MSE), jaccard similarity index (JSI), Dice similarity index, Accuracy, geometric mean (GM) and Matthew's correlation coefficient (MCC). Such analysis has not been done before in this area of BAA and hand bone segmentation.
4. A robust feature extraction methods have been implemented for BAA from segmented hand radiographs. Further, different classification techniques have been used for predicting bone age of a person with high classification accuracy. Finally, experimental results reveal that fully automated BAA system provided better results as compared to other existing BAA methods.

## 1.8 Organization of the thesis

The thesis is organized into six chapters as follows.

Chapter 2, discusses the work done in the field of bone age assessment. The literature survey is divided into 3 parts; (1) pre-processing and ROI extraction, (2) segmentation of bones and (3) feature extraction and classification based on bone features extracted.

Chapter 3, presents the proposed ROI extraction methods for PROI and RUROI. This chapter also presents the extraction results of proposed ROI extraction methods and summarizes the work done in fulfilling the first objective.

Chapter 4, discusses the proposed segmentation techniques for PROI and RUROI images. A quantitative and qualitative analysis is presented and quantitative as well as qualitative results are compared with state-of-the-art segmentation techniques. The results have also been validated by medical experts. The work is summarized at the end which fulfills the second objective.

Chapter 5, analyses various feature extraction methods by applying it on segmented PROI images. The classification results have been presented in this chapter and the work is summarized in the end. Work presented in this chapter fulfills the third objective.

Chapter 6 concludes with the contribution of the thesis. This chapter also presents possible extensions and future work.

# Chapter 2

## LITERATURE REVIEW

This chapter discusses the work carried out by various researchers in the field of bone age assessment and critically analyses their work to a very minute detail. The literature review is divided into sections based on the various stages of BAA. Hence, the literature review is divided into pre-processing and ROI extraction, segmentation, and feature extraction with classification. Lastly, the research gaps and opportunities for further work in the same domain are listed.

### 2.1 Literature review on pre-processing and ROI extraction techniques

The pre-processing stage is an important step before hand radiograph segmentation as it prepares the image for extracting the required information. A pre-processing stage may involve noise removal, contrast enhancement or any other technique based on application to improve the quality of image for further stages. Region of interest (ROI) extraction is done to apply the algorithm only on required areas of the image, so that it eases the segmentation procedure and reduces complexity.

Michael and Nelson (1989) made the first attempt to automate bone age assessment procedure and was called as HANDX system. HANDX system is a semi-automated system which uses pre-processing and segmentation. It reduced the variability of the observer to give a slightly better result. The accuracy was still not reasonable and there were some overlapping pixels between the background and segmented bones.

Various methods have been designed to remove the background of radiograph as pre-processing. Sharif *et al.* (1994) used the derivative of Gaussian (DoG) for pre-processing and segmentation of bones by thresholding, but the results were not promising. Pietka *et al.* (2001) proposed epiphyseal-metaphyseal region of interest (EMROI) extraction technique, which also included a good pre-processing unit. Pre-processing steps involved orientation correction and background removal. EMROI extraction is done by first detecting the phalangeal tip and then step wedge function to extract the fingers. Later, gradient function is used to mark the epiphyseal region. But thresholding was not good enough to separate out the spongy region and the bone tissue.

Park *et al.* (2007) developed a method to extract the epiphysis using horizontal profile. In this paper, authors first removed the background using least squares algorithm and then boundary was traced. Later, the central axis of each finger was estimated using 3rd order polynomial, because of which even if the fingers were slightly curved, the central axis could be estimated. Giordano *et al.* (2007) developed a semi-automated system for skeletal bone age evaluation. This proposed method was based on derivative of Gaussian (DoG) filtering and adaptive thresholding for enhancement, but it was not feasible for low contrast images. Thresholding method identifies the spongy tissue region also as an object of interest which is its major drawback.

Lee and Kim (2008) proposed an EMROI extraction method for the TW2 system in which the boundary was removed using least squares algorithm and then long axis of each finger was extracted. EMROI were localized by studying the intensity profile along the axis. Chai *et al.* (2013) proposed a histogram equalization technique called as multi-objective beta-optimized bi-histogram equalization was designed which used multi-objective optimization technique for histogram equalization. Before segmentation, anisotropic diffusion was also used to smoothen the image. Hsieh *et al.* (2012) have focused on PROI extraction using projection profile of the fingers and gamma parameter enhancement. Authors compared the results with and without gamma enhancement for two popular segmentation techniques namely k-means algorithm and gradient vector flow (GVF) snakes. The summary of different pre-processing and ROI extraction techniques is presented in Table 2.1.

**Table 2.1:** Summary of different pre-processing techniques used for bone age assessment on hand radiographs.

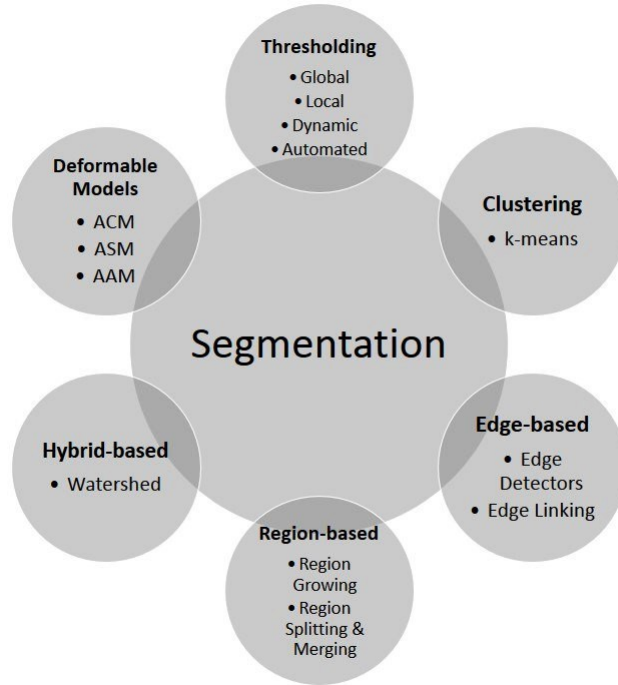
Pre-processing Technique	Advantages	Disadvantages
<b>Histogram Equalization</b> Michael and Nelson (1989), Sharif <i>et al.</i> (1994)	Simple and basic method for image enhancement	Overlapping of pixels between bone and background.
<b>Orientation correction and background removal</b> Pietka <i>et al.</i> (2001)	Simple mathematical steps to correct the orientation and background removal	Not highly effective method.
<b>DoG filtering</b> Giordano <i>et al.</i> (2007, 2010)	Does not depend on X-ray acquisition	Fails in noisy images. Requires good contrast images.
<b>Background Removal</b> Park <i>et al.</i> (2007)	Better than previous PROI extraction methods	Complex and consumes more time.
<b>Noise Removal</b> Han <i>et al.</i> (2007)	Using mathematical morphology is simple and fast	Manual extraction of ROI and not a convincing method.
<b>Gamma Enhancement</b> Hsieh <i>et al.</i> (2012)	Gives better results and its easier for segmentation.	Huge training data required to set the gamma value.
<b>Bi-histogram equalization</b> Chai <i>et al.</i> (2013)	Uses optimization technique to find the best possible value.	Complex and takes time.
<b>Contrast Enhancement &amp; Noise Filtering</b> Guraksin <i>et al.</i> (2016)	Simple morphological operators used.	Not very effective and applied only on carpal and radius bones.

## 2.2 Literature review on hand bone segmentation techniques

For extracting the bone region from ROI image, segmentation techniques are essential. Image segmentation techniques are classified into thresholding, clustering, edge-based, region-based, deformable models and hybrid techniques. Different classes of segmentation techniques are shown in Figure 2.1.

Thresholding is the earliest and first segmentation technique, also the most widely applied segmentation technique. It is based on the postulation that both object and background have a different range of pixel intensities. In other words, if an object or background is mutually exclusive in terms of intensity range, then it could be separated in different regions using a single or multiple values of pixels intensity. Segmenting the bones from soft tissue region are achieved by Sobel gradient (Pietka *et al.* (1991,





**Figure 2.1:** Different types of segmentation techniques.

2001)). This method has limitations as the gradient image cannot be further used for segmentation. Overlapping of pixels are also present in the resulting image. Similar segmentation techniques like Derivative of Gaussian (DoG) and dynamic thresholding are also implemented on hand radiographs (Pietka *et al.* (1993), Sharif *et al.* (1994), Giordano *et al.* (2007)). But these techniques also hold the same problems as the previous technique. Otsu thresholding which is based on maximizing the inter-class variance was implemented on hand radiographs, but the major problem with the technique was that results were not accurate (Kashif *et al.* (2015)).

Clustering is unsupervised learning strategy that groups similar patterns into clusters. Most popular clustering technique used for segmentation is k-means clustering wherein the pixels are classified into k clusters, based on distance measure such as Euclidean distance. Clustering process is carried out by optimizing an objective function, in this case, to minimize a squared error function. Adaptive clustering algorithm based on k-means clustering along with Gibbs random fields (GRF) was formulated by Pappas (1992). This clustering technique was implemented on hand radiographs by many researchers, but the results were appalling as it was not effective on finely

varying textures (Gertych *et al.* (2007), Tristan-Vega and Arribas (2008), Giordano *et al.* (2010)). The k-means clustering along with gray-level co-occurrence matrix was used by Chai *et al.* (2011) for hand radiograph segmentation. The main drawbacks of this method were that the number of gray levels were decided manually and it was computationally intensive.

Edges are pixels which undergo abrupt changes in gray level intensity, known as discontinuities. These edges are connected and linked to constitute closed boundary. Pixels within the closed boundary are then labeled as objects. This type of labeling is referred to edge-based segmentation. Particle Swarm Optimization (PSO) was used along with edge detectors by Liu *et al.* (2007) and also with graph-based segmentation by Thangam *et al.* (2012).

Region-based segmentation techniques seek to segment an image by classifying the image into two sets of pixels: Interior and exterior, based on the similarity of selected image features. It is based on the concept that the object to be segmented has common image properties and similarities such as a homogeneous distribution of pixel intensity, texture, and pattern of pixel intensity that is unique enough to distinguish it from another object (Gonzalez *et al.* (2004)). Region growing and region merging technique was applied by Manos *et al.* (1994) on hand radiographs. This technique is insensitive to image semantics and is unable to separate multiple disconnected objects simultaneously.

Watershed algorithm is a classic example of hybrid segmentation technique. It is based on the basic concepts; thresholding, region growing, and edge detection techniques. Han *et al.* (2007) implemented it on hand radiographs but it had limitations due to sensitivity towards noise and heavy dependence on gradient of the image.

Deformable model is a class of methods that implement an estimated model of the targeted object using the model constructed by the prior information. Prior information can be edge information, image texture and shape variability of a specific class of object. The three main classes of deformable models are active contour model (ACM), active shape model (ASM) and active appearance model (AAM). The word active suggests that the curves adapt themselves to fit the targeted object. Each class

differs mainly from the prior information that they use for segmentation. Niemeijer *et al.* (2003) segmented middle phalanx of the third finger using ASM. In this paper, authors achieved an accuracy of 80 percent in terms of the observer. However, the dataset consisted of images of age group 9-17 years. Other authors also tried using ACM for segmentation (Luis-Garcia *et al.* (2003)).

Thodberg *et al.* (2009) proposed a complete BAA system called as BoneXpert method. The architecture of BoneXpert can be divided into three major layers: Layer A to reconstruct the bone borders, Layer B to compute bone age value for each bone based on image and gender, and Layer C to transform the intrinsic bone age value to final bone age value that can be used by the clinician. The bone reconstruction is based on active appearance model (AAM). However, the age groups 17-19 and 0-2 were omitted from the dataset. Also, radius and ulna bones were poorly reconstructed. The summary of different segmentation techniques is presented in Table 2.2.

## 2.3 Literature review on feature extraction methods and classification techniques

Based on the TW2 method, a computer-based skeletal age scoring system (CASAS) using phalanges and radius-ulna bones was designed by Tanner and Gibbons (1994). The result minimized the root-mean-square error between Fourier transform from the unknown bone and Fourier transform of the available bone templates. The templates were produced by averaging the Fourier transform coefficients using 10 images from bone stages. The system coped well with overexposed or underexposed images but demanded a well-positioned hand. It was highly dependent on the templates which had been used to design the system. Rucci *et al.* (1995) proposed a method based on a trained neural network for feature extraction of X-ray hand bone images. The method was tested on 56 radiographs of low quality. Gross *et al.* (1995) used a neural network which was based on linear distance measures. It did not use morphological features that were used in GP or TW methods.

Mahmoodi *et al.* (1997) developed an automated system based on analysis of PROI utilizing an active shape model and knowledge-based technique. The system applied

**Table 2.2:** Summary of different segmentation techniques for bone age assessment of hand radiographs.

Segmentation Technique	Advantages	Disadvantages
<b>Binary overlay &amp; Adaptive contour</b> Michael and Nelson (1989)	Simple and very basic method	Contour follower fails at very noisy edges & at corners.
<b>Sobel Gradient</b> Pietka <i>et al.</i> (1991, 2001)	Takes less processing time.	Some overlapping pixels still present. Depends heavily on contrast of the image.
<b>Dynamic-thresholding</b> Pietka <i>et al.</i> (1993)	Performs better than local and global thresholding.	Only suitable selection of kernel size and constant can produce optimum result.
<b>DoG &amp; thresholding</b> Sharif <i>et al.</i> (1994), Giordano <i>et al.</i> (2007)	Advantages of DoG and thresholding makes it slightly better.	Fails in noisy images. Requires good contrast images.
<b>Region growing &amp; Region merging</b> Manos <i>et al.</i> (1994)	Better than thresholding as it divides regions into interior and exterior	Insensitive to image semantics. Unable to separate multiple disconnected objects simultaneously.
<b>Active Shape Models</b> Mahmoodi <i>et al.</i> (1997), Niemeijer <i>et al.</i> (2003)	Gives high segmentation accuracy.	Landmark placement is manual. Number of landmarks has to be specified. Alignment phase is critical. Large data required for training set.
<b>k-means with GRF</b> Pietka <i>et al.</i> (2003), Gertych <i>et al.</i> (2007), Tristan-Vega and Arribas (2008), Giordano <i>et al.</i> (2010, 2016)	Very high segmentation accuracy	Bad results if noise is present. Very slow compared to k-means clustering. Effective for slow varying textures.
<b>Active Contour Models</b> Luis-Garcia <i>et al.</i> (2003)	Processes only specific areas. High computational efficiency. Can be easily governed.	High sensitivity to noise. High dependency on initial snake. Does not consider region information.
<b>Watershed</b> Han <i>et al.</i> (2007)	Overcomes drawbacks of edge-based segmentation.	Sensitive towards noise. Heavily depends on the gradient.
<b>PSO with Edge set</b> Liu <i>et al.</i> (2007, 2008)	Better than edge-based segmentation methods.	Not effective for fused bones.
<b>Active Appearance Model</b> Thodberg <i>et al.</i> (2009)	Powerful segmentation method. Follows ASM method but slightly better.	Low efficiency in real time systems. Low discriminative ability. Inconsistent robustness.
<b>Canny edge detector</b> Giordano <i>et al.</i> (2010), Guraksin <i>et al.</i> (2016)	Simple and basic methods	Depends heavily on the gradient and contrast of the image.
<b>GLCM with k-means</b> Chai <i>et al.</i> (2011)	Simple and effective for largely similar regions in image.	No. of gray levels manually decided. Computationally intensive & time consuming.
<b>Graph-based Segmentation</b> Thangam <i>et al.</i> (2012)	Overcomes drawbacks of edge-based methods	Requires manual landmarks if gradient are not clear. Cannot segment multiple disconnected objects simultaneously.
<b>Otsu thresholding</b> Kashif <i>et al.</i> (2015, 2016)	Most simplest and basic method.	Manual threshold values to be given. End segmentation results are not accurate.

a hierarchical search to localize the bones and then an active shape model was performed by a bone contour. Age estimation was done using the Bayesian estimator and regression model. Pietka *et al.* (2003) developed an end-to-end system using k-means

clustering algorithm and Gibbs random fields for segmentation (Pappas (1992)). The features were extracted using wavelet transform, which was then further classified using fuzzy classifiers.

Aja-Fernández *et al.* (2004) designed a computational TW3 classifier for bone age assessment. The classifier was built upon a modified version of a fuzzy ID3 decision tree. A unique advantage was that it did not require a large dataset to train, but only a few to fine tune it. Tristán and Arribas (2005) developed an end-to-end system focussing on radius and ulna bones. It used a modified k-means algorithm for segmentation (Pappas (1992)). Further, 89 features were extracted from each bone and classification was done with the help of generalized softmax perceptron (GSP) neural network. Feature selection was done using linear discrimination analysis (LDA). The dataset was really small with only 4 stages of TW3. As a further attempt by Tristán-Vega and Arribas (2008), a detailed methodology was described but it did not cover all the stages of TW3.

Liu *et al.* (2008) proposed automatic bone age assessment based on intelligent algorithms. In this paper, the main focus of authors was on the extraction of RUS and carpal features as well as classification technique using back-propagation algorithm. Even though accuracy achieved was good, the training of neural network took a lot of time. Hsieh *et al.* (2007) focused on the extraction of features from PROI and classify them using fuzzy logic. The feature selection was done using principal component analysis (PCA). In their further attempt, Hsieh *et al.* (2010) demonstrated the same work with a slightly larger database and also showed which features were dominant.

Thodberg *et al.* (2009) proposed a complete BAA system called as BoneXpert method. Features include shape, intensities, texture information. Final stage maps the result to either GP Bone age or TW2 bone age. Giordano *et al.* (2010) developed a fully automated system for bone age assessment. Authors compared their results with Pietka *et al.* (1991, 1993) and Gertych *et al.* (2007). The performance was good but not as high as the BoneXpert method. But the system can evaluate low-quality images as compared to BoneXpert as it rejects such images.

Recently Harmsen *et al.* (2013) have used support vector machines (SVM) with

**Table 2.3:** Summary of various feature extraction techniques and classification methods.

Segmentation Method	Features Extracted	Classification	Results
<b>Sobel Gradient</b> Pietka <i>et al.</i> (1991)	Phalangeal length		ME = 1.57 Std = 0.32
<b>ASM</b> Mahmoodi <i>et al.</i> (1997)	Principal Components E-M width ratio	Bayes decision theory	Acc = 83(M)/85(F)
<b>k-means with GRF</b> Pietka <i>et al.</i> (2003)	Wavelet Transform Morphological features	Fuzzy classifiers	ME = 0.94(M), 1.13(F)
<b>ASM</b> Niemeijer <i>et al.</i> (2003)	Correlation values	TW model compare	Acc = 73.2
<b>Manual Segmentation</b> Aja-Fernández <i>et al.</i> (2004)	Epiphysis curvature measure. E-M width Ratio.	Fuzzy Decision tree	Acc = 93.5
<b>k-means with GRF</b> Gertych <i>et al.</i> (2007)	Wavelet Transform Morphological features	Fuzzy classifiers	Acc = 80
<b>DoG and thresholding</b> Giordano <i>et al.</i> (2007)	E-M width ratio Morphological features		Acc = 87
<b>k-means with GRF</b> Tristan-Vega and Arribas (2008)	E-M width ratio Zerinke Moments, Fourier and Haar wavelet	Neural networks	ME= 0.89
<b>PSO with edge set</b> Liu <i>et al.</i> (2008)	E-M width ratio Morphological features	Neural Networks	ME = 0.84 Std = 4.4
<b>AAM</b> Thodberg <i>et al.</i> (2009)	Shape of phalange Gabor energies	Calibrated GP/TW	Std(GP) = 0.42 Std(TW) = 0.8
<b>k-means with GRF</b> Giordano <i>et al.</i> (2010)	E-M width ratio Convex hull of Epiphysis	TW model compare	ME = 0.67 Std = 0.43
<b>Region growing</b> Harmsen <i>et al.</i> (2013)	Cross corellation values	SVM	ME = 0.83 (Gender) Me = 0.96 (No Gender)
<b>Semi-auto with Otsu</b> Kashif <i>et al.</i> (2016)	SIFT	SVM	ME = 0.6053 (Gender) ME = 0.7461 (No Gender)
<b>Deep Learning</b> Lee <i>et al.</i> (2017)	Deep CNN transfer	CNN	ME = 0.93(F) ME = 0.82 (M)
<b>Deep Learning</b> Spampinato <i>et al.</i> (2017)	CNN features	CNN	ME = 0.79

cross-correlation to prototype age for each class. Guraksin *et al.* (2016) have worked on morphological operators for pre-processing, segmentation and feature extraction. In this paper, authors have used SVM for classification and their main work was focused on carpal bones and radius bone only for an age group of 0-6 years. Scale Invariant Feature Transform (SIFT) feature extraction was used for BAA by Kashif *et al.* (2015) and later Kashif *et al.* (2016) proved that SIFT is better than other feature extraction

techniques like BRISK, FREAK etc. But the authors use a semiautomatic procedure involving Otsu's thresholding as the main segmentation technique. Seok *et al.* (2016) have extracted 17 ROI's altogether from phalanges and radius, ulna bones and used multi-layered fuzzy classifiers for classification. Lee *et al.* (2017) and Spampinato *et al.* (2017) have used deep learning techniques for bone age assessment. The summary of various feature extraction techniques and classification methods is presented in Table 2.3.

## 2.4 Research gap analysis

### 1 The TW2 system is obsolete.

The differences between TW2 and TW3 systems have been discussed earlier. The creators of TW system do not recommend the use of TW2 system after it has been revised. The TW3 system mentions that the skeletal maturity scores have been mapped to bone ages which have been derived from larger populations (European, North-American and European derived populations).

### 2 Need for a larger dataset.

Ideally, to test the technique and derive a conclusion on the fitness of the technique there is a need to have a large dataset. There has been good work done in this field, with various approaches to tackle the BAA problem, but the major drawback is the limited number of images used for validating the results.

### 3 A system to cater the whole age group.

The TW3 system can be used to predict ages from 0-18 years. The literature survey clearly shows that researchers have not tested their BAA systems on the whole age group except for a few systems which gave bad accuracy. This may be due to the failure in segmenting the bones at different ages or failing to classify them.

### 4 End-to-end TW3 system for BAA.

For the benefit of larger and rural masses, the BAA system should be simple, easy-to-use and fast. Hence, there is a need to have a fully automated system that will assess the bone age from a radiograph with minimal or no human intervention. The underlying software should be light, so that it can run on any processing machine, from a desktop to a mobile phone.

# Chapter 3

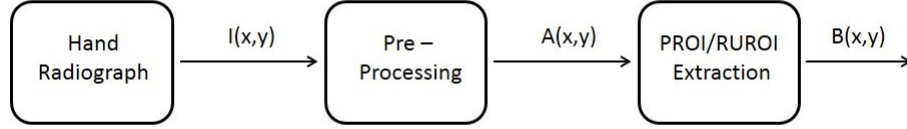
## PRE-PROCESSING AND ROI EXTRACTION

### 3.1 Introduction

This chapter presents pre-processing and ROI extraction blocks of the ABAA system. Pre-processing and ROI extraction techniques used for the phalangeal region of interest (PROI) and radius-ulna region of interest (RUROI) are discussed. Later the segmentation stage is applied which common to both ROI's i.e. PROI and RUROI, which will be discussed in the chapter 4.

Pre-processing of an image is a set of operations applied to image data that will either suppress unwanted distortions or enhance particular image features. It is an important procedure which prepares the image for further analysis. Pre-processing techniques are broadly divided into contrast enhancement, noise filtering, histogram modification and geometrical transformations. Contrast or image enhancement is basically a set of operations that are used to improve the quality of an image such that it is better suited for human or machine interpretation. Noise filtering is used to remove any unnecessary information if present. Histogram reflects the characteristics of an image. Thus, by varying the histogram it can unlock any hidden information that can be useful for any particular application. Geometric transformations such as scaling, rotation, translation, skewing were not considered as pre-processing techniques until recently. The region of interest (ROI) is a portion of an image under study, on which further image processing techniques are applied.





**Figure 3.1:** Block diagram of the proposed ROI extraction technique.

The schematic block diagram of the proposed ROI extraction technique for both phalangeal and radius-ulna is shown in Figure 3.1. In this figure, the first pre-processing stage involves noise removal and preparation of the hand radiograph image  $I$  for ROI extraction stage. Let the output image after this stage be called as  $A$ . The next step is the extraction of ROI's (Phalangeal and Radius-Ulna ROI). Let the extracted image be  $B$ . In the next stage edge enhancement or edge preservation is performed and then segmentation of bones is carried out in ROI which is discussed in the chapter 4.

## 3.2 Pre-processing and extraction of PROI and RUROI

It is important to prepare the image before an extensive procedure of ROI extraction followed by segmentation stage. The pre-processing stage is same for both ROI extraction techniques. For efficient and accurate ROI extraction, the X-ray image of the left hand is subjected to Gaussian filtering (Gonzalez and Woods (2004)). The Gaussian filter removes the noise present in the hand radiograph to give image  $A$ . After studying the shape and structure of fingers, the extraction of ROI is done with the help of morphological operators (Dougherty and Lotufo (2003)) using SDC morphology toolbox.

### 3.2.1 Pre-processing and PROI extraction technique

The steps for PROI extraction technique are as follows:

1. Gaussian filtering for noise removal (Gonzalez and Woods (2004)). The filter has a Gaussian profile which is convolved with the image and presented in equation

(3.1)

$$O(x, y) = I(x, y) * G(x, y) \quad (3.1)$$

where  $O(x, y)$  is the output image after filtering stage and  $I(x, y)$  is the input radiograph and  $G(x, y) = \frac{1}{2\pi\sigma^2} e^{-\frac{x^2+y^2}{2\sigma^2}}$ . In the equation (3.1),  $*$  stands for convolution and  $\sigma$  is the standard deviation.

2. Multi-level Otsu thresholding to get the boundary of hand (Otsu (1975)).

$$\sigma_w^2(t_h) = \omega_1(t_h)\sigma_1^2(t_h) + \omega_2(t_h)\sigma_2^2(t_h) \quad (3.2)$$

where  $\omega_i(t_h)$  stands for probabilities of two classes ( $i = 1, 2$ ) separated by a threshold  $t_h$ . In Otsu (1975), author proved that minimizing the intra-class variance  $\sigma_w^2(t_h)$  is same as maximizing the inter-class variance  $\sigma_b^2(t_h)$ .

3. Morphological erosion is used to smoothen the boundary of hand. Assume the output after thresholding stage is  $T$ , then the morphological erosion operation on the input image  $T$  by structuring element  $S$  is given by equation (3.3):

$$T \ominus S = x : S_x \subset T \quad (3.3)$$

where  $\subset$  denotes subset and  $T \ominus S$  is made up of all the points  $x$  for which the translation of  $S$  by  $x$  fits in  $T$  (Dougherty and Lotufo (2003)). The structuring element used for this step is cross.

4. Unnecessary objects present in the binary image are removed with the help of edge-off function and area opening function. The edge-off function discards any object connected to borders of the image. Area opening filter removes an object from the image if it's size is less than some value  $\nu$ , which is given in equation (3.4).

$$T \circ (\nu)_n = \bigcup P, \text{area}(P) \geq \nu \quad (3.4)$$

where  $T$  is the input image and  $P$  is the area of n-connected component, (Dougherty and Lotufo (2003)).

5. Skeleton function and thinning operation to get the skeleton of thresholded image.
6. Use region properties function to find bounding box, orientation and area of all skeletons.

7. Use above properties to draw a rectangular box around the phalanges and crop to get PROI. The output PROI image is  $B(x, y)$ .

### 3.2.2 Pre-processing and RUROI extraction technique

The steps for RUROI extraction technique are as follows:

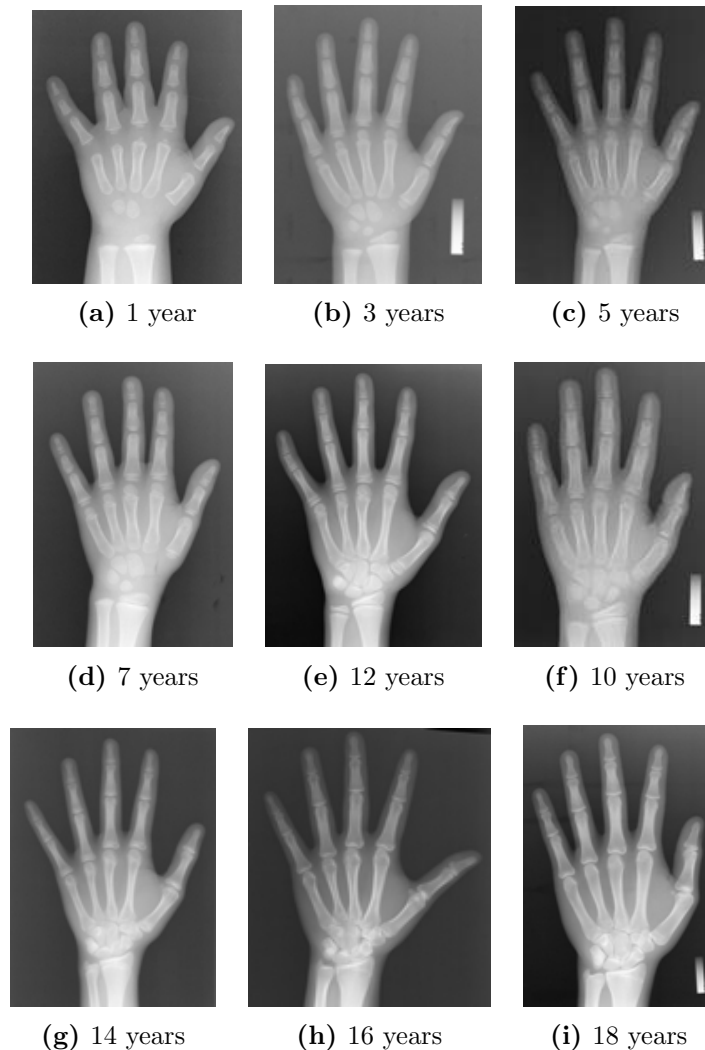
1. Gaussian filtering for noise removal as defined in equation (3.1).
2. Multi-level Otsu thresholding to get the boundary of hand as defined in the equation (3.2).
3. Morphological erosion to smoothen the boundary of hand as defined in the equation (3.3).
4. Edge off and area opening function to remove any unnecessary objects present in the binary image as defined in the equation (3.4).
5. Find the mean of all the columns to get the column with maximum value and use this as a reference line for finding the vertical borders of the ROI.
6. With the help of reference column from previous step which divides the hand into two parts, first non-zero values are found from the left and right borders of hand radiograph. These non-zero values form the left and right borders of RUROI.
7. To find the top horizontal border of RUROI, the mean of all the rows is used to choose a border line of RUROI based on the information extracted.
8. Use the above properties to crop a rectangular region containing the bones radius and ulna.

## 3.3 Experimental results and discussion

In this section, the results of PROI and RUROI extraction techniques on digital hand radiographs between age group of 0-18 years is presented. All results are obtained on a 64-bit system with MATLAB 2015a software, having an 8 GB RAM and an Intel i7 processor with clock speed of 3.6 GHz. The section consists of image database details, MATLAB implementation procedure, results obtained and discussion.

### 3.3.1 Image database

The database used for experimentation is acquired from an online website, <http://www.ipilab.org/BAAweb/>. The images in this database were collected from Childrens Hospital Los Angeles (CHLA), United States of America (Gertych *et al.* (2007)). This database consists of 1101 digital radiographs of left hand out of which 552 were of male and 549 were of female children. The manual segmentation or ground truth images are constructed with the help of different medical experts from Goa Medical College (GMC), Bambolim, Goa, India for result comparison. Test hand radiograph images used for experimentation are shown in Figure 3.2.



**Figure 3.2:** Test hand radiograph images used for ROI extraction and segmentation.

### 3.3.2 Implementation of PROI extraction technique

The implementation steps of proposed fully automatic PROI extraction are given as follows:

1. **Noise removal:** The first step is pre-processing, where Gaussian low pass filtering is used for noise removal as given in equation (3.1). The filter size is  $3 \times 3$  with sigma value set to 5. Please note that hand radiographs are not resized.
2. **Boundary extraction:** The PROI extraction stage begins with multi-level Otsu thresholding to extract the boundary of hand. Matlab function *multithresh* and morphology toolbox function *mmthreshad* are used to perform this operation. The resulting output image is binary. Smoothen the boundary of hand in radiograph using erosion operation *mmero* as given in the equation (3.3). Structuring element used here is cross with size 2. Please note that functions starting with *mm* are morphology toolbox functions and rest are Matlab functions.
3. **Superfluous object removal:** Unnecessary objects present in the image are removed by using *mmedgeoff* and *mmareaopen* functions.
4. **PROI extraction:** The skeleton of hand is extracted using *mmskelm*, *mmthin*, *mmendpoints* functions and then labeled using *bwlabel* function. These labeled objects are further processed using *regionprops* function to extract information and then cropped to get the PROI image from hand radiograph. Orientation option from *regionprops* function is used to align the PROI's vertically.

### 3.3.3 Implementation of RUROI extraction technique

The implementation of the proposed automatic RUROI extraction is explained in following steps:

1. **Noise removal:** As mentioned earlier, as a pre-processing step, Gaussian low pass filtering is used for noise removal as given in equation (3.1). The filter size is kept  $3 \times 3$  and the sigma value is set to 5. The hand radiographs are not resized before applying this step.
2. **Extracting boundary of hand:** Boundary of hand is extracted using multi-level Otsu thresholding. Matlab functions used are *multithresh* and SDC toolbox function *mmthreshad* for this operation. The binary image obtained after

thresholding is further smoothed using erosion operation *mmero* as given in the equation (3.3) and structuring element used here is cross with size 2.


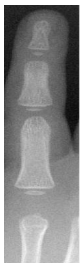


















3. **Vestigial object removal:** Unwanted objects present in the image are removed with the help of *mmedgeoff* and *mmareaopen* functions.
4. **RUROI extraction:** The borders of RUROI image are found using simple mathematical logic as explained in the earlier section. The MATLAB functions used in this step are *mean* and *find*. The *mean* function is used to find the mean of all column and rows whereas *find* function is used to find the first non-zero values from the left and right borders of hand radiograph.

### 3.3.4 PROI and RUROI extraction results











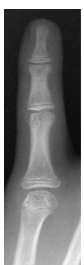














The extraction of PROI and RUROI images is done according to the guidelines of TW3 assessment as given in Tanner *et al.* (2001). For assessing the score, phalanges and a small part of a metacarpal bone in PROI are required, whereas in RUROI extraction, only radius and ulna bones are required. The PROI images extracted are shown in the Figures 3.3 and 3.4 along with the CPU processing time required for extraction and the RUROI images extracted are shown in Figure 3.5. The adjoining phalange if present in the PROI is removed in the post-processing step after segmentation stage which is explained in chapter 4. Note that the CPU processing time taken for extraction varies due to the different sizes of the images.

### 3.3.5 Discussion

The pre-processing stage involves only noise removal as the enhancement of the image is done after ROI extraction stage. The PROI and RUROI extraction results are fairly accurate by isolating the required bones for further application of segmentation technique. The extraction process is fairly swift as mentioned in Figures 3.3 and 3.4. Figures 3.3, 3.4, and 3.5 shows the CPU processing time in seconds taken by the PROI and RUROI extraction techniques respectively. It clearly indicates that computational cost of each ROI extraction technique is very less. Also, the automatic ROI extraction stage is independent of hand placement and orientation. The automatic ROI extraction stage (PROI and RUROI) is simple and takes a negligible amount of time because it does not involve any complex mathematical procedure.

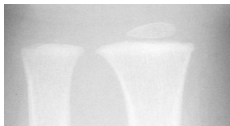
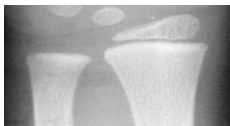
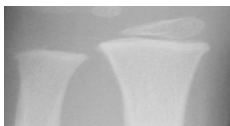

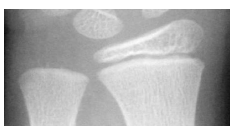
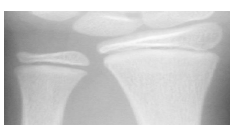
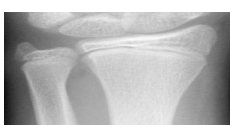
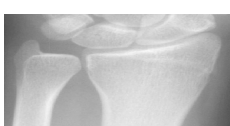

Image	Pinky	Ring	Middle	Index	Thumb	Time(sec)
1 year old 5173.jpg [1430x1099]						8.635
3 years old 6102.jpg [1542x1152]						12.438
5 years old 7143.jpg [1728x1248]						9.538
7 years old 5154.jpg [1890x1330]						16.937

**Figure 3.3:** PROI images extracted from the hand radiographs.

Image	Pinky	Ring	Middle	Index	Thumb	Time(sec)
10 years old 5113.jpg [1900x1380]						17.587
12 years old 5322.jpg [2081x1592]						16.511
14 years old 5237.jpg [2509x1844]						36.529
16 years old 5257.jpg [2149x1879]						21.368
18 years old 6145.jpg [2376x1616]						31.869

**Figure 3.4:** PROI images extracted from the hand radiographs.



Image	RUIOI Image	Time(sec)
1 year old 5173.jpg [1099x1430]		0.730
3 year old 6102.jpg [1542x1152]		0.777
5 year old 7143.jpg [1728x1248]		0.774
7 year old 5154.jpg [1890x1330]		0.874
10 year old 7076.jpg [1728x1216]		0.771
12 year old 5322.jpg [2081x1592]		0.923
14 year old 5237.jpg [2509x1844]		1.127
16 year old 5257.jpg [2149x1879]		1.009
18 year old 6145.jpg [2376x1616]		0.943

**Figure 3.5:** RUIOI images extracted from the hand radiographs.

## 3.4 Summary

- Fully automated ROI extraction techniques are designed for phalanges (PROI) and radius-ulna bones (RUROI).
- Both ROI extraction techniques are simple, accurate and fast.
- Both ROI extraction techniques are robust as they performed well on hand radiographs of varying intensities.
- Proposed ROI extraction techniques are independent of hand placement and orientation.
- The extracted regions are quite adequate to be processed further by next stages of ABAA system.

# Chapter 4

## SEGMENTATION OF HAND BONES

### 4.1 Introduction

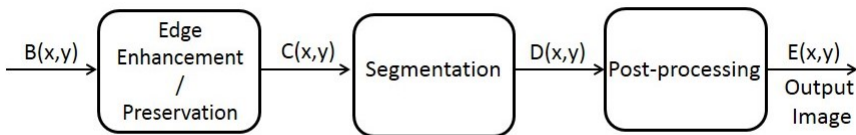
This chapter describes the segmentation stage of ABAA system. In this connection, two segmentation techniques are proposed for PROI and RUROI images. The results of both proposed segmentation techniques are discussed and compared with other state-of-the-art segmentation techniques. The chapter also presents the validation of obtained results by different medical experts.

Segmentation is a mathematical process which divides an image into separate regions, where each region is homogeneous. It is meaningful or useful for image analysis and interpretation only, if the regions are strongly related to the depicted objects or features of interest. Meaningful segmentation is the first step of transforming an image from low level image processing into high-level image description in terms of features and objects. An accomplishment of image analysis depends highly on segmentation, but an accurate partitioning of an image is a very challenging task. As mentioned earlier, intensity inhomogeneity and overlapping pixels between the soft tissue region and hand bones are the major challenges in the segmentation of hand bones from the digital hand radiograph.

The extraction of a phalangeal region of interest(PROI) and radius-ulna bones region of interest (RUROI) is done separately as explained in the chapter 3. Next

step is the segmentation of extracted PROI and RUROI images for BAA. In this context, robust segmentation techniques are proposed. The schematic block diagram of proposed segmentation techniques for PROI and RUROI images is shown in Figure 4.1. The proposed segmentation technique is subdivided into 3 stages which are:

1. Edge Preservation for PROI/Edge Enhancement for RUROI,
2. Segmentation of the bones in ROI's and
3. Post processing of the segmented image.



**Figure 4.1:** Schematic block diagram of the proposed segmentation technique.

In Figure 4.1,  $B$  is the extracted ROI image, pre-processing is performed for edge enhancement or edge preservation to give image  $C$ . Segmentation of bones in ROI is done based on level set method (Osher and Sethian (1988)). Segmented image  $D$  is further post-processed and the end result is given in image  $E$ . Due to non-uniform distribution of X-ray intensities in hand radiograph, the segmentation step is followed by post-processing stage to increase the segmentation accuracy. This stage removes any vestigial regions that might be present after segmentation stage.

## 4.2 Edge preservation for PROI

Prior to segmentation of the bones in the PROI, anisotropic diffusion algorithm is applied for edge preservation (Perona and Malik (1990)). The reason for applying anisotropic diffusion on extracted PROI images is that it selectively diffuses regions having less gradient while preserving the edges. The output of previous stage is  $B(x, y)$  which is the extracted PROI image and input image for the segmentation stage. The mathematical formulation of anisotropic diffusion is defined in equation (4.1).

$$\frac{\delta(B(x, y, t))}{\delta t} = \text{div}(J(x, y, t)\nabla(B(x, y, t))) \quad (4.1)$$

where  $\nabla(B)$  is the image gradient and the diffusion function  $J(x, y)$  depends on the image gradient magnitude  $\|\nabla(B)\|$ . For larger gradient values, the diffusion is low and for smaller gradient values, the diffusion is high (Hum (2013)).

The anisotropic diffusion algorithm preserves the edges by smoothing the texture inside the object and sharpening the edges of the object. Two diffusion functions were proposed by Perona and Malik (1990) which are defined in equations (4.2) and (4.3) respectively.

$$G(x, y, t) = \exp\left(-\left(\frac{\nabla(B(x, y, t))}{\lambda}\right)^2\right) \quad (4.2)$$

$$G(x, y, t) = \frac{1}{1 + \left(\frac{\|\nabla(B(x, y, t))\|}{\lambda}\right)^{1+a}}; a > 0 \quad (4.3)$$

where  $a$  is empirical constant and  $\lambda$  is a parameter which is used to control the diffusion strength. The equation (4.2) is used for implementation with  $\lambda$  value set to the variance of the image.

### 4.3 Edge enhancement for RUROI

Prior to segmentation of RUROI images, edge enhancement is required for better segmentation accuracy. In this case, the image is modified in such a way that edges and other features of bones in the RUROI are enhanced. This is achieved by three steps which are given below:

1. Use alternating sequential filtering to diffuse the image with less effect on the edges and curves (Dougherty and Lotufo (2003)). The output of close-open filter with  $m = 3$  is given in equation (4.4).

$$F_{CO}^m = (((((B \bullet S) \circ S) \bullet 2S) \circ 2S) \dots \bullet mS) \circ mS \quad (4.4)$$

where  $m$  is the number of times structuring element ( $S$ ) is applied to the image  $B$ , and disk is used as the structuring element in all these steps. In equation (4.4),  $\bullet$  and  $\circ$  stand for morphological closing and opening respectively.

2. Take morphological gradient of negative image of resulting filtered image which is given in equation (4.5).

$$K = (F' \oplus S) - (F' \ominus S) \quad (4.5)$$

where  $F'$  is compliment of image  $F$ ,  $\oplus$  and  $\ominus$  are dilation and erosion operators respectively.

3. Add the resulting image  $K$  from previous step to the extracted RUROI image  $B$  to get edge-enhanced image  $C$ .

## 4.4 Segmentation using Level Set Method

The pre-processed and edge-enhanced/edge-preserved ROI images  $C$  are modeled by the mathematical equation (4.6):

$$C = bZ + n \quad (4.6)$$

where  $Z$  is the true image,  $b$  is the bias field and  $n$  is the additive noise.

In the equation (4.6), the true image  $Z$  is the depiction of physical characteristics of hand. Therefore, it might be safe to assume that true image is approximately constant. The image  $C$  is a function  $C : \Omega \rightarrow R$ , defined on the continuous domain  $\Omega$ . The bias field  $b$  is assumed to be smoothly varying. The true image  $Z$  is divided into  $N$  different regions  $\Omega = \cup_{i=1}^N \Omega_i$ . Each of this region takes a constant value  $p_1, p_2, \dots, p_N$ .

Consider a centre point  $c$  of a circular area with radius  $r$ ,  $c$  belongs to  $\Omega$ ,  $V_c = x : |x - c| < r$ . If  $\Omega$  is divided into  $N$  regions  $\Omega_{i=1}^N$ , this will divide the circular area  $V_c \cap \Omega_i$ , (Li *et al.* (2011)). According to above formulation, equation (4.6) is reformulated as given in equation (4.7).

$$C(x) = b(x)p_i + n(x) \text{ for } x \text{ belongs to } V_c \cap \Omega \quad (4.7)$$

The equation (4.7) is similar to k-means clustering (Theodoridis *et al.* (2010)) and can be written in continuous energy form which is given in equation (4.8).

$$W = \int_{V_c} |C(x) - q_i|^2 u_i(x) dx \quad (4.8)$$

where  $q_i$  is the cluster center of the  $i^{th}$  cluster and  $u_i$  is the membership function of region  $\Omega_i$ .

Further, it can be safely assumed that  $q_i \approx b(x)p_i$  and is defined in the region  $V_c$ . The membership function will have a value 1 in this region and zero outside, hence equation (4.8) is rewritten as follows:

$$W(b, p) = \int_{\Omega} |C(x) - b(x)p_i|^2 dx \quad (4.9)$$

Using the Chan and Vese (CV) model (Chan *et al.* (2001)), now level set function is used to minimize the energy function. Level set methods are one of the many numerical techniques designed to track the evolution of interfaces (Osher and Sethian (1988)). Level set function focuses on moving boundaries by exploiting a strong link between moving interfaces and equations from computational fluid dynamics (Sethian (1987), Osher and Sethian (1988)). The mathematical expression of CV model is given in equation (4.10).

$$\begin{aligned} Q(b, p, \phi) = & \int_{\Omega} |C(x) - b(x)p_1|^2 H(\phi(x)) dx \\ & + \int_{\Omega} |C(x) - b(x)p_2|^2 (1 - H(\phi(x))) dx \\ & + \mu \int_{\Omega} |\nabla H(\phi(x))| dx \end{aligned} \quad (4.10)$$

where  $\phi$  is the level set function and  $H$  is the Heaviside function.

In the equation (4.10), the Heaviside function is a discontinuous function which is zero for all negative arguments and one for all positive arguments. The first two terms in the equation (4.10) are data fitting terms, whereas the last term regularizes the zero level contour (Osher and Sethian (1988)). The level set function performs division of the image into two parts  $\Omega_1 = x : \phi(x) < 0$  and  $\Omega_2 = x : \phi(x) > 0$ . Hence, the segmentation of bones is fulfilled by finding parameters like level set function  $\phi$ , bias field  $b$  and a constant  $p$  that minimizes the energy function.

In order to divide image into object and background, it is defined as  $u_1(\phi) = H(\phi)$

and  $u_2(\phi) = 1 - H(\phi)$ , where  $u_i$  represents membership function for the regions  $\Omega_i$ . Hence, the revised form of energy function is defined in equation (4.11).

$$W(b, p, \phi) = \int_{\Omega} \sum_{i=1}^N |C(x) - b(x)p_i|^2 u_i(\phi(x)) dx \quad (4.11)$$

Now this energy term is used as data term in equation (4.10) and it is reformulated as given in equation (4.12).

$$Q(b, p, \phi) = W(b, p, \phi) + \varpi R(\phi) \quad (4.12)$$

where  $\varpi$  is the weight and  $R(\phi)$  is the regularization term which is equal to  $\int_{\Omega} |\nabla H(\phi(x))| dx$ . The above equation (4.12) is minimized with respect to variables  $b$ ,  $p$  and  $\phi$  to segment the bones from hand radiograph. The minimization is achieved by performing iterations, where in each iteration any two variables are fixed and then minimize the equation (4.12) with respect to the third variable. The output image of segmentation stage is  $D(x, y)$  which is the input for the post-processing stage. The minimization steps are as follows:

1. Energy minimization with respect to  $\phi$ : For fixed values of  $p$  and  $b$ , the minimization of  $Q(b, p, \phi)$  is achieved by using standard gradient descent method and solving gradient flow equation.

$$\frac{\partial \phi}{\partial t} = -\frac{\partial Q}{\partial \phi} \quad (4.13)$$

From calculus of variations:

$$\frac{\partial \phi}{\partial t} = -\delta(\phi)(d_1 - d_2) + \mu \delta(\phi) \operatorname{div} \left( \frac{\nabla(\phi)}{|\nabla(\phi)|} \right) \quad (4.14)$$

where  $d_i = \int |C(x) - b(x)p_i|^2 dx$  and  $i = 1, 2$ .

2. Energy minimization with respect to  $p$ : For fixed values of  $\phi$  and  $b$ , the optimized value of  $p$  is denoted as:

$$\tilde{p}_i = \frac{\int bC(x)u_i(\phi(x))dx}{\int b^2u_i(\phi(x))dx} \text{ where } i = 1, 2 \quad (4.15)$$

3. Energy minimization with respect to  $b$ : For fixed values of  $\phi$  and  $p$ , the optimized



value of  $b$  is denoted as:

$$\tilde{b} = \frac{C(x)[(p_1 u_1(\phi(x))) + (p_2 u_1(\phi(x)))]}{[(p_1^2 u_1(\phi(x))) + (p_2^2 u_1(\phi(x)))]} \quad (4.16)$$

## 4.5 Post-processing

This step is necessary for the procedure to extract accurate information from the segmented bones. Sometimes the contours which are initialized by level set function to track the bone edges might not behave in the required way. This is due to either or both of the following reasons:

1. It tracks the cancellous bone region along with the cortical bone region.
2. Due to intensity inhomogeneity and overlapping pixels between bone and soft tissue, the tissue region also gets identified as an object of interest.

To mitigate these errors morphological operators are used. To rectify the first type of error, image filling function along with erosion and dilation operations are used. To correct the second type of error, area opening function along with erosion and dilation operations are used. The area opening and erosion operations are given in equations (3.4) and (3.3) respectively. The dilation operation is defined as:

$$I \oplus S = \left( I' \ominus S^c \right)' \quad (4.17)$$

where  $I$  denotes the input image,  $S^c$  is the 180 degrees rotated version of structuring element and  $I'$  denotes the complement of an image. The dilation operation is denoted by  $\oplus$ . The structuring element used for post-processing steps is cross as it performs better than disk and there is no loss of information.

At last, edge off function is used to remove any unnecessary objects or other bone parts that might be present at the boundary of ROI. All the functions and operators used in pre and post-processing operations are applied from SDC morphology toolbox based on Dougherty and Lotufo (2003).

## 4.6 Implementation and illustrations

In this section, the proposed techniques are implemented and illustrated in a stepwise manner with the help of output images from each stage.

### 4.6.1 Implementation of phalangeal segmentation technique

The implementation steps of proposed fully automatic segmentation technique for extracted PROI images are given as follows:

1. **Anisotropic Diffusion:** Anisotropic diffusion algorithm is used to preserve the edges present in the image. Time step  $t$  in equation (4.1) is set to 5 and the value of  $\lambda$  in equation (4.2) is made equal to variance of the image.
2. **Initialization of level set function:** Initialization of level set contour on the image is done randomly. The contours initialized in a shape of box or circle get trapped in a region and are not able to proceed further. The Heaviside function  $H$  used during implementation is the smoothed version of Heaviside function which is defined in the equation (4.18) (Osher and Sethian (1988)).

$$H_\nu(x) = \frac{1}{2} \left[ 1 + \frac{2}{\pi} \arctan\left(\frac{x}{\nu}\right) \right] \quad (4.18)$$

where  $\nu = 1$ .

3. **Energy minimization:** For energy minimization the weight of regularization parameter ( $\varpi$ ) in equation (4.12) is set to any smaller value. It is found to be best if it is made equal to the standard deviation of the extracted PROI image. Energy minimization is achieved by using the equations (4.14), (4.15) and (4.16). The number of iterations is set to 100.
4. **Post-processing:** The functions used for post processing are image filling function *imfill* and dialtion operation *mmdil*. Area-opening and edge-off functions are used to remove unnecessary bone parts present in the ROI.

### 4.6.2 Illustration of phalangeal segmentation technique

From the theory explained in sections 4.2 and 4.4, the proposed segmentation technique is divided into three stages which are: (1) edge-preservation (Pre), (2) segmentation (Seg) and (3) post-processing (Post). The stage-wise results are illustrated in

Figures 4.2 to 4.4, which presents the implementation of proposed technique on hand radiographs of ages 1, 10 and 16-year-old person respectively. Quantitative results of each stage are evaluated and compared in terms of quality metrics like peak signal to noise ratio (PSNR), mean squared error (MSE), and structure similarity (SSIM) index, which are given in the Table 4.1. The mathematical expressions of these quality metrics is given in sub-section 4.7.1. Please note that the output image after an edge-preservation stage is compared with PROI image where both are grayscale images, whereas the output images of other two stages are compared with ground truth image in which all images are binary. It is noticed that there is a considerable improvement in the results at each stage of the proposed technique and the final output image is similar to ground truth image.

### 4.6.3 Implementation of radius and ulna segmentation

The implementation steps of the proposed automatic segmentation technique for extracted RUROI images are explained as follows:

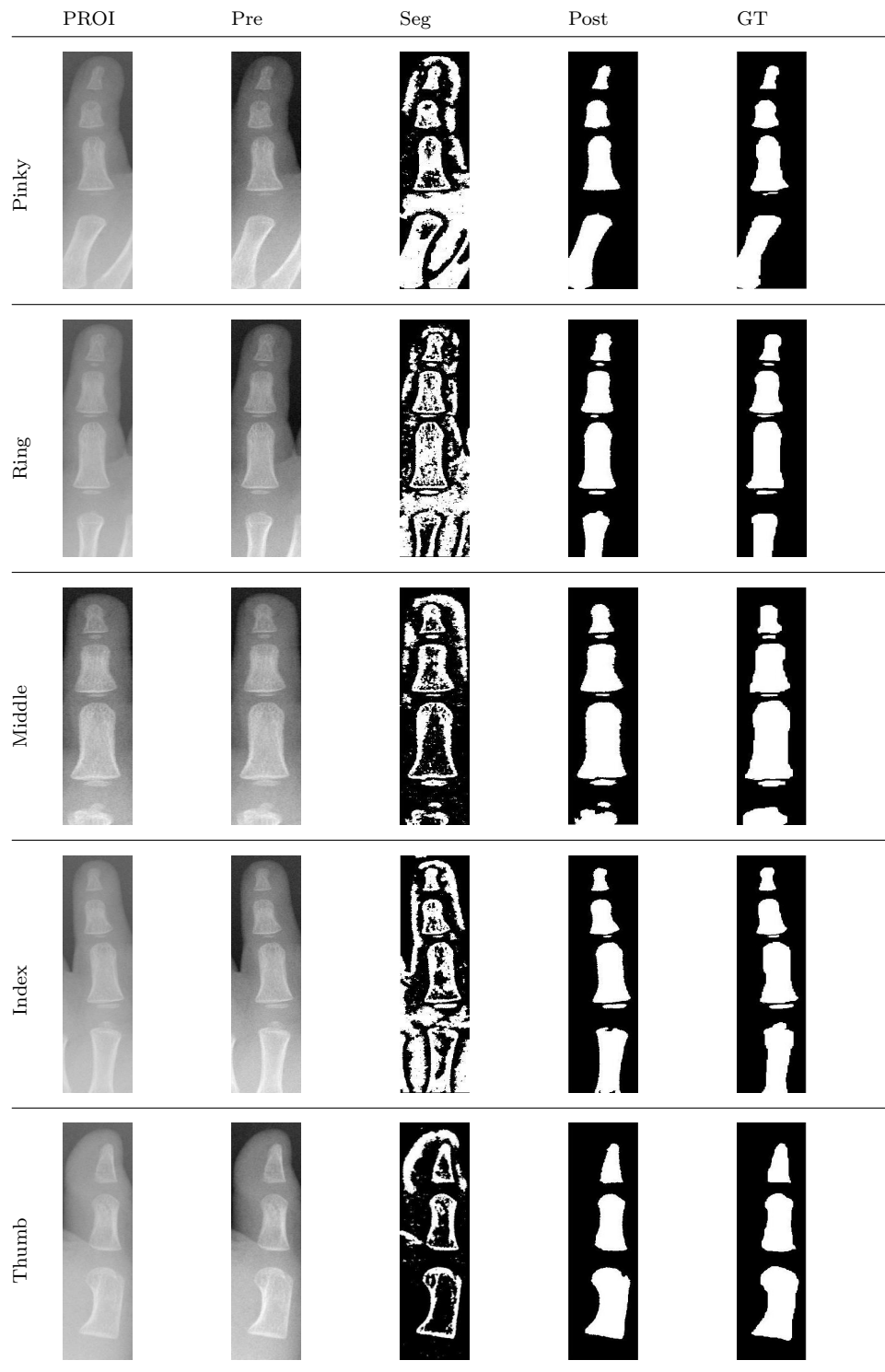
1. **Edge - Enhancement:** The steps for edge-enhancement are described in the section 4.3 and section 4.4. Function *mmsfrec* is used for alternate sequential filtering of image. Close-open-close filtering is done as value of *m* was set to 3. Structuring element used is disk with size 1. Further *mmgradm* function is used with disk structuring element of size 2 to get the gradient.
2. **Level set function:** Level set contour is initialized randomly on the image as contours initialized in a shape of box or circle get trapped in some regions. Smoothed version of Heaviside function is used for implementation purposes which is given in equation (4.18) (Osher and Sethian (1988)).
3. **Energy minimization:** The weight of regularization parameter ( $\varpi$ ) in equation (4.12) is set to any smaller value or it is made equal to the standard deviation of the extracted RUROI image. Energy minimization is achieved by using the equations (4.14), (4.15) and (4.16). The number of iterations is set to 100.
4. **Post-processing:** The functions such as image filling function *imfill* and dilation operation *mmdil* are used for post processing. Area-opening function *mmareaopen* and edge-off function *mmedgeoff* are used to remove carpal bones and other vestigial parts present in the RUROI.

**Table 4.1:** PSNR, MSE, and SSIM performance comparison of results after each stage of the proposed technique on hand radiographs of ages 1, 10 and 16 year old person.

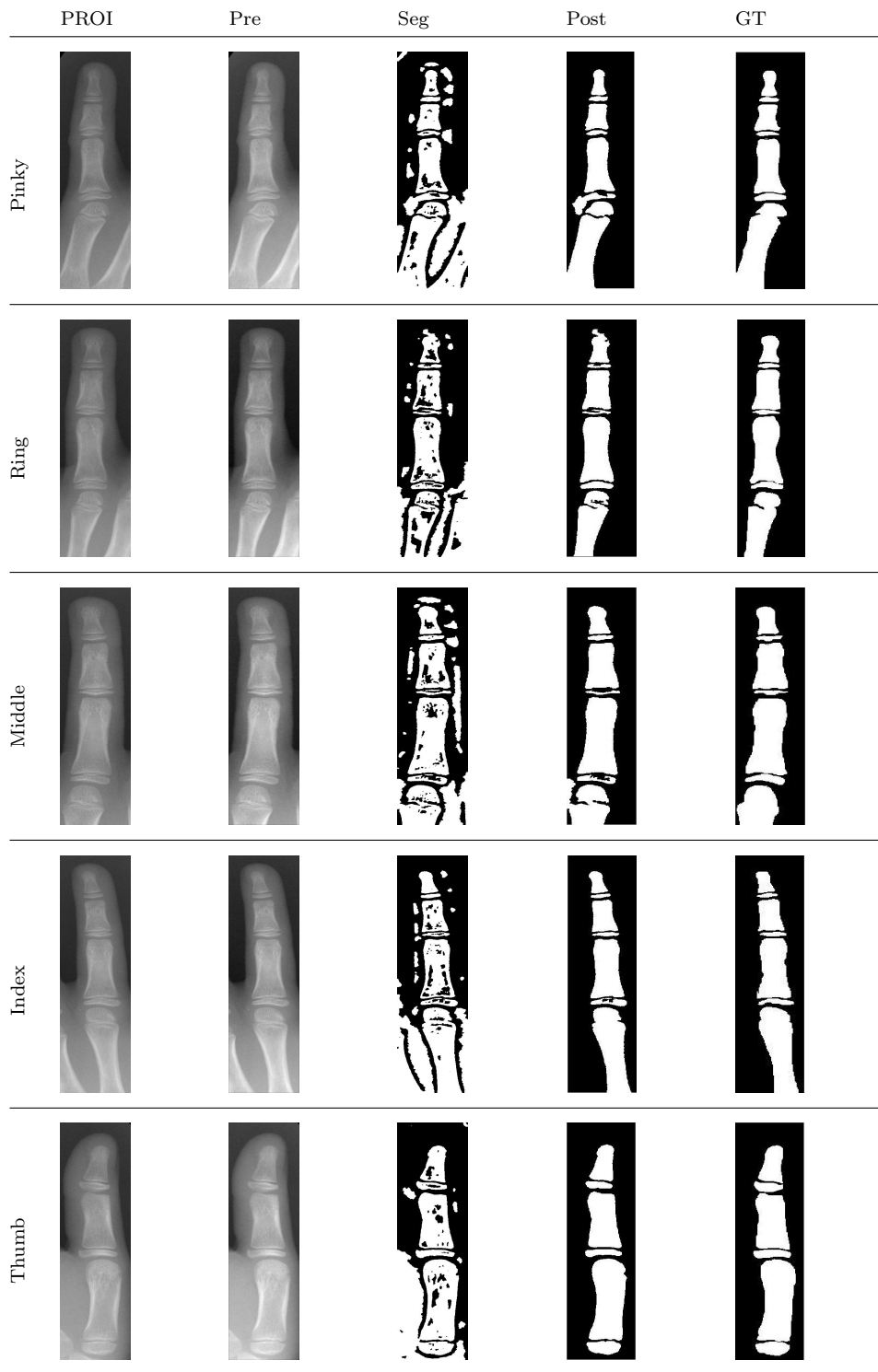
Image	PROI	QM	Edge Preservation	Segmentation	Post-processing
1 year, [5173.jpg]	Pinky	PSNR	19.977	45.592	65.079
		MSE	653.660	1.794	0.020
		SSIM	0.914	0.812	0.999
	Ring	PSNR	19.117	45.840	65.142
		MSE	796.786	1.695	0.020
		SSIM	0.907	0.825	0.999
	Middle	PSNR	19.830	47.787	61.864
		MSE	676.210	1.082	0.042
		SSIM	0.897	0.880	0.996
	Index	PSNR	21.807	45.944	64.269
		MSE	428.892	1.655	0.024
		SSIM	0.943	0.831	0.998
	Thumb	PSNR	20.772	47.787	65.115
		MSE	544.356	1.082	0.020
		SSIM	0.933	0.875	0.999
10 year, [5113.jpg]	Pinky	PSNR	19.085	46.240	62.606
		MSE	802.816	1.546	0.036
		SSIM	0.848	0.838	0.997
	Ring	PSNR	24.133	46.730	63.070
		MSE	251.062	1.381	0.032
		SSIM	0.849	0.855	0.997
	Middle	PSNR	23.000	46.904	61.824
		MSE	325.894	1.326	0.043
		SSIM	0.869	0.860	0.997
	Index	PSNR	25.790	46.403	64.823
		MSE	171.436	1.489	0.021
		SSIM	0.864	0.845	0.998
	Thumb	PSNR	21.172	46.470	64.218
		MSE	496.485	1.466	0.025
		SSIM	0.861	0.849	0.998
16 years, [5257.jpg]	Pinky	PSNR	21.16	47.088	62.601
		MSE	497.145	1.272	0.036
		SSIM	0.887	0.877	0.997
	Ring	PSNR	22.573	47.537	61.874
		MSE	359.611	1.147	0.042
		SSIM	0.919	0.877	0.996
	Middle	PSNR	20.563	47.663	61.835
		MSE	571.167	1.114	0.043
		SSIM	0.973	0.880	0.996
	Index	PSNR	24.310	46.969	63.972
		MSE	241.055	1.307	0.026
		SSIM	0.956	0.859	0.998
	Thumb	PSNR	21.657	47.133	60.181
		MSE	444.010	1.258	0.062
		SSIM	0.905	0.868	0.994

#### 4.6.4 Illustration of radius and ulna segmentation technique

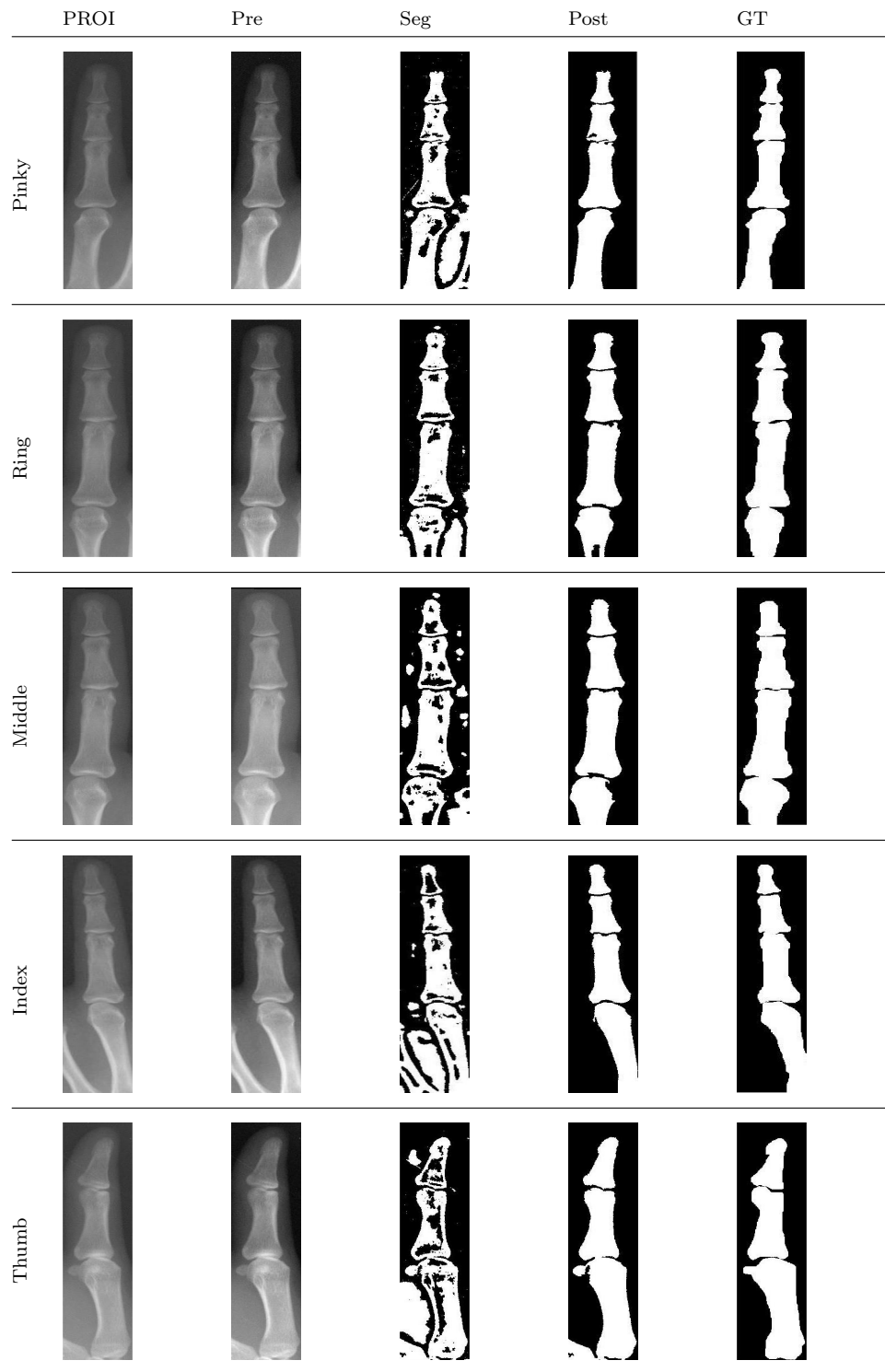
The proposed segmentation technique is divided into 3 major stages as discussed in section 4.3 and section 4.4. Quantitative results of each stage are evaluated using the quality metrics (QM) like PSNR, MSE, SSIM (Gupta *et al.* (2015)) which are given in the Table 4.2. Please note that the edge-enhanced image is compared with RUROI image and the output image of other two stages are compared with ground truth image



**Figure 4.2:** Output images from each stage of the proposed technique on extracted PROI image of 1 year old person [5173.jpg].



**Figure 4.3:** Output images from each stage of the proposed technique on extracted PROI image of 10 year old person [5113.jpg].

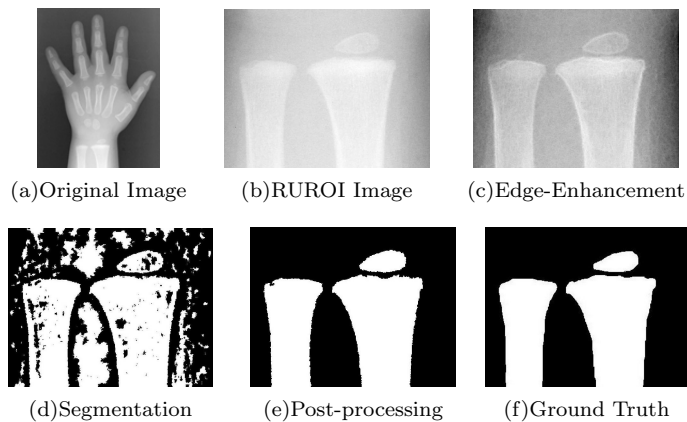


**Figure 4.4:** Output images from each stage of the proposed technique on extracted PROI image of 16 year old person [5257.jpg].

for calculating PSNR, MSE and SSIM. Output images of each stage is given in Figures 4.5, 4.6 and 4.7 respectively. After edge-enhancement stage, a clear demarkation of edges which is apparent in the Figures 4.5, 4.6 and 4.7 has been achieved. Figure 4.5 shows the implementation of proposed technique on hand radiograph of 1 year old child. The smaller bone is ulna and the larger is radius. The small bone above radius is called epiphysis which will fuse with metaphysis of radius as the child grows. Metaphysis is the head portion of any bone. These bones are a part of analysis for BAA (Tanner *et al.* (2001), Gilsanz and Ratib (2005)). Similarly Figure 4.6 presents the output results using hand radiograph of 7 year old person. A part of carpal bone is present in RUROI, which is removed after post-processing. It is clear from Figure 4.6, that the epiphysis has grown in size and will later fuse with radius bone. In Figure 4.7, the output images of hand radiograph of 18 year old person at each stage of proposed technique are presented.

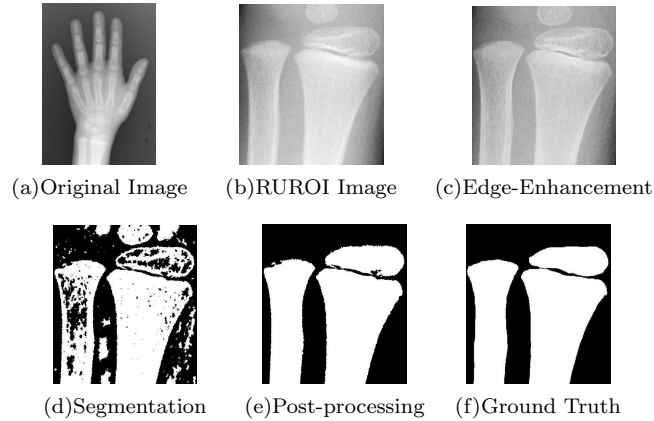
**Table 4.2:** Performance results after each stage of the proposed technique

Image	QM	Edge-Enhancement	Segmentation	Post-processing
1 year [5173.jpg]	PSNR	33.109	46.471	65.891
	MSE	31.781	1.466	0.017
	SSIM	0.967	0.847	0.999
7 years [5154.jpg]	PSNR	32.150	47.430	65.172
	MSE	39.635	1.175	0.020
	SSIM	0.960	0.881	0.999
18 years [6145.jpg]	PSNR	30.751	45.941	68.753
	MSE	54.702	1.656	0.009
	SSIM	0.956	0.830	0.999

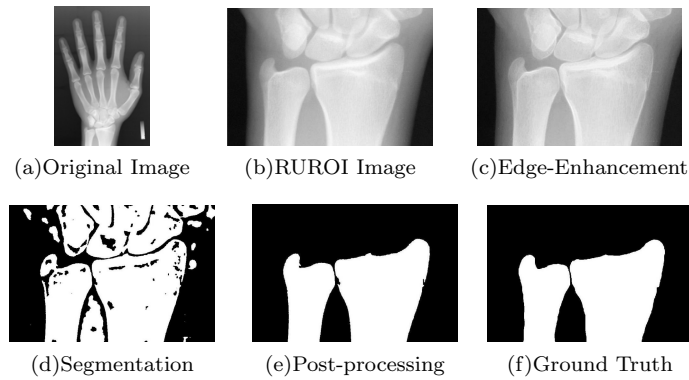


**Figure 4.5:** Output images from each stage of the proposed technique on extracted RUROI image of 1 year old [5173.jpg].





**Figure 4.6:** Output images from each stage of the proposed technique on extracted RUROI image of 7 year old [5154.jpg].



**Figure 4.7:** Output images from each stage of the proposed technique on extracted RUROI image of 18 year old [6145.jpg].

## 4.7 Experimental results and discussion

The experimental results of the proposed segmentation techniques and other state-of-the-art segmentation techniques are evaluated and discussed in this section. All segmentation results are obtained on a 64-bit system with MATLAB 2015a software, having an 8 GB RAM and an Intel i7 processor with clock speed of 3.6 GHz.

### 4.7.1 Performance metrics

To evaluate the quantitative performance of proposed technique (PT), improvement at each stage is validated by using quality metrics like PSNR, MSE and SSIM. The math-

emathical expression for PSNR, MSE and SSIM are given in equations (4.20), (4.19), and (4.21) respectively. To judge the robustness of proposed technique with other state-of-the-art segmentation techniques mentioned earlier, various quality metrics such as Structure similarity index (SSIM), Jaccard Similarity Index (JSI), Dice, Accuracy (ACC), Geometric Mean (GM) and Matthews Correlation Coefficient (MCC) are the automatic choice for the researchers in the field of medical image segmentation. The mathematical expressions for PSNR and MSE are as follows:

$$MSE = \frac{1}{MN} \sum_{i=1}^M \sum_{j=1}^N \left( S(i, j) - G(i, j) \right)^2 \quad (4.19)$$

where  $S$  stands for segmented image and  $G$  for ground truth image.

$$PSNR(dB) = 10 * \log_{10} \left( \frac{255^2}{MSE} \right) \quad (4.20)$$

Structure similarity (SSIM) index is given by equation:

$$SSIM(S, G) = \frac{(2\mu_S\mu_G + \lambda_1)(2\sigma_{SG} + \lambda_2)}{(\mu_S^2 + \mu_G^2 + \lambda_1)(\sigma_S^2 + \sigma_G^2 + \lambda_2)} \quad (4.21)$$

where  $\mu_S$  is the mean of segmented image,  $\sigma_S^2$  is the variance of segmented image,  $\mu_G$  is the mean of ground truth image,  $\sigma_G^2$  is the variance of ground truth image,  $\sigma_{SG}$  is the covariance between segmented and ground truth images,  $\lambda_1$  and  $\lambda_2$  are small constants to stabilize the denominator. The numerical value of SSIM lies between 0 and 1. If the proximity of SSIM value is closer to 1, better the segmentation technique.

Jaccard similarity index (JSI) and Dice similarity index as mentioned by Gupta *et al.* (2015) is used for performance analysis:

$$JSI = \frac{|S \cap G|}{|S \cup G|} \quad (4.22)$$

$$Dice = 2 \frac{|S \cap G|}{|S + G|} \quad (4.23)$$

Dice coefficient is also called as the F1 score. Jaccard coefficient and Dice coefficient look similar but they are not same. Both are used to measure the similarity index but Dice does not satisfy the triangle inequality. The numerical values of both coefficients

lie between 0 and 1. If the proximity of JSI and Dice values are closer to 1, better the segmentation technique.

Accuracy (ACC) as used by Gupta *et al.* (2015) gives information about the ratio of the pixels contained within the segmented region achieved by the test algorithm with the pixels of the manually segmented region. The segmentation accuracy is defined as,

$$ACC = \frac{t_p + t_n}{t_p + f_p + t_n + f_n} \quad (4.24)$$

where  $t_p$  = true positive,  $t_n$ = true negative,  $f_p$ = false positive and  $f_n$ =false negative. The numerical value of ACC lies between 0 and 1, where 0 corresponds to failed segmentation and 1 corresponds to best segmentation accuracy.

The geometric mean (GM) given by Orlando *et al.* (2017) is calculated as:

$$GM = \sqrt{\frac{t_p t_n}{(t_p + f_n)(t_n + f_p)}} \quad (4.25)$$

The numerical value of GM lies between 0 and 1. If the proximity of GM value is closer to 1, better the segmentation technique.

The mathematical equation for Matthews Correlation Coefficient (MCC) as used by Orlando *et al.* (2017) is given as in equation (4.26).

$$MCC = \frac{(t_p t_n) - (f_p f_n)}{\sqrt{(t_p + f_p)(t_p + f_n)(t_n + f_p)(t_n + f_n)}} \quad (4.26)$$

MCC is considered as a balanced measure as it can be used also when the classes vary in sizes. The MCC value varies between -1 and +1. Where +1 means a perfect segmentation and -1 indicates complete fallout between segmented and ground truth images.

#### 4.7.2 Experimental settings for segmentation of phalanges

The hand radiograph is divided into 3 regions namely background, the soft tissue region, and the bones. Hence, the parameter values of segmentation techniques used for

result comparison are set accordingly. Otsu’s thresholding is done using two levels to separate the 3 regions while other techniques like k-means algorithm (KMS), k-means with Gibb’s random fields (KGRF) and PSO based segmentation algorithm (PSO) have a number of classes set to 3 for segmentation. Table 4.3 shows the parameters used for simulation of these segmentation techniques and their values. The first four techniques namely Otsu, KMS, KGRF, and PSO are implemented in the field of hand bone segmentation by Kashif *et al.* (2015), Pietka *et al.* (2003), Tristan-Vega and Arribas (2008), Liu *et al.* (2007) respectively. Adaptively Regularised Kernel-based Fuzzy C-means clustering technique (AKFM) is a recent fuzzy based clustering algorithm which was implemented on brain tissues by Elazab *et al.* (2015), and it is also included for result comparison. BFV algorithm (BFV) developed by Gong *et al.* (2015) is a recent fuzzy based level set algorithm, which is also included for comparison. All hand radiographs used for comparison are also been subjected to anisotropic diffusion as pre-processing step before applying various segmentation techniques for fair comparison with PT.

**Table 4.3:** Simulation parameters and their values used for various segmentation techniques of PROI images

Parameters	Otsu	KMS	KGRF	PSO	AKFM	BFV	PT
Number of thresholds	2						
Number of clusters		3	3	3	3		
Number of iterations			30	150		200	100
Clique potential			0.5				
Local filtering					median	gaussian	gaussian
Local window size					3	10	3
Population				150			
Inertial weight				1.2			
Weight 1				0.8		1	
Weight 2				0.8		1	
Min velocity				-5			
Max velocity				5			
Lower bound of position				1			
Upper bound of position				256			
Constant positive integer						2	
Time step						0.1	0.1
Heavyside weight							1

### 4.7.3 Quantitative and qualitative analysis of phalangeal segmentation

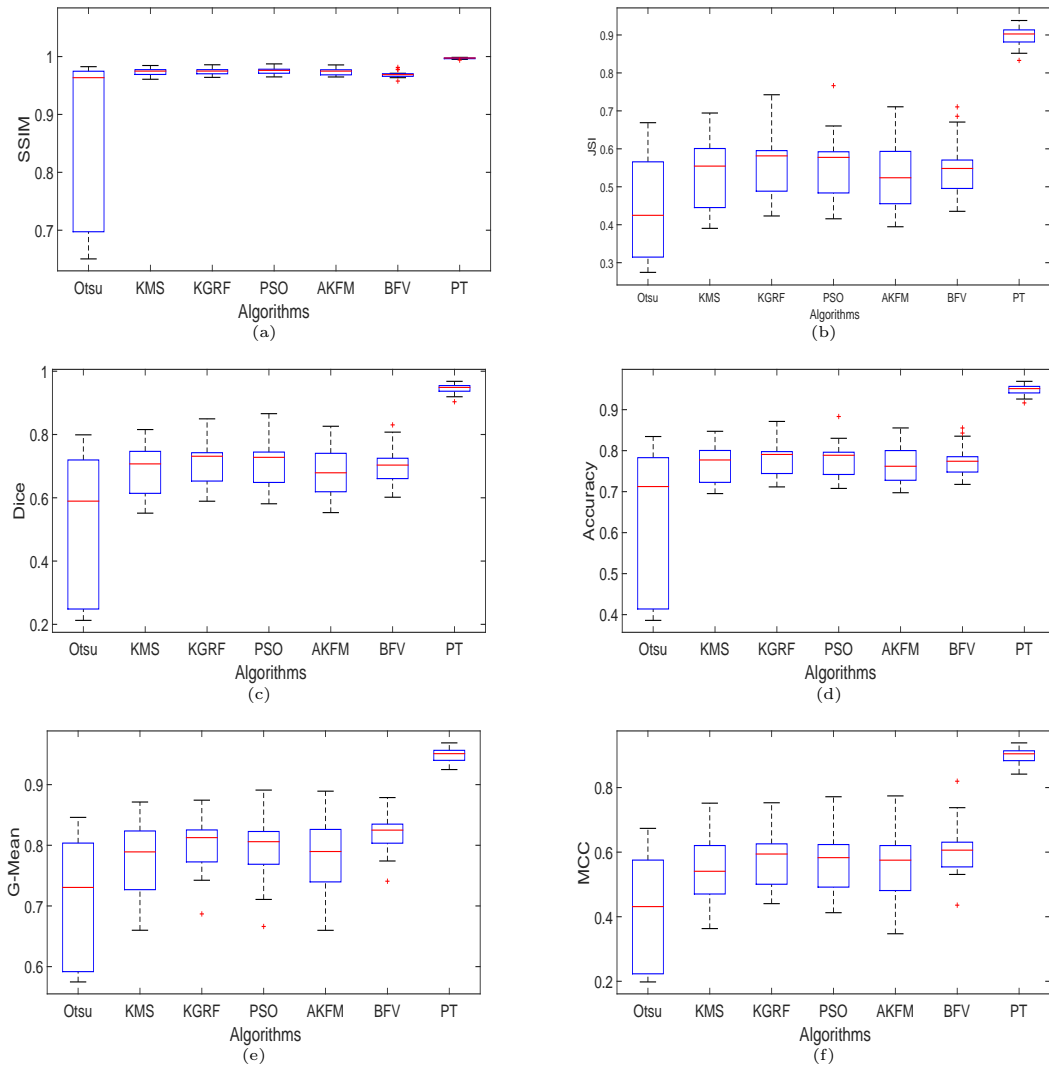
The quantitative performance analysis of proposed fully automatic segmentation technique and other existing segmentation techniques are obtained on extracted PROI images at ages 1, 3, 5, 7, 10, 12, 14, 16 and 18 which are given in Table 4.4. In Table 4.4, the results shown are the average values of all 5 fingers i.e. pinky, ring, middle, index and thumb. The qualitative results of proposed fully automatic segmentation technique and other state-of-the-art segmentation techniques are given in Figures 4.9 to 4.17 for ages 1, 3, 5, 7, 10, 12, 14, 16 and 18 respectively. Ground truth images (GT) are also included for comparison in the Figures 4.9 to 4.17.

Box-plot is used to compare all the segmentation techniques with respect to various quality metrics and is shown in Figure 4.8, wherein the sample size is 9 (number of images). The interquartile range (IQR) is denoted by box and whiskers denoted by line with breaks which define the range. The median is denoted by a line in the IQR which is skewed in some cases due to the sample distribution being skewed positively or negatively. From the box-plot shown in Figure 4.8, it is noticed that PT has less variation as compared to other segmentation techniques and also achieves higher segmentation accuracy. The SSIM values of other segmentation techniques are above 0.95 whereas the proposed technique has values around 0.99. The boxplot of JSI shown in Figure 4.8(b) shows proposed technique takes the value around 0.9 and supersedes other state-of-the-art techniques. Similarly in all other boxplots i.e. Figures 4.8(c), 4.8(d), 4.8(e) and 4.8(f) the proposed technique has higher quality metric values against other existing techniques (approximately 0.95).

The visual comparison of segmentation results of the proposed technique and other state-of-the-art segmentation techniques are given from Figures 4.9 to 4.17. It is noticed from Figures 4.9 to 4.8 that proposed segmentation technique (PT) for PROI images gives better segmentation results as compared to other state-of-the-art techniques. The statistical values such as minimum (MIN), maximum (MAX), mean, median and standard deviation (SDEV) of various quality metrics against segmentation techniques are presented in Table 4.5.

**Table 4.4:** Performance comparison of different segmentation techniques on PROI

Image	QM	Otsu	KMS	KGRF	PSO	AKFM	BFV	PT
<b>1 year</b> [5173.jpg]	SSIM	0.650	0.965	0.966	0.967	0.967	0.965	<b>0.998</b>
	JSI	0.274	0.468	0.462	0.461	0.415	0.491	<b>0.912</b>
	DICE	0.213	0.634	0.629	0.628	0.580	0.655	<b>0.954</b>
	ACC	0.386	0.734	0.731	0.731	0.708	0.745	<b>0.956</b>
	GM	0.575	0.760	0.767	0.764	0.767	0.801	<b>0.955</b>
	MCC	0.198	0.475	0.483	0.478	0.482	0.547	<b>0.913</b>
<b>3 years</b> [6102.jpg]	SSIM	0.681	0.978	0.977	0.977	0.978	0.970	<b>0.994</b>
	JSI	0.287	0.603	0.595	0.593	0.595	0.549	<b>0.833</b>
	DICE	0.231	0.748	0.741	0.740	0.741	0.703	<b>0.904</b>
	ACC	0.403	0.802	0.798	0.796	0.798	0.774	<b>0.916</b>
	GM	0.586	0.832	0.832	0.831	0.831	0.828	<b>0.925</b>
	MCC	0.212	0.630	0.629	0.626	0.632	0.606	<b>0.842</b>
<b>5 years</b> [7143.jpg]	SSIM	0.676	0.969	0.969	0.970	0.968	0.969	<b>0.996</b>
	JSI	0.317	0.436	0.529	0.525	0.417	0.548	<b>0.881</b>
	DICE	0.245	0.594	0.690	0.686	0.569	0.706	<b>0.936</b>
	ACC	0.403	0.718	0.764	0.762	0.709	0.774	<b>0.941</b>
	GM	0.582	0.660	0.791	0.784	0.672	0.774	<b>0.941</b>
	MCC	0.217	0.375	0.543	0.532	0.406	0.820	<b>0.882</b>
<b>7 years</b> [5154.jpg]	SSIM	0.673	0.975	0.975	0.975	0.975	0.966	<b>0.998</b>
	JSI	0.315	0.592	0.588	0.586	0.588	0.536	<b>0.912</b>
	DICE	0.243	0.741	0.738	0.746	0.738	0.697	<b>0.954</b>
	ACC	0.401	0.796	0.794	0.793	0.794	0.768	<b>0.956</b>
	GM	0.581	0.824	0.826	0.825	0.827	0.825	<b>0.957</b>
	MCC	0.216	0.615	0.618	0.615	0.618	0.600	<b>0.913</b>
<b>10 years</b> [7076.jpg]	SSIM	0.700	0.975	0.977	0.977	0.976	0.971	<b>0.997</b>
	JSI	0.314	0.506	0.595	0.590	0.575	0.575	<b>0.901</b>
	DICE	0.253	0.653	0.743	0.739	0.725	0.728	<b>0.948</b>
	ACC	0.415	0.753	0.798	0.795	0.788	0.788	<b>0.951</b>
	GM	0.592	0.747	0.817	0.812	0.824	0.837	<b>0.951</b>
	MCC	0.226	0.512	0.606	0.596	0.617	0.632	<b>0.904</b>
<b>12 years</b> [5322.jpg]	SSIM	0.697	0.978	0.978	0.979	0.978	0.968	<b>0.995</b>
	JSI	0.309	0.617	0.615	0.615	0.616	0.549	<b>0.852</b>
	DICE	0.249	0.758	0.757	0.757	0.757	0.707	<b>0.919</b>
	ACC	0.413	0.809	0.808	0.808	0.808	0.775	<b>0.926</b>
	GM	0.591	0.822	0.828	0.827	0.823	0.830	<b>0.925</b>
	MCC	0.223	0.622	0.628	0.628	0.621	0.614	<b>0.851</b>
<b>14 years</b> [5237.jpg]	SSIM	0.705	0.976	0.976	0.976	0.976	0.971	<b>0.996</b>
	JSI	0.302	0.575	0.581	0.577	0.524	0.563	<b>0.858</b>
	DICE	0.248	0.726	0.731	0.728	0.679	0.717	<b>0.924</b>
	ACC	0.417	0.787	0.791	0.789	0.762	0.782	<b>0.929</b>
	GM	0.595	0.748	0.813	0.806	0.791	0.832	<b>0.928</b>
	MCC	0.224	0.506	0.594	0.583	0.575	0.620	<b>0.859</b>
<b>16 years</b> [5257.jpg]	SSIM	0.804	0.969	0.973	0.972	0.975	0.978	<b>0.996</b>
	JSI	0.370	0.413	0.475	0.446	0.586	0.671	<b>0.893</b>
	DICE	0.347	0.575	0.632	0.610	0.728	0.800	<b>0.943</b>
	ACC	0.496	0.706	0.738	0.723	0.793	0.835	<b>0.946</b>
	GM	0.647	0.676	0.687	0.666	0.790	0.861	<b>0.946</b>
	MCC	0.296	0.469	0.483	0.463	0.597	0.697	<b>0.893</b>
<b>18 years</b> [6145.jpg]	SSIM	0.714	0.985	0.986	0.987	0.986	0.981	<b>0.998</b>
	JSI	0.379	0.694	0.742	0.766	0.711	0.706	<b>0.938</b>
	DICE	0.294	0.816	0.850	0.866	0.826	0.828	<b>0.968</b>
	ACC	0.431	0.847	0.871	0.883	0.855	0.853	<b>0.969</b>
	GM	0.596	0.871	0.874	0.891	0.889	0.879	<b>0.969</b>
	MCC	0.247	0.752	0.753	0.772	0.774	0.738	<b>0.938</b>

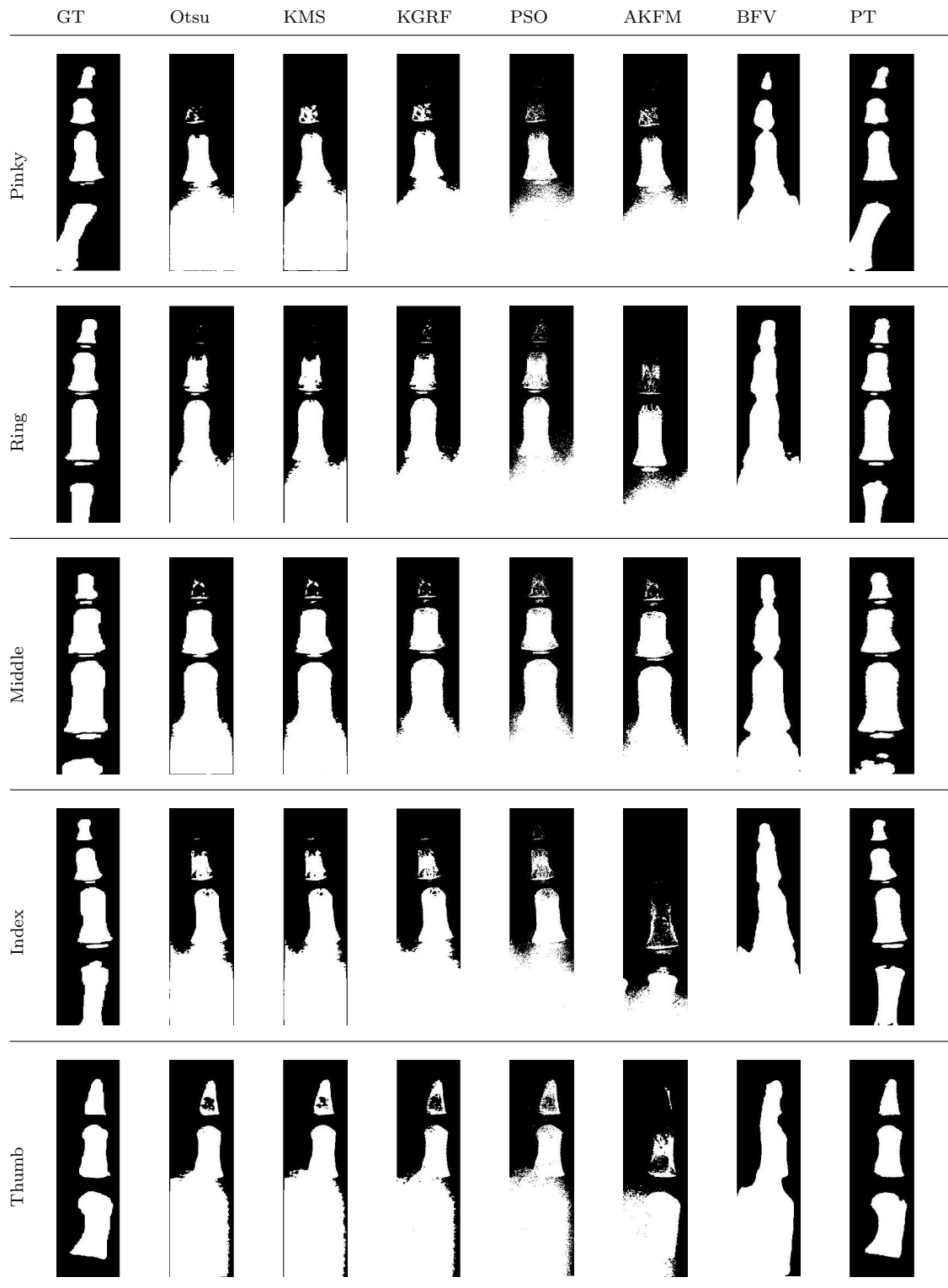


**Figure 4.8:** Boxplots of segmentation techniques against various quality metrics for segmented PROI images.

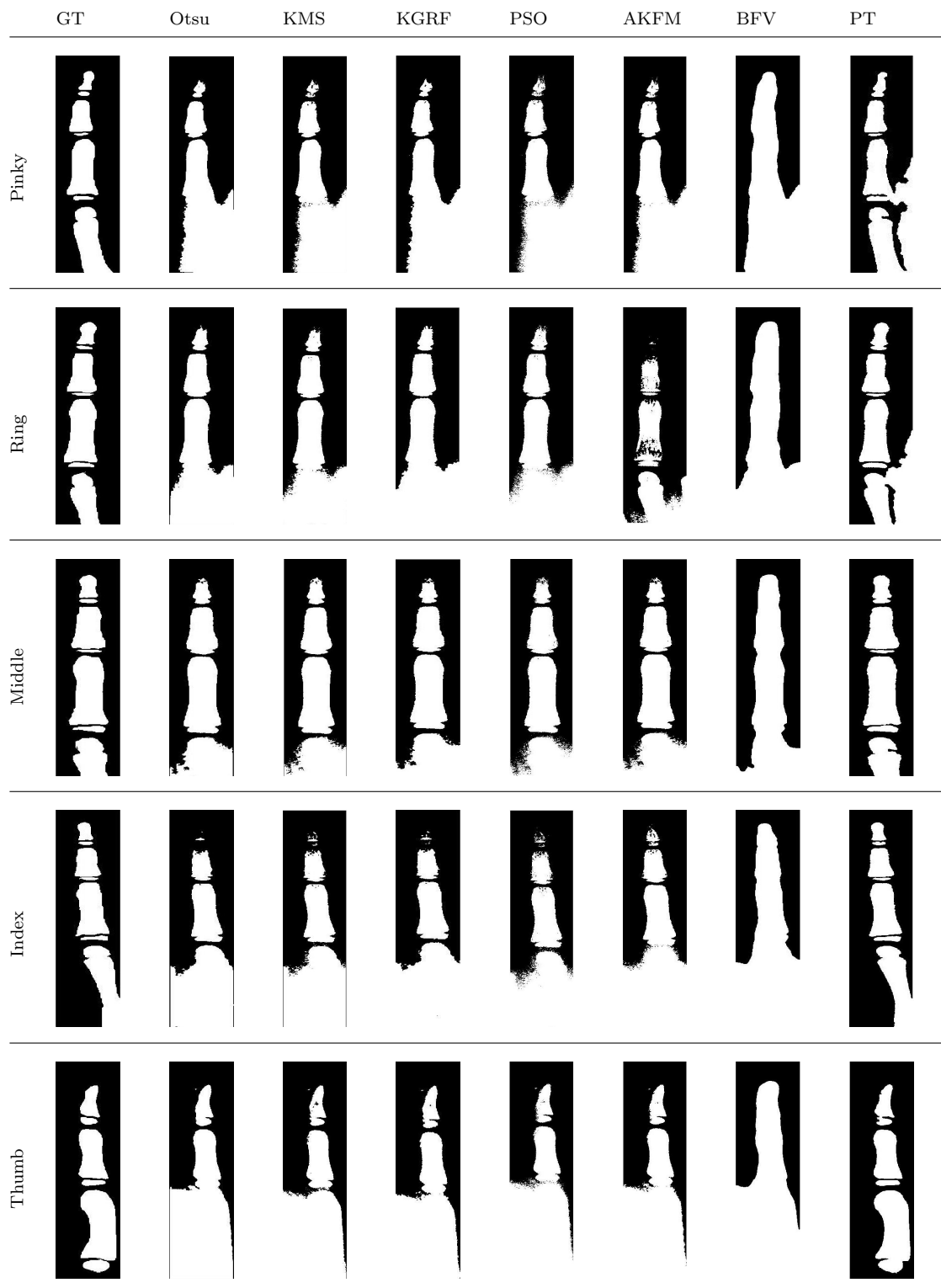
**Table 4.5:** Statistical values of various quality metrics against segmentation techniques

QM	Statistic	Otsu	KMS	KGRF	PSO	AKFM	BFV	PT
<b>SSIM</b>	MIN	0.650	0.961	0.964	0.965	0.965	0.958	0.994
	MAX	0.983	0.985	0.986	0.987	0.986	0.981	0.999
	MEAN	0.844	0.974	0.974	0.975	0.974	0.969	0.997
	MEDIAN	0.964	0.975	0.975	0.976	0.975	0.969	0.997
	SDEV	0.139	0.006	0.005	0.005	0.005	0.005	0.001
<b>JSI</b>	MIN	0.274	0.390	0.423	0.416	0.395	0.435	0.833
	MAX	0.669	0.694	0.742	0.766	0.711	0.711	0.938
	MEAN	0.440	0.540	0.561	0.556	0.532	0.548	0.895
	MEDIAN	0.425	0.554	0.581	0.577	0.524	0.548	0.903
	SDEV	0.130	0.091	0.079	0.085	0.087	0.073	0.026
<b>DICE</b>	MIN	0.213	0.551	0.589	0.581	0.553	0.602	0.904
	MAX	0.799	0.816	0.850	0.866	0.826	0.830	0.968
	MEAN	0.492	0.691	0.711	0.708	0.683	0.703	0.944
	MEDIAN	0.589	0.707	0.731	0.728	0.679	0.703	0.949
	SDEV	0.228	0.080	0.065	0.071	0.077	0.060	0.015
<b>ACC</b>	MIN	0.386	0.695	0.712	0.708	0.697	0.718	0.916
	MAX	0.834	0.847	0.871	0.883	0.855	0.855	0.969
	MEAN	0.606	0.770	0.780	0.778	0.767	0.774	0.948
	MEDIAN	0.712	0.777	0.791	0.789	0.762	0.774	0.951
	SDEV	0.181	0.045	0.039	0.043	0.044	0.037	0.013
<b>GM</b>	MIN	0.575	0.660	0.687	0.666	0.660	0.741	0.925
	MAX	0.846	0.871	0.874	0.891	0.889	0.879	0.969
	MEAN	0.699	0.775	0.800	0.794	0.780	0.822	0.947
	MEDIAN	0.731	0.789	0.813	0.806	0.790	0.825	0.951
	SDEV	0.104	0.061	0.041	0.049	0.057	0.031	0.012
<b>MCC</b>	MIN	0.198	0.363	0.440	0.412	0.347	0.436	0.842
	MAX	0.674	0.752	0.753	0.772	0.774	0.820	0.938
	MEAN	0.401	0.544	0.576	0.567	0.549	0.614	0.897
	MEDIAN	0.431	0.541	0.594	0.583	0.575	0.606	0.905
	SDEV	0.174	0.105	0.078	0.087	0.103	0.082	0.025

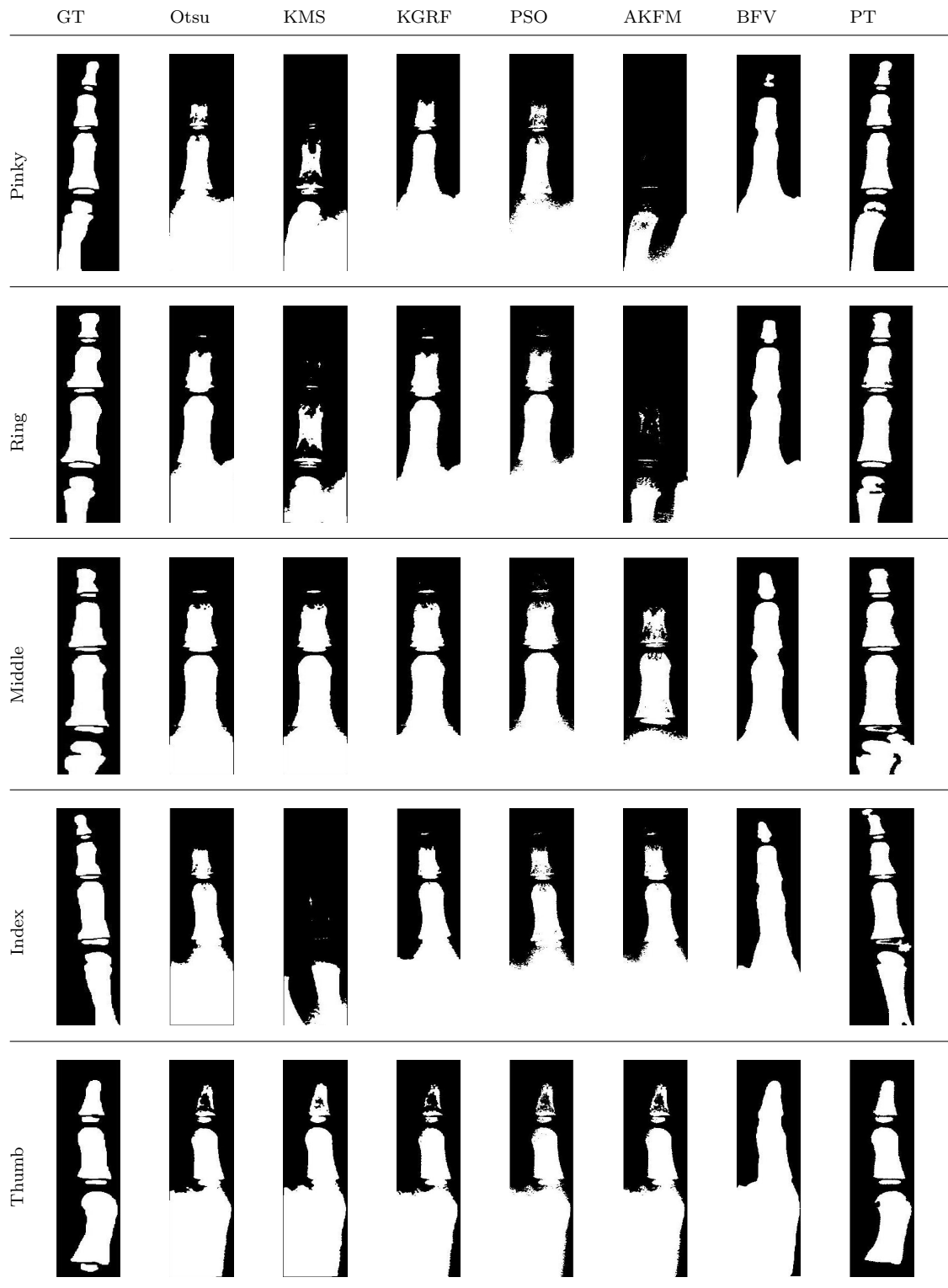




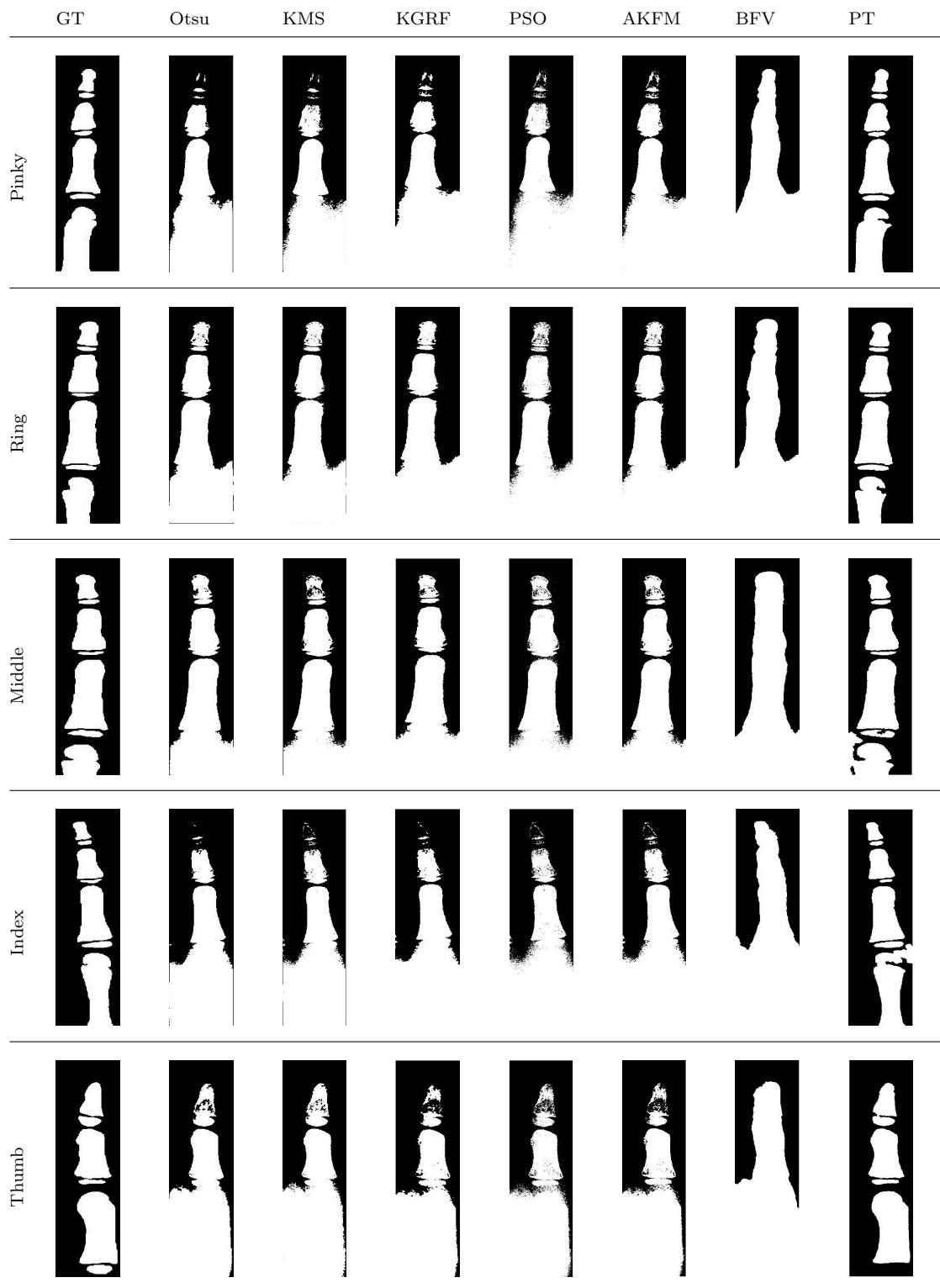
**Figure 4.9:** Segmentation results of different algorithms on hand radiograph taken from 1 year old person [5173.jpg].



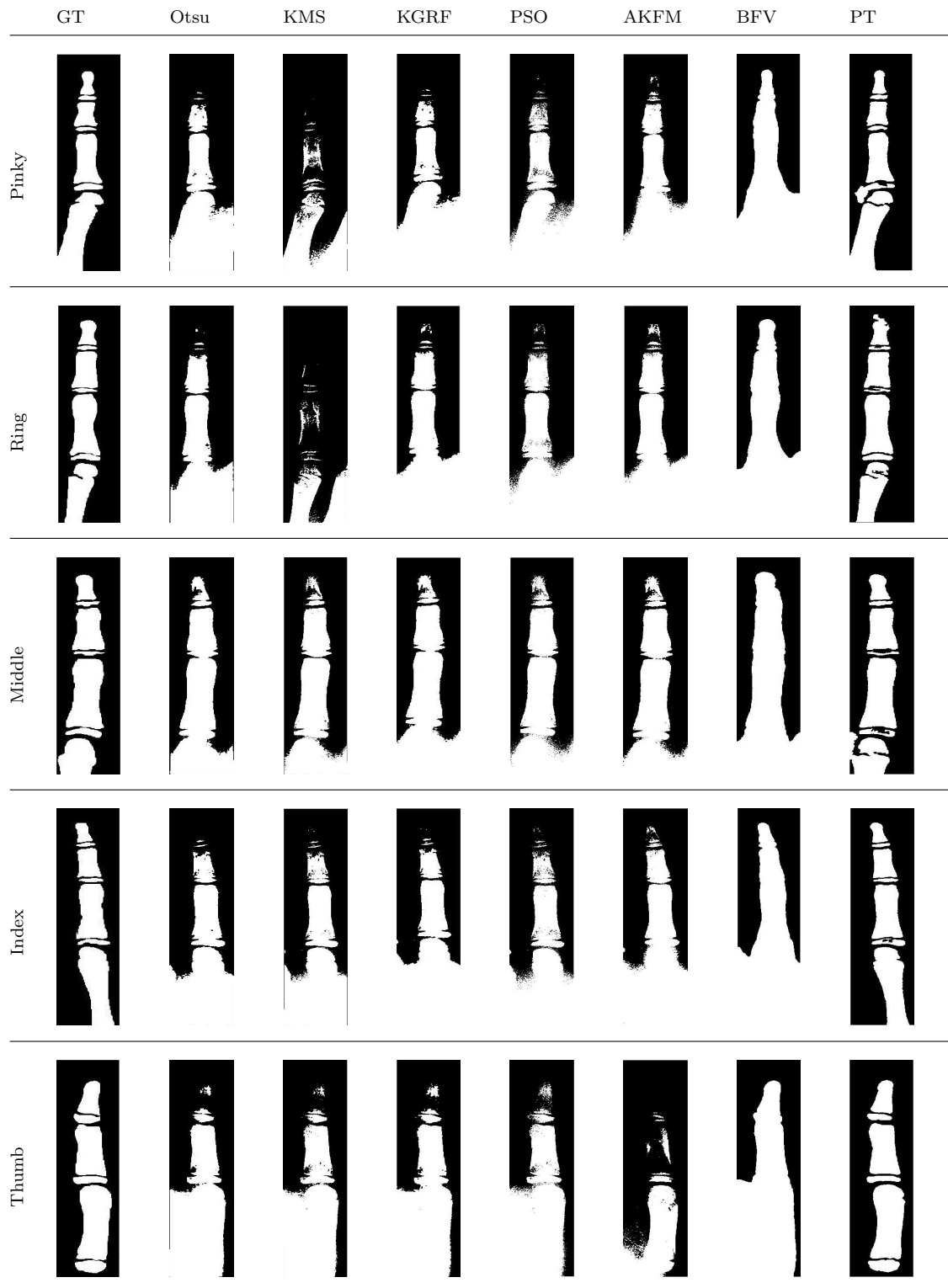
**Figure 4.10:** Segmentation results of different algorithms on hand radiograph taken from 3 year old person [6102.jpg].



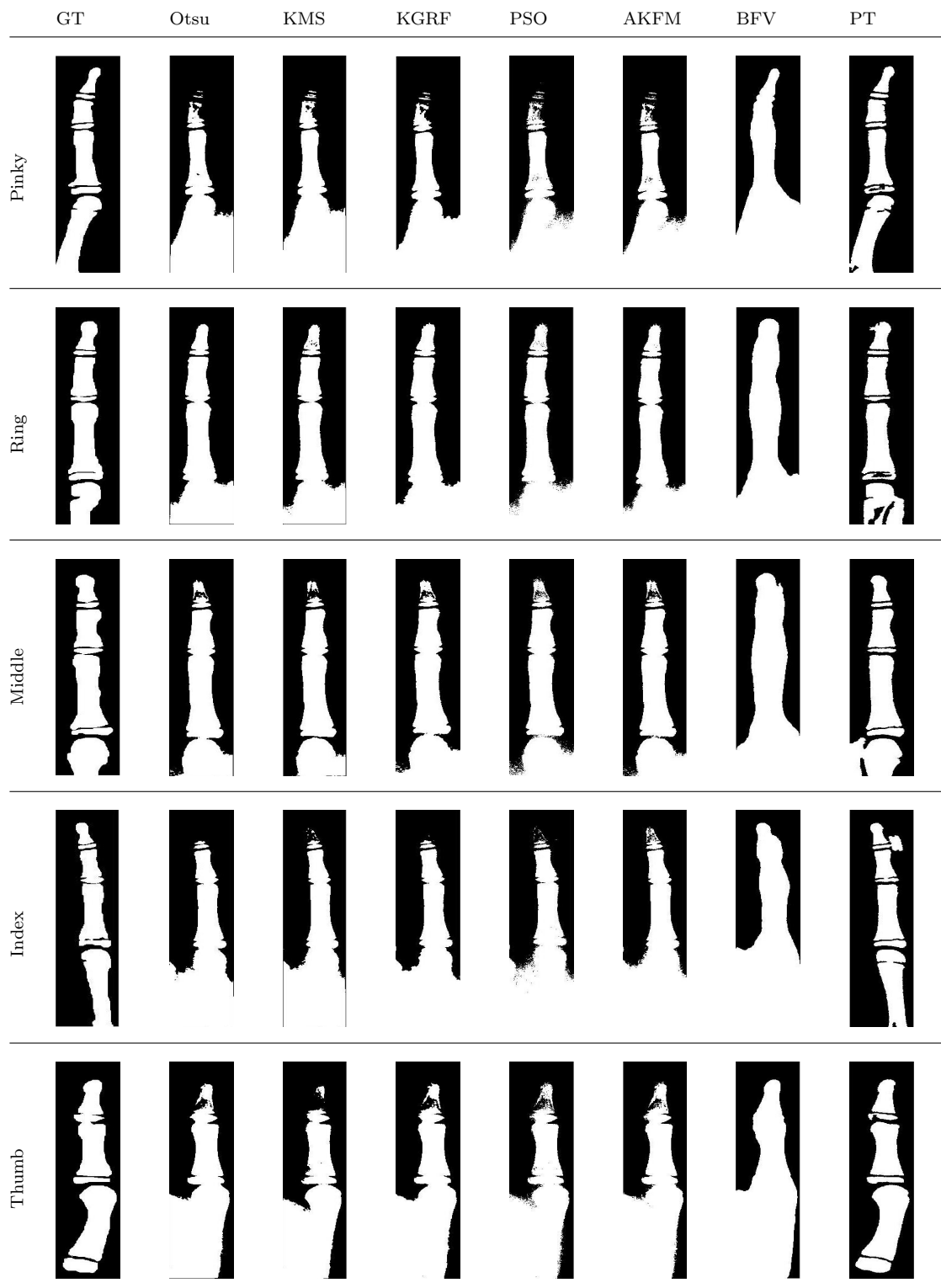
**Figure 4.11:** Segmentation results of different algorithms on hand radiograph taken from 5 year old person [7143.jpg].



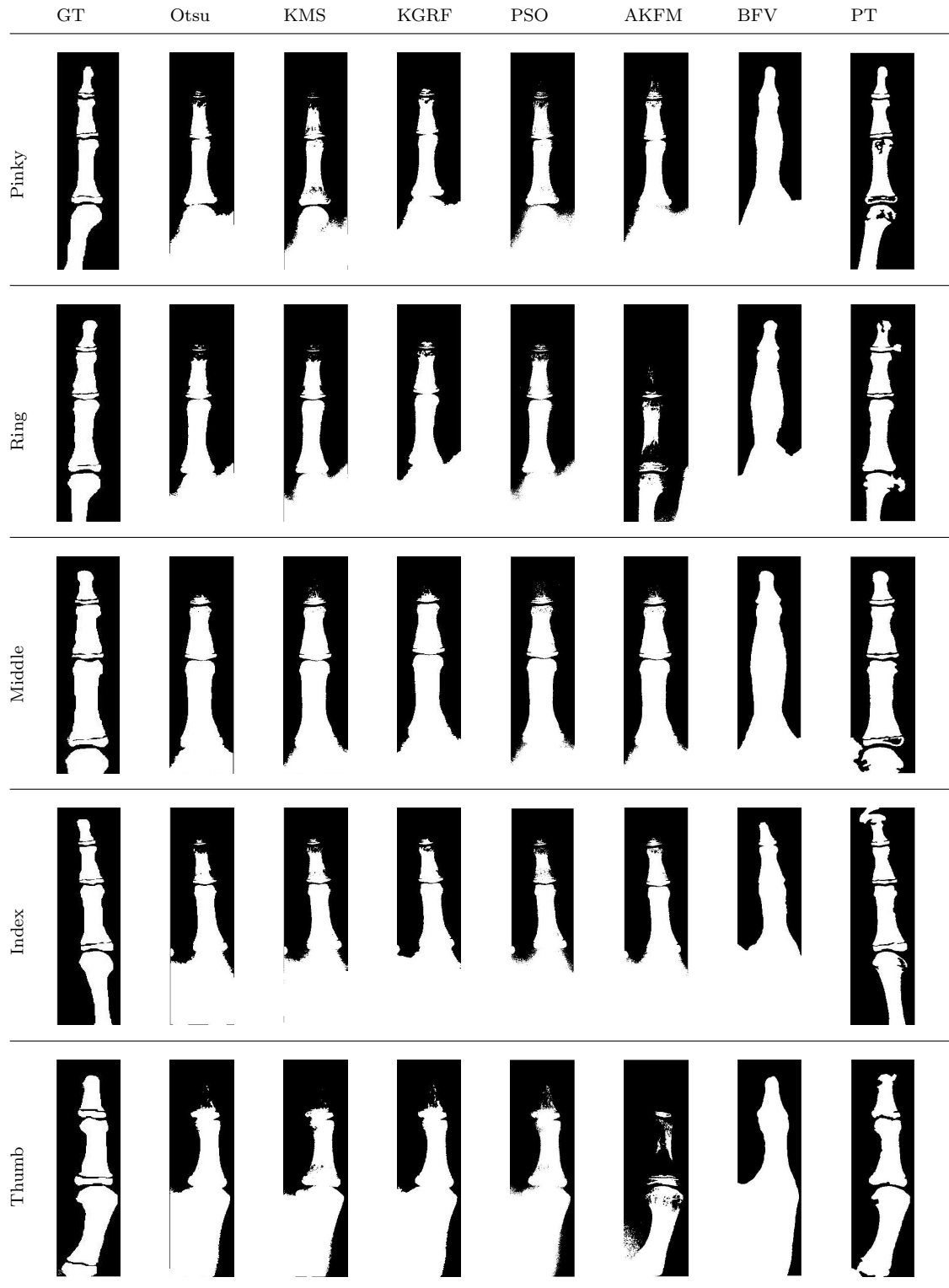
**Figure 4.12:** Segmentation results of different algorithms on hand radiograph taken from 7 year old person [5154.jpg].



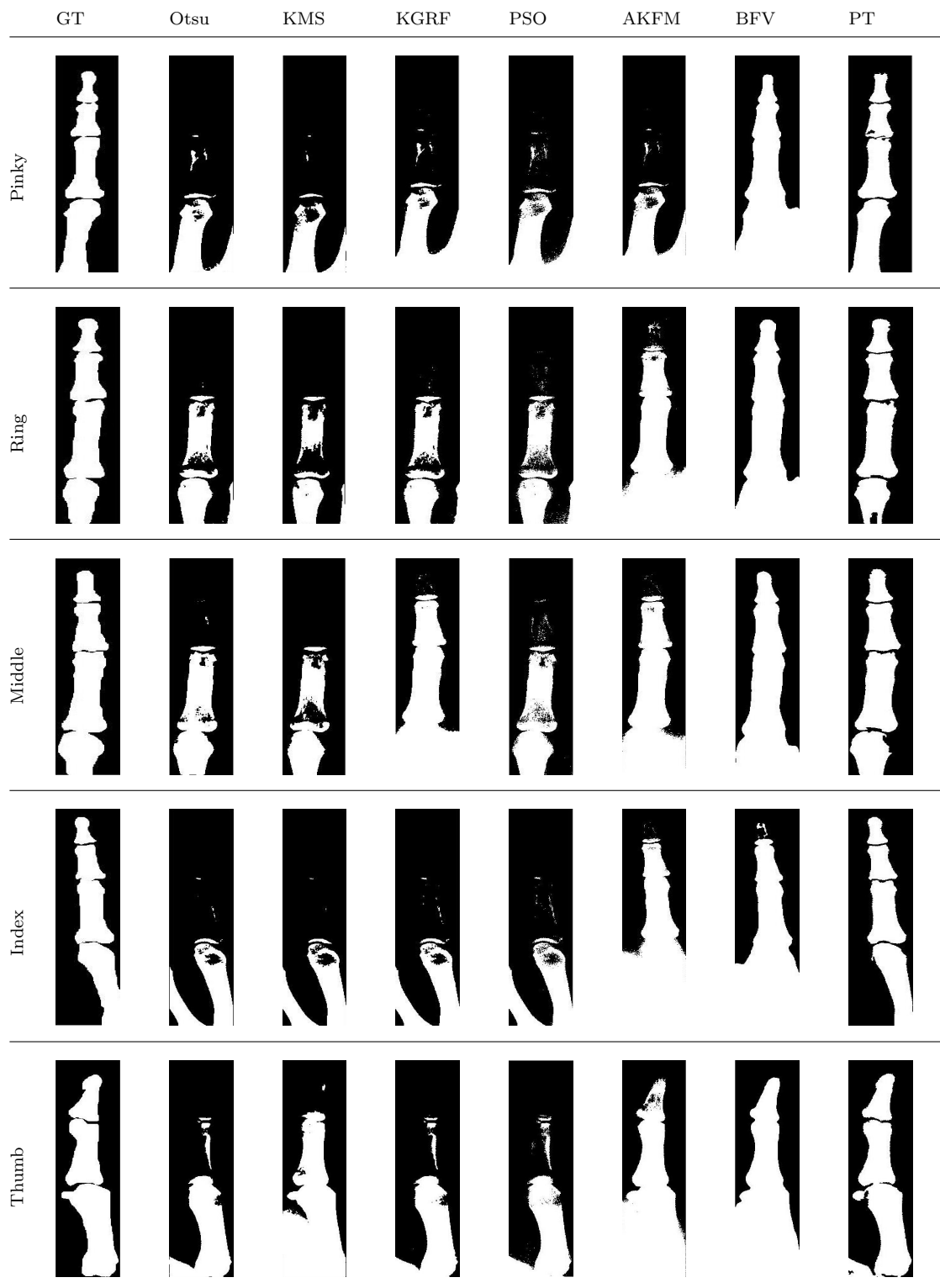
**Figure 4.13:** Segmentation results of different algorithms on hand radiograph taken from 10 year old person [5113.jpg].



**Figure 4.14:** Segmentation results of different algorithms on hand radiograph taken from 12 year old person [5322.jpg].

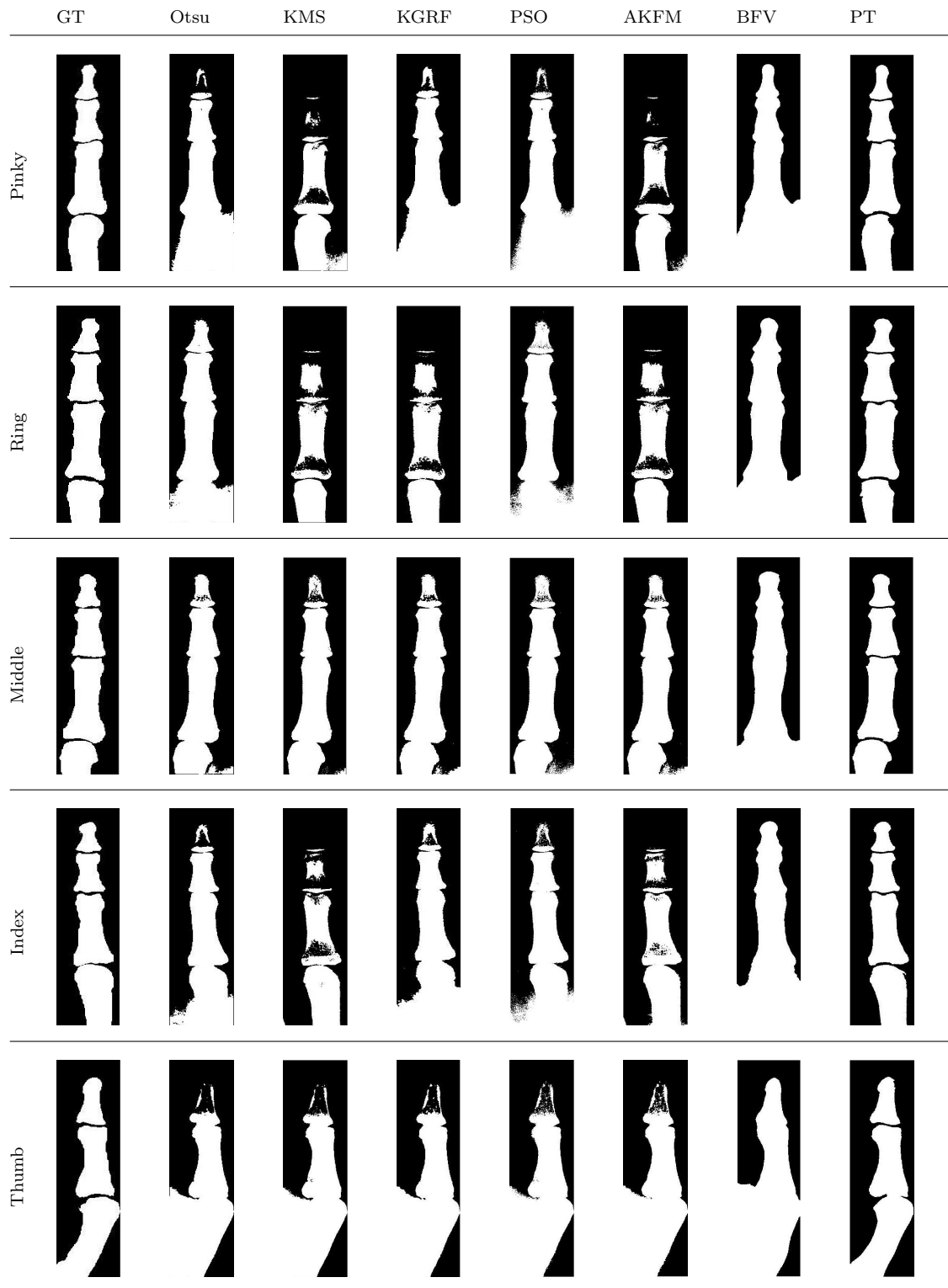


**Figure 4.15:** Segmentation results of different algorithms on hand radiograph taken from 14 year old person [5237.jpg].



**Figure 4.16:** Segmentation results of different algorithms on hand radiograph taken from 16 year old person [5257.jpg].





**Figure 4.17:** Segmentation results of different algorithms on hand radiograph taken from 18 year old person [6145.jpg].

#### 4.7.4 Experimental settings for segmentation of Radius-Ulna

Experimental results of the proposed segmentation technique are evaluated compared with popular and widely used segmentation techniques such as KMS (Hartigan and Wong (1979)), KGRF (Pappas (1992)), PSO based segmentation technique (PSO) (Eberhart and Kennedy (1995)), DPSO based segmentation technique (DPSO) (Tillett *et al.* (2005)), and AKFM technique (Elazab *et al.* (2015)). The first three techniques namely KMS, KGRF and PSO have been used in the field of hand bone segmentation (Pietka *et al.* (2003), Tristán and Arribas (2005), Liu *et al.* (2007)). Hence, the parameter values of state-of-the-art segmentation techniques are set accordingly. Table 4.6 shows the parameters used for these segmentation techniques and their values.

**Table 4.6:** Simulation parameters and their values used for various segmentation techniques of RUROI images

Parameters	KMS	KGRF	PSO	DPSO	AKFM	PT
Number of clusters	3	3	3	3	3	
Number of iterations		30	150	150		100
Clique potential		0.5				
Local filtering					median	gaussian
Local window size					3	3
Population			150	30		
Inertial weight			1.2	1.2		
Weight 1			0.8	0.8		
Weight 2			0.8	0.8		
Min velocity			-5	-1.5		
Max velocity			5	1.5		
Lower bound of position			1	1		
Upper bound of position			256	256		
Stagnancy				10		
Time step						0.1
Heavyside weight						1

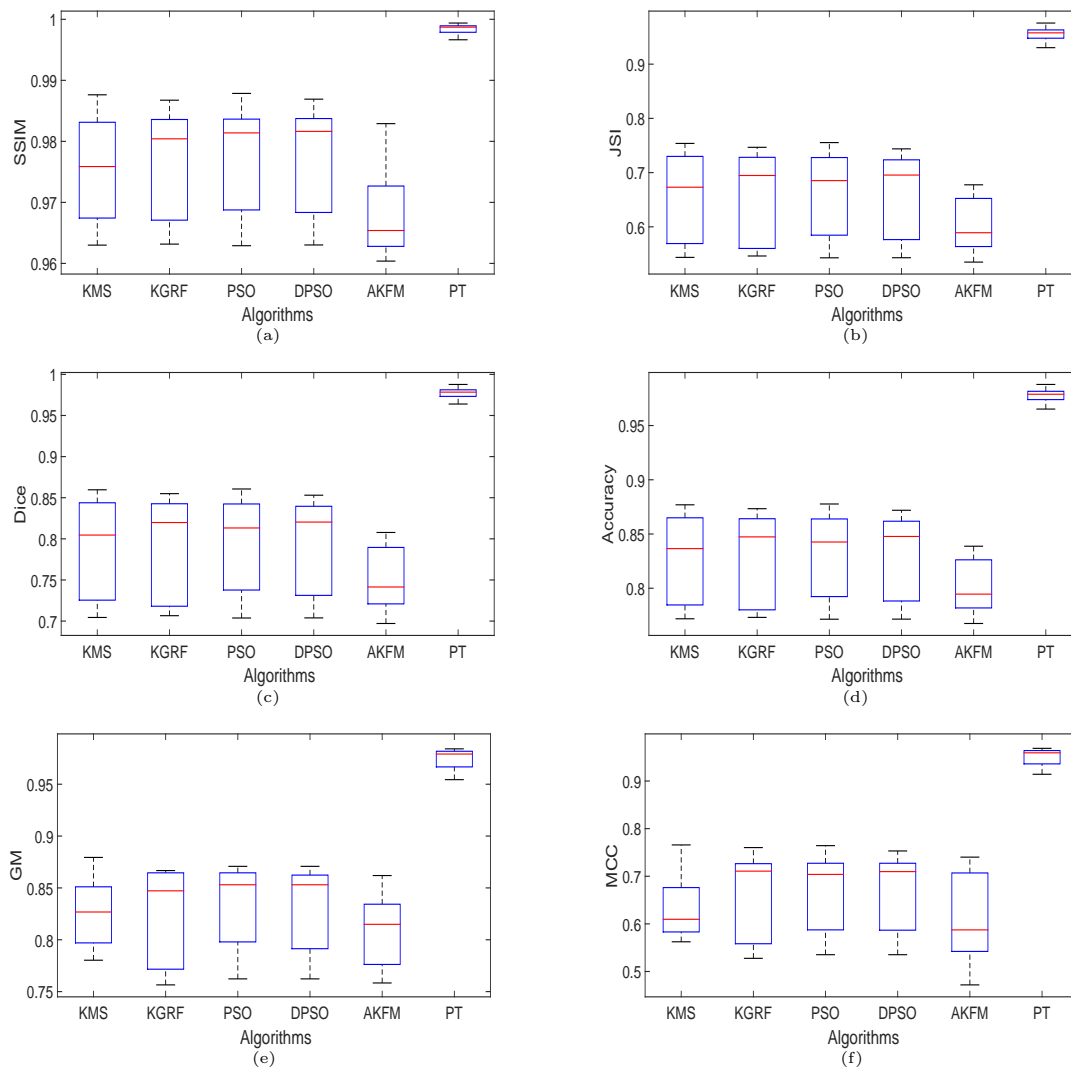
#### 4.7.5 Quantitative and qualitative analysis of radius and ulna segmentation

The quantitative results comparison of different segmentation techniques on extracted RUROI images are presented in Tables 4.4 and 4.7 in terms of different quality metrics.

**Table 4.7:** Performance comparison between different segmentation techniques on RUROI based on various quality metrics

Image	QM	KMS	KGRF	PSO	DPSO	AKFM	PT
<b>1 year</b> [5173.jpg]	SSIM	0.980	0.981	0.981	0.983	0.965	<b>0.999</b>
	JSI	0.688	0.695	0.685	0.695	0.570	<b>0.956</b>
	DICE	0.815	0.820	0.813	0.820	0.726	<b>0.977</b>
	ACC	0.844	0.847	0.843	0.848	0.785	<b>0.978</b>
	GM	0.827	0.865	0.862	0.864	0.782	<b>0.978</b>
MCC	0.610	0.711	0.704	0.710	0.472	<b>0.956</b>	
<b>3 years</b> [6102.jpg]	SSIM	0.986	0.986	0.986	0.987	0.960	<b>0.999</b>
	JSI	0.728	0.745	0.742	0.744	0.570	<b>0.960</b>
	DICE	0.843	0.854	0.852	0.853	0.726	<b>0.980</b>
	ACC	0.864	0.872	0.871	0.872	0.785	<b>0.980</b>
	GM	0.832	0.867	0.871	0.871	0.862	<b>0.984</b>
MCC	0.623	0.743	0.738	0.738	0.740	<b>0.969</b>	
<b>5 years</b> [7143.jpg]	SSIM	0.988	0.987	0.988	0.987	0.983	<b>0.998</b>
	JSI	0.754	0.747	0.755	0.739	0.677	<b>0.950</b>
	DICE	0.860	0.855	0.861	0.850	0.808	<b>0.974</b>
	ACC	0.877	0.873	0.878	0.870	0.839	<b>0.975</b>
	GM	0.879	0.864	0.870	0.860	0.823	<b>0.981</b>
MCC	0.766	0.760	0.764	0.753	0.708	<b>0.963</b>	
<b>7 years</b> [5154.jpg]	SSIM	0.982	0.980	0.982	0.982	0.978	<b>0.999</b>
	JSI	0.735	0.715	0.723	0.715	0.677	<b>0.964</b>
	DICE	0.847	0.834	0.839	0.834	0.808	<b>0.982</b>
	ACC	0.868	0.858	0.861	0.857	0.839	<b>0.982</b>
	GM	0.854	0.847	0.853	0.853	0.835	<b>0.979</b>
MCC	0.681	0.721	0.724	0.724	0.707	<b>0.959</b>	
<b>10 years</b> [7076.jpg]	SSIM	0.976	0.983	0.983	0.983	0.971	<b>0.999</b>
	JSI	0.673	0.723	0.718	0.718	0.644	<b>0.963</b>
	DICE	0.805	0.839	0.836	0.836	0.784	<b>0.981</b>
	ACC	0.837	0.861	0.859	0.859	0.822	<b>0.981</b>
	GM	0.850	0.862	0.863	0.862	0.834	<b>0.980</b>
MCC	0.675	0.719	0.717	0.717	0.684	<b>0.962</b>	
<b>12 years</b> [5322.jpg]	SSIM	0.974	0.969	0.973	0.972	0.970	<b>0.998</b>
	JSI	0.648	0.580	0.620	0.607	0.589	<b>0.942</b>
	DICE	0.786	0.734	0.765	0.756	0.741	<b>0.970</b>
	ACC	0.824	0.790	0.810	0.804	0.795	<b>0.971</b>
	GM	0.780	0.775	0.802	0.794	0.791	<b>0.969</b>
MCC	0.571	0.562	0.606	0.592	0.587	<b>0.941</b>	
<b>14 years</b> [5237.jpg]	SSIM	0.968	0.968	0.970	0.970	0.963	<b>0.997</b>
	JSI	0.568	0.563	0.594	0.585	0.616	<b>0.930</b>
	DICE	0.724	0.721	0.745	0.738	0.762	<b>0.964</b>
	ACC	0.784	0.782	0.797	0.793	0.808	<b>0.965</b>
	GM	0.802	0.761	0.784	0.784	0.759	<b>0.954</b>
MCC	0.603	0.547	0.577	0.577	0.546	<b>0.914</b>	
<b>16 years</b> [5257.jpg]	SSIM	0.964	0.963	0.964	0.964	0.963	<b>0.998</b>
	JSI	0.570	0.550	0.557	0.551	0.535	<b>0.958</b>
	DICE	0.726	0.710	0.716	0.710	0.697	<b>0.978</b>
	ACC	0.785	0.775	0.779	0.775	0.767	<b>0.979</b>
	GM	0.781	0.756	0.762	0.762	0.758	<b>0.959</b>
MCC	0.562	0.528	0.535	0.535	0.530	<b>0.922</b>	
<b>18 years</b> [6145.jpg]	SSIM	0.963	0.965	0.963	0.963	0.964	<b>0.999</b>
	JSI	0.544	0.546	0.543	0.543	0.546	<b>0.976</b>
	DICE	0.704	0.707	0.704	0.704	0.706	<b>0.988</b>
	ACC	0.772	0.773	0.771	0.772	0.773	<b>0.988</b>
	GM	0.815	0.811	0.817	0.817	0.815	<b>0.983</b>
MCC	0.587	0.581	0.591	0.590	0.587	<b>0.966</b>	

Box-plot has been used to compare all the segmentation techniques with respect to various quality metrics and has been shown in Figure 4.18, wherein the sample size is 9 (number of images). The statistical values such as minimum (MIN), maximum (MAX), mean, median and standard deviation (SDEV) of various quality metrics against segmentation techniques are presented in Table 4.8.



**Figure 4.18:** Boxplots of segmentation techniques against various quality metrics for segmented RUROI images.

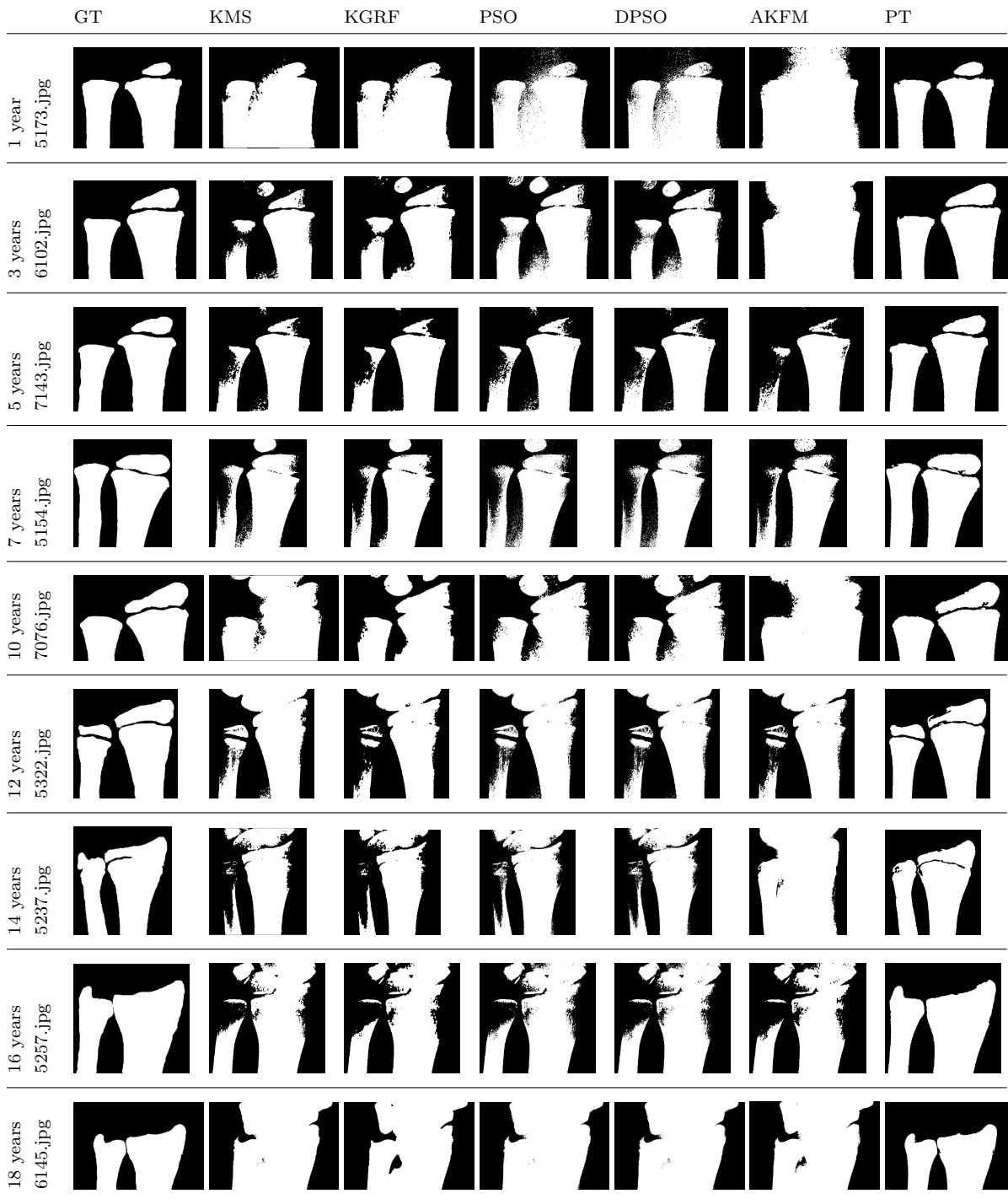
**Table 4.8:** Statistical values of various quality metrics against segmentation techniques

QM	Statistic	KMS	KGRF	PSO	DPSO	AKFM	PT
SSIM	MIN	0.963	0.963	0.963	0.963	0.960	0.997
	MAX	0.988	0.987	0.988	0.987	0.983	0.999
	MEAN	0.976	0.976	0.977	0.977	0.969	0.998
	MEDIAN	0.976	0.980	0.981	0.982	0.965	0.999
	SDEV	0.009	0.009	0.009	0.009	0.007	0.001
JSI	MIN	0.544	0.546	0.543	0.543	0.535	0.930
	MAX	0.754	0.747	0.755	0.744	0.677	0.976
	MEAN	0.656	0.652	0.660	0.655	0.603	0.955
	MEDIAN	0.673	0.695	0.685	0.695	0.589	0.958
	SDEV	0.075	0.084	0.078	0.078	0.051	0.012
DICE	MIN	0.704	0.707	0.704	0.704	0.697	0.964
	MAX	0.860	0.855	0.861	0.853	0.808	0.988
	MEAN	0.790	0.786	0.792	0.789	0.751	0.977
	MEDIAN	0.805	0.820	0.813	0.820	0.741	0.978
	SDEV	0.055	0.062	0.057	0.058	0.039	0.007
ACC	MIN	0.772	0.773	0.771	0.772	0.767	0.965
	MAX	0.877	0.873	0.878	0.872	0.839	0.988
	MEAN	0.828	0.826	0.830	0.828	0.801	0.978
	MEDIAN	0.837	0.847	0.843	0.848	0.795	0.979
	SDEV	0.037	0.042	0.039	0.039	0.025	0.006
GM	MIN	0.780	0.756	0.762	0.762	0.758	0.954
	MAX	0.879	0.867	0.871	0.871	0.862	0.984
	MEAN	0.825	0.823	0.832	0.830	0.807	0.974
	MEDIAN	0.827	0.847	0.853	0.853	0.815	0.979
	SDEV	0.032	0.045	0.039	0.039	0.034	0.010
MCC	MIN	0.562	0.528	0.535	0.535	0.472	0.914
	MAX	0.766	0.760	0.764	0.753	0.740	0.969
	MEAN	0.631	0.652	0.662	0.659	0.618	0.950
	MEDIAN	0.610	0.711	0.704	0.710	0.587	0.959
	SDEV	0.062	0.090	0.079	0.079	0.089	0.019

The qualitative results of proposed segmentation technique (PT) for RUROI images and other state-of-the-art segmentation techniques are given in Figure 4.19 for ages 0-18 years old respectively.

#### 4.7.6 Segmentation accuracy and its validation

The quality metrics like SSIM, JSI, Dice, and Accuracy are used for quantitative results comparison of proposed segmentation techniques and other state-of-the-art segmentation techniques. The experimental results of proposed segmentation techniques for PROI and RUROI images are validated by different medical experts from Goa Medical College, Goa, India. The ratings are given between values 1-5 with value 1 being very poor, 2 for a poor result, 3 for average, 4 for good result and 5 for an excellent result achieved. These ratings are given in Table 4.9 for segmented PROI images and Table 4.10 is for segmented RUROI images. These ratings used for de-



**Figure 4.19:** Segmentation results of different techniques on RUROI of different ages.

noting segmentation accuracy of the proposed technique are given after assessment by same medical experts who created the ground truth images for hand radiographs.

**Table 4.9:** Ratings given by medical experts to the PROI segmentation results of proposed technique.

Age (years)	Finger	Expert-1	Expert-2	Expert-3	Expert-4	Average Rating	Overall Average
<b>01</b>	Pinky	5	5	5	5	5	<b>4.4</b>
	Ring	5	5	5	5	5	
	Middle	3	4	3	4	3.5	
	Index	3	4	4	3	3.5	
	Thumb	5	5	5	5	5	
<b>03</b>	Pinky	3	3	4	3	3.25	<b>4.4</b>
	Ring	4	3	4	4	3.75	
	Middle	5	5	5	5	5	
	Index	5	5	5	5	5	
	Thumb	5	5	5	5	5	
<b>05</b>	Pinky	4	4	4	4	4	<b>3.3</b>
	Ring	4	4	4	4	4	
	Middle	3	3	3	3	3	
	Index	2	3	3	3	2.75	
	Thumb	2	3	3	3	2.75	
<b>07</b>	Pinky	5	5	5	5	5	<b>4.45</b>
	Ring	4	5	5	5	4.75	
	Middle	5	3	4	4	4	
	Index	4	3	4	3	3.5	
	Thumb	5	5	5	5	5	
<b>10</b>	Pinky	5	2	4	3	3.5	<b>4.25</b>
	Ring	4	4	4	4	4	
	Middle	4	4	4	5	4.25	
	Index	5	4	5	4	4.5	
	Thumb	5	5	5	5	5	
<b>12</b>	Pinky	3	4	4	3	3.5	<b>3.6</b>
	Ring	3	3	3	4	3.25	
	Middle	3	4	4	3	3.5	
	Index	3	3	3	4	3.25	
	Thumb	4	4	5	5	4.5	
<b>14</b>	Pinky	3	3	4	3	3.25	<b>3.85</b>
	Ring	2	3	4	4	3.25	
	Middle	5	4	5	4	4.5	
	Index	4	4	5	4	4.25	
	Thumb	2	4	5	5	4	
<b>16</b>	Pinky	4	4	4	4	4	<b>4.45</b>
	Ring	4	4	5	5	4.5	
	Middle	4	4	4	4	4	
	Index	5	5	5	5	5	
	Thumb	5	4	5	5	4.75	
<b>18</b>	Pinky	5	5	5	5	5	<b>5</b>
	Ring	5	5	5	5	5	
	Middle	5	5	5	5	5	
	Index	5	5	5	5	5	
	Thumb	5	5	5	5	5	

**Table 4.10:** Ratings given by medical experts to the RUROI segmentation results of proposed technique.

Age (years)	Expert-1	Expert-2	Expert-3	Expert-4	Overall Average
1	4	5	5	5	4.75
3	5	5	5	5	5
5	5	5	5	5	5
7	5	5	5	4	4.75
10	3	4	4	5	4
12	3	3	4	4	3.5
14	2	4	3	3	3
16	5	5	5	5	5
18	3	5	4	5	4.25

## 4.8 Discussion

From the sub-sections 4.7.3 and 4.7.5, it is clear that SSIM, JSI, Dice, Accuracy, GM, and MCC provide indispensable information regarding the precision of segmented output from various segmentation techniques which are used for comparison. The boxplots in Figure 4.8 clarify that proposed segmentation technique for phalanges is far better as compared to other existing segmentation techniques. It achieves the highest segmentation accuracy which is well above 0.9. Other quality metrics also present that proposed segmentation technique (PT) performs far better than other existing segmentation techniques with values above 0.95. Figures 4.9 to 4.17 along with the segmentation results in Table 4.4 present the best results of phalangeal segmentation by proposed technique (PT). Table 4.5 indicates, the performance of PT for PROI is spotless with very less variation in mean and standard deviation.

Similarly, the box-plot shown in Figure 4.18, indicates that the proposed segmentation technique (PT) for RUROI has very less variation as compared with other existing segmentation techniques. It also achieves a higher segmentation accuracy among all the techniques compared, with respect to all quality metric values. SSIM values of all techniques are above 0.95 but proposed technique has a value of almost 1 as shown in Figure 4.18(a). The boxplot of JSI shows that k-means, KGRF, PSO, and DPSO have similar ranges shown in Figure 4.18(b), and also the proposed technique takes the value around 0.9. Similarly in other boxplots, i.e. Figures 4.18(c), 4.18(d),



4.18(e) and 4.18(f), PT has higher values ( $\sim 0.95$ ) for quality metrics like Dice, ACC, GM and MCC respectively. Figure 4.19 along with the segmentation results in Table 4.7 clearly show that the proposed technique gives best results among all other state-of-the-art techniques. The mean and standard deviation statistics of various quality metrics tabulated in Table 4.8 indicates that the performance of PT for RUROI is best among compared segmentation techniques.

The ratings given by medical experts which are presented in the Tables 4.9 and 4.10 are high, with all of them being above average values. The values allocated in Table 4.9 to hand radiographs of 5-year-old person and 12-year-old person in phalangeal segmentation are slightly less as the radiographs have high-intensity inhomogeneity. Similarly in Table 4.10 hand radiographs of 12-year-old person and 14-year-old person have less rated values. But the ratings further strengthen the claim that proposed segmentation technique provides very good segmentation results for bones of both PROI and RUROI.

The advantages of the proposed segmentation technique are: (1) It is very effective and robust as it tackles intensity inhomogeneity problem in hand radiographs, (2) It clearly delineates phalanges from hand radiographs of different ages which make it easier for further assessment, (3) It successfully removes all spurious regions and achieves a higher segmentation accuracy. The disadvantages of proposed segmentation techniques are that it is slightly complex than other existing segmentation techniques.

## 4.9 Summary

- The segmentation of phalanges and radius-ulna bones have been fully automatized while achieving a very high accuracy.
- Quantitative and qualitative results of proposed segmentation techniques for PROI and RUROI were compared with other state-of-the-art segmentation techniques with the help of various quality metrics.
- The segmentation accuracy for phalangeal bones is around 94% and for radius-ulna bones is 97%.
- Quality metrics revealed that proposed segmentation techniques (PT) have performed far better than other state-of-the-art segmentation techniques.
- Ground truth images were created with the help of medical experts and the results of proposed segmentation techniques were also rated by them.
- The ratings given by medical experts were above the average value (3), which proved that the proposed segmentation techniques have achieved high accuracy.

# Chapter 5

## FEATURE EXTRACTION AND CLASSIFICATION

### 5.1 Introduction

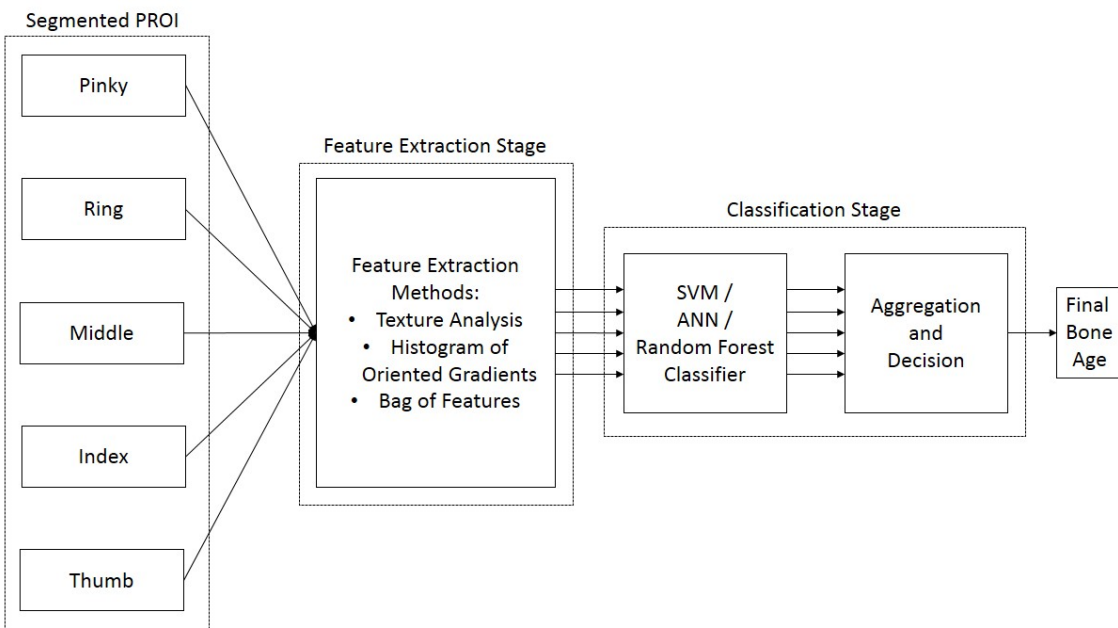
This chapter presents the implementation of final two blocks of ABAA system, which are Feature Extraction and Classification stages. The segmentation results of phalanges are reported earlier in chapter 4. Segmented PROI images are used further to predict the age of a person using robust features extraction methods and suitable classification techniques. Robust and efficient feature extraction methods along with conducive classification techniques are explored in this chapter.

In the field of image processing and machine learning, feature extraction plays a very important role in helping to identify the object or a scene. Application of feature extraction also includes identifying cancer in human body from medical images. The process starts from an initial set of measured data and derives prominent and distinct features which are intended to be informative and non-redundant. This further promotes subsequent learning and in some cases leads to a better human interpretation of the data. Feature extraction can also be viewed as a dimensionality reduction process because it involves reducing the number of resources which are required to describe a large set of data. The complexity of a problem depends on the number of variables involved, and with a large number of variables, requires a large amount of memory and computation power. Hence, feature extraction is a general term for various methods wherein the variables are used to solve these problems, while still being able to

describe the data with sufficient accuracy.

Classification is one of the main topics in machine learning which involves teaching machines how to group together data based on a particular criteria. This can be divided into two types which are supervised and unsupervised learning. When machines group data together based on some predetermined characteristics, it is called as supervised learning. In unsupervised learning/clustering, machines try to find shared characteristics with the help of which the data can be grouped together when categories are not specified.

The block diagram of feature extraction and classification stage of ABAA system is shown in the Figure 5.1. In the feature extraction stages, various feature extraction methods like texture feature analysis, Histogram of Oriented Gradients (HOG) and Bag of Features (BoF) are applied on segmented PROI images. In the classification stage, various classification techniques like Artificial Neural Networks (ANN), Support Vector Machines (SVM) and Random Forest classifier are used for BAA from extracted features.



**Figure 5.1:** Block diagram of Feature extraction and Classification stages of ABAA system.

## 5.2 Feature extraction methods

In this section, different feature extraction methods such as texture feature analysis, HOG, and BoF are presented in brief.

### 5.2.1 Texture feature analysis

Bone texture provides useful information for classification and prediction of bone age. A total of 61 different texture features are extracted as explored by Loizou *et al.* (2014) and they are listed below.

1. Statistical Features (SF): Mean, Median, Variance, Skewness and Kurtosis.
2. Spatial Gray Level Dependence Matrices (SGLDM): Angular second moment (ASM), Contrast, Correlation, Sum of squares variance (SOSV), Inverse difference moment (IDM), Sum average (SA), Sum variance (SV), Sum entropy (SE), Entropy, Difference variance (DV), Difference entropy (DE), and Information measures of correlation.
3. Gray level difference statistics (GLDS): Homogeneity, contrast, energy, entropy, and mean.
4. Neighborhood gray tone difference matrix (NGTDM): Coarseness, contrast, busyness, complexity, and strength.
5. Statistical feature matrix (SFM): Coarseness, contrast, periodicity, and roughness.
6. Laws texture energy measures (LTEM): using four vectors representing texture features to create sixteen 2D masks from the outer products of the pairs of vectors called as texture kernels or energy maps.
7. Fractal dimension texture analysis (FDTA): The Hurst coefficients for dimensions 4, 3 and 2.
8. Fourier Power Spectrum (FPS): Radial sum and angular sum.

### 5.2.2 Histogram of oriented gradients

In the field of computer vision and image processing, a histogram of oriented gradients (HOG) is one of the widely used feature descriptor which is usually employed

for object detection and recognition (Dalal and Triggs (2005)). A feature descriptor is a portrayal of an image or an image patch that simplifies the image by extracting useful information. The histograms of directions of oriented gradients are actually the features in the HOG feature descriptor. The importance of using gradients is that the magnitude of gradients is large around edges and corners, hence it is used as a feature.

Steps for HOG feature calculation as explored by Dalal and Triggs (2005) are listed below:

**1. Computation of gradient values.**

Use 1-D centered discrete derivative mask in both vertical and horizontal directions as is given in equation (5.1).

$$\nabla I = \begin{bmatrix} g_x \\ g_y \end{bmatrix} = \begin{bmatrix} \frac{\delta I}{\delta x} \\ \frac{\delta I}{\delta y} \end{bmatrix} \quad (5.1)$$

where  $\frac{\delta I}{\delta x}$  is the derivative in  $x$  direction and  $\frac{\delta I}{\delta y}$  is the derivative in  $y$  direction.

**2. Creating the cell histograms.**

The image is divided into cells which can be rectangular or radial. Each pixel within the cell affects histogram channel depending on the gradient values.

**3. Normalization.**

The gradient values are locally normalized to take in an account for any changes in illumination and contrast. For this purpose, group the cells together into larger blocks. Normalization is carried out by using the equation (5.2).

$$\nu = \frac{v}{\sqrt{\|v\|_2^2 + \epsilon^2}} \quad (5.2)$$

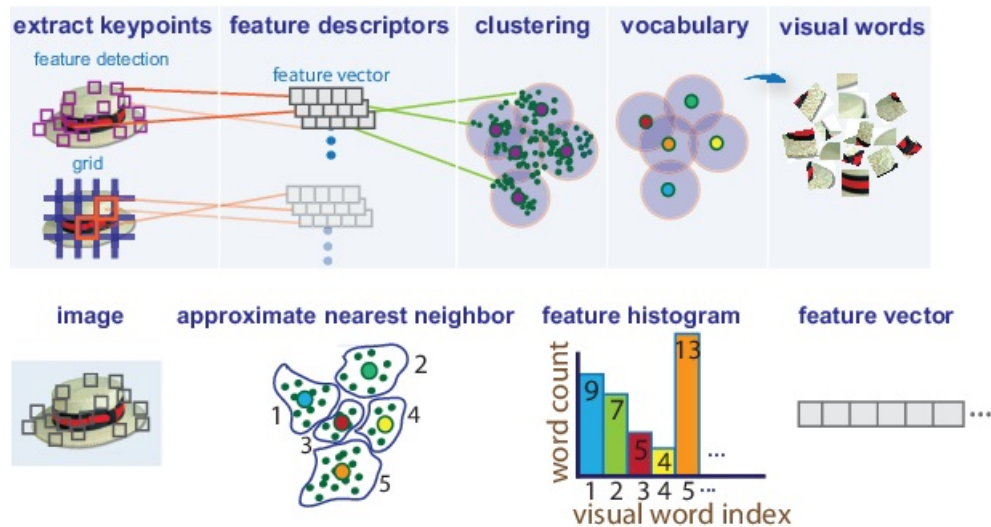
where  $v$  is the unnormalised descriptor vector of the block and  $\epsilon$  is a constant.

**4. Concatenation.**

Normalized cell histograms are then concatenated from all of the block regions to give the final HOG descriptor. The blocks usually overlap, so that each cell contributes to final descriptor more than once.

### 5.2.3 Bag of features

In computer vision domain, the bag-of-words model (BoW) is applied to image classification, by treating image features as words, hence the name Bag-of-Features (BoF) (Csurka *et al.* (2004)). For image classification, computer vision toolbox is used and classification is performed by creating a bag of visual words or BoF. The process generates a histogram of visual word occurrences that represent an image. These histograms are used to train an image classifier. The bag of words is treated as a bag of features because it basically contains image features. The steps to obtain BoF are as follows and also presented in Figure 5.2 (Image courtesy: www.mathworks.com).



**Figure 5.2:** Overview of Bag of Features method

1. Create a bag of features, by extracting feature descriptors from images of each class.
2. The BoF function derives the features by using the k-means clustering algorithm on the feature descriptors extracted from training set images. The algorithm iteratively groups the descriptors into  $k$  mutually exclusive clusters. Each cluster center represents a feature.
3. Then, encode method is used to encode each image from the training set. It uses the approximate nearest neighbor algorithm to construct a feature histogram for each image.

4. The function then increments histogram bins based on the proximity of the descriptor to a particular cluster center. The histogram length corresponds to the number of visual words. The histogram then becomes a feature vector for the image.

The actual implementation steps of BoF function in matlab are divided into following steps:

1. **Extracts SURF features from all images.**

Speeded Up Robust Features (SURF) uses box filters as an approximation of Laplacian of Gaussian (LoG) (Bay *et al.* (2006)). For implementation, box filters are used because convolution is easy and can be calculated using integral images. Also, this step is performed parallelly for different scales. The equations for LoG and integral images are given in equation (5.3) and (5.4) respectively.

$$L(x, y) = \frac{\delta^2}{\delta x^2} O(x, y) + \frac{\delta^2}{\delta y^2} O(x, y) \quad (5.3)$$

$$S(x, y) = \sum_{i=0}^x \sum_{j=0}^y I(i, j) \quad (5.4)$$

SURF depends on determinant of Hessian matrix for calculating both scale and location. The determinant of a Hessian matrix gives information about the change around that point. The points are then selected in such a way that determinant is maximal at that location (Bay *et al.* (2006)). Given a point  $p = (x, y)$  in an image  $I$ , the Hessian matrix  $\tilde{H}(p, \sigma)$  at point  $p$  and scale  $\sigma$ , is given in equation (5.5).

$$\tilde{H}(p, \sigma) = \begin{bmatrix} L_{xx}(p, \sigma) & L_{xy}(p, \sigma) \\ L_{yx}(p, \sigma) & L_{yy}(p, \sigma) \end{bmatrix} \quad (5.5)$$

2. **Construction of visual vocabulary using k-means clustering.**

The number of features can be reduced using k-means clustering algorithm (Gonzalez *et al.* (2004)). The algorithm aims at minimizing an objective function



which is known as squared error function and is given in equation (5.6).

$$J(V) = \sum_{i=1}^c \sum_{j=1}^{c_i} (\|x_i - v_j\|)^2 \quad (5.6)$$

where  $\|x_i - v_j\|^2$  is the Euclidean distance between pixel  $x_i$  and centre  $v_j$ .

### 3. Use encode method.

Encoding of images is done to produce a histogram of visual word occurrences that becomes a new and reduced representation of an image. This histogram now is the basis for training any classifier for image classification. Basically, it encodes an image into a feature vector (Csurka *et al.* (2004)).

## 5.3 Classification techniques

In this section, different classification techniques such as ANN, SVM and random forest classifiers are presented and discussed.

### 5.3.1 Artificial Neural Networks

Artificial Neural Networks (ANN) are biologically inspired network of artificial neurons with a particular activation function to perform specific tasks (Haykin (1998)). The network is made up of a collection of nodes called artificial neurons and each connection between artificial neurons can transmit a signal from one to another. This system mimics the natural brain of a human. The artificial neuron receives an input signal and process it to give an output signal based on the activation function or threshold value. Most commonly, artificial neurons are organized in different layers, input layer, hidden layers and output layer. Different layers may perform different kinds of operations on their inputs based on the activation functions and also the weights attached to it. ANNs have been used to solve many real-life problems in the areas such as computer vision, face and voice recognition, and medical diagnosis.

### 5.3.2 Support Vector Machines

Support Vector Machine (SVM) is one of the most powerful and widely used classifiers in signal and image processing field. It is applied on a given set of training data which

generates a model and then used to classify any new data (Cortes and Vapnik (1995)). Usually a kernel function is used to map any input data to feature space, such that a hyperplane is found that can divide the data into sets or classes. Kernel function can be linear, polynomial, sigmoid, radial basis etc. Most commonly used kernel function is the Radial Basis Function (RBF).

### 5.3.3 Random Forest Classifier

Random Forest Classifier is an ensemble algorithm. Ensemble algorithms combine more than one algorithms of a same or different kind of classification of objects, (Breiman (2001)). Random forest classifier creates a set of decision trees from a randomly selected subset of a training set. It then aggregates the votes from different decision trees to decide the final class of the test object. Decision tree concept is more like the rule-based system. Given the training dataset with targets and features, the decision tree algorithm will come up with some set of rules. The same set of rules can be used to perform prediction on the test dataset. The steps for building a random forest classifier are mentioned below and is shown in Figure 5.3 (Image courtesy: www.youtube.com).

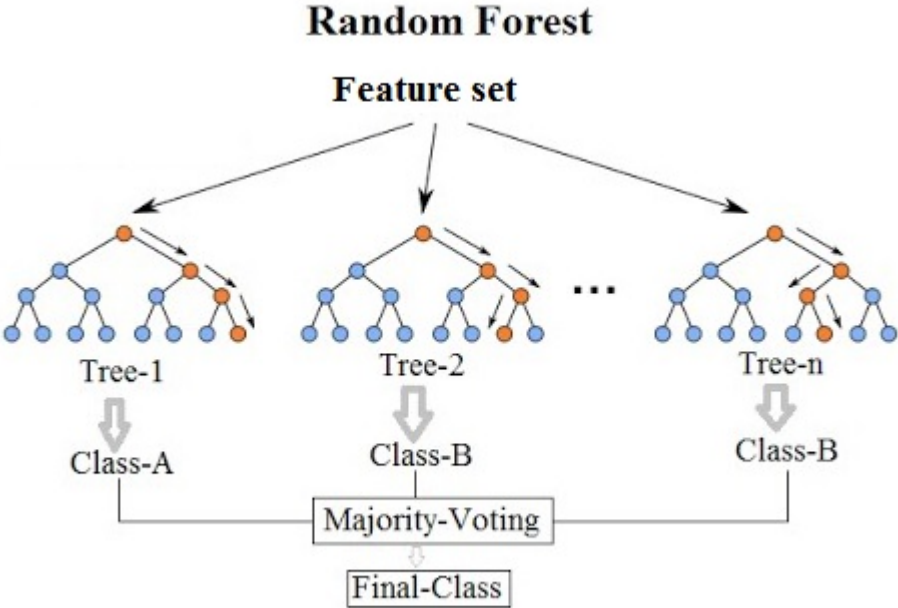


Figure 5.3: Steps for building a Random Forest Classifier

1. Select  $k$  features out of  $m$  features randomly, where  $k \ll m$ .
2. Calculate the node  $d$  using the best split point from the  $k$  features.
3. Using best split point, divide the node into daughter nodes.
4. Repeat the steps 1 to 3 until only one node remains.
5. Repeat the steps 1 to 4 for  $n$  number times to create a forest of  $n$  number of trees.

## 5.4 Implementation

The feature extraction and classification techniques are implemented on a 64-bit system having an Intel i7 processor with clock speed of 3.6 GHz and an 8 GB RAM. The implementation of feature extraction methods is simple and straightforward. Texture based feature analysis is based on the research work by Loizou *et al.* (2014). HOG feature descriptor with  $64 \times 64$  as cell size is used for implementation. BoF using SURF descriptor is implemented with varying vocabulary size for analysis and finally fixed to 500.

Implementation of SVM is done using LIBSVM library version 3.22 (Chang and Lin (2011)). In this case, a multiclass SVM function is used for classification using one-versus-rest approach. The kernel function used is third-degree polynomial rather than radial basis function as it is not suitable for a large number of features (Kashif *et al.* (2016)). ANN is designed with 2 hidden layers and the learning constant is set to 0.1. The activation function used is *tanh* with a maximum number of iterations set to 100. Random Forest classifier is designed using *treebagger* function from MATLAB 2015a software. For implementation, number of trees is set to 200 and minimum leaf size to 5.

## 5.5 Experimental results and discussion

This section presents the experiments performed on segmented regions (PROI) with and without gender specification. Lower error rates are achieved on subsets of regions. Using iterative adding and removal of regions, the best combinations can be chosen.

### 5.5.1 Results

In this section, the experiments are performed on segmented PROI images (Simu *et al.* (2017a)). To compare the results with preceding work presented in Thodberg *et al.* (2009) and Kashif *et al.* (2016), a separate dataset of 2-17 years is created. Each hand radiograph will give 5 PROI regions. Some segmented PROI images are rejected due to bad results. Finally, we have used a total of 3082 PROI images for feature extraction out of which 1396 male segmented PROI images and 1686 female segmented PROI images. The images were resized to a common size which is a mean size of all segmented PROI. Table 5.1 shows the age groups and corresponding number of segmented PROI images used for feature extraction and classification. The analysis was accomplished using five-fold cross-validation and each of the datasets were divided into training (80%) and testing phase (20%). The dataset is imbalanced because the hand radiograph dataset acquired from USC is an imbalanced dataset.

**Table 5.1:** Age group and corresponding number of segmented PROI images

Age	0	1	2	3	4	5	6	7	8	9	10	11	12	13	14	15	16	17	18
<b>Male (1396)</b>	18	31	34	39	14	66	61	66	70	56	103	159	89	123	104	86	107	81	89
<b>Female (1686)</b>	8	24	49	51	35	66	73	70	74	81	121	139	166	164	121	122	122	75	125
<b>Combined (3082)</b>	26	55	83	90	49	132	134	136	144	137	224	298	255	287	225	208	229	156	214

For the bone age assessment analysis, mean error (Merr), root mean squared error (RMSE), and standard deviation of error (Sdev) are the automatic choice for the researchers for results comparison of different bone age assessment methods. The experimental results obtained from all 3 feature extraction methods using ANN, SVM, and Random Forest are presented in Tables 5.2-5.4 for combined, male and female datasets respectively. Tables 5.2-5.4 present the mean error (Merr), root mean square error (RMSE) and standard deviation of error (Sdev). The values shown are an average of all 5 PROI's (Avg5) and an average of the ring, middle and index fingers (Avg3) in the bone age range of 0-18 years. From the Tables 5.2-5.4, it is observed that random forest classifier provided the lowest value of Merr, RMSE, and Sdev on combined dataset as well as separate datasets. Hence, random forest classifier is best suited for BAA analysis as compared to ANN and SVM classifiers.

**Table 5.2:** Classification results for different feature extraction methods on combined dataset

Segmented PROI	ANN			SVM			Random Forest		
	Merr	RMSE	Sdev	Merr	RMSE	Sdev	Merr	RMSE	Sdev
Texture (Avg5)	1.967	2.661	1.797	1.646	2.496	1.634	1.090	1.459	0.976
Texture (Avg3)	1.963	2.687	1.840	1.518	2.314	1.501	1.064	1.435	0.970
HOG (Avg5)	2.062	2.687	1.672	1.457	1.969	1.328	0.723	0.968	0.644
HOG (Avg3)	2.046	2.688	1.655	1.443	1.952	1.319	0.694	0.944	0.642
BoF (Avg5)	1.737	2.252	1.438	1.318	1.540	1.511	0.681	0.872	0.550
BoF (Avg3)	<b>1.697</b>	<b>2.216</b>	<b>1.430</b>	<b>1.061</b>	<b>1.203</b>	<b>1.232</b>	<b>0.634</b>	<b>0.816</b>	<b>0.514</b>

**Table 5.3:** Classification results for different feature extraction methods on male dataset

Segmented PROI	ANN			SVM			Random Forest		
	Merr	RMSE	Sdev	Merr	RMSE	Sdev	Merr	RMSE	Sdev
Texture (Avg5)	1.776	2.459	1.708	1.630	2.486	1.648	1.092	1.485	1.016
Texture (Avg3)	1.797	2.379	1.563	1.506	2.419	1.702	1.057	1.438	0.990
HOG (Avg5)	1.901	2.517	1.657	1.429	1.943	1.329	0.707	0.984	0.692
HOG (Avg3)	1.947	2.528	1.615	1.398	1.935	1.345	0.692	0.980	0.704
BoF (Avg5)	1.403	1.837	1.193	1.201	1.749	1.235	0.587	0.773	0.506
BoF (Avg3)	<b>1.401</b>	<b>1.777</b>	<b>1.119</b>	<b>1.095</b>	<b>1.508</b>	<b>1.102</b>	<b>0.536</b>	<b>0.702</b>	<b>0.458</b>

**Table 5.4:** Classification results for different feature extraction methods on female dataset

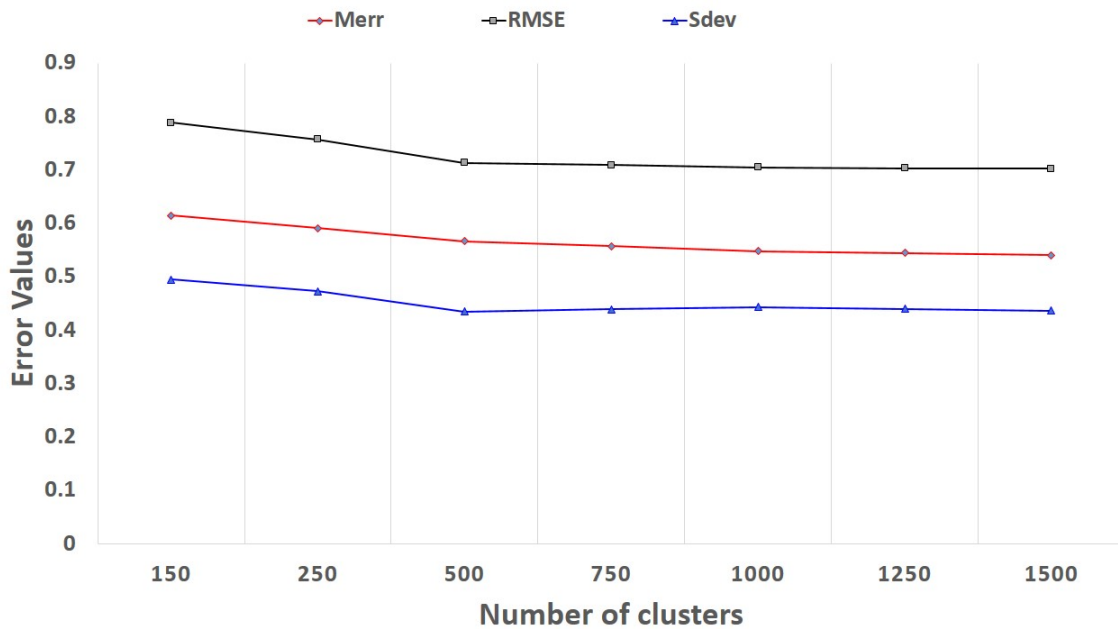
Segmented PROI	ANN			SVM			Random Forest		
	Merr	RMSE	Sdev	Merr	RMSE	Sdev	Merr	RMSE	Sdev
Texture (Avg5)	2.145	2.880	1.926	1.500	2.386	1.655	1.165	1.583	1.080
Texture (Avg3)	2.199	2.886	1.868	1.395	2.272	1.605	1.104	1.527	1.059
HOG (Avg5)	2.108	2.623	1.571	1.638	2.089	1.308	0.744	0.966	0.620
HOG (Avg3)	2.117	2.595	1.511	1.562	1.982	1.231	0.706	0.921	0.593
BoF (Avg5)	1.592	2.065	1.324	1.565	1.958	1.273	0.687	0.888	0.562
BoF (Avg3)	<b>1.565</b>	<b>2.012</b>	<b>1.273</b>	<b>1.377</b>	<b>1.648</b>	<b>1.168</b>	<b>0.630</b>	<b>0.815</b>	<b>0.517</b>

From the Tables 5.2-5.4, it is deduced that Bag of Features (BoF) method performs better as compared with other two feature extraction methods. Texture feature analysis performs better than HOG features for the case of classification using ANN. But the best results are achieved by BoF method as given in Tables 5.2-5.4. For classification using SVM, similar results are obtained for all feature extraction methods

as given in Table 5.2-5.4. Tables 5.2-5.4 also show that BoF provides the lowest values for mean error, RMSE and standard deviation of error. Best results in Tables 5.2-5.4 are highlighted. Further, from the Tables 5.2-5.4, it is also observed that BoF method using ANN, SVM, and random forest classifiers provided the lowest value of Merr, RMSE, and Sdev as compared to texture feature analysis and HOG feature extraction methods. In the experimental results analysis, it is found that some regions (e.g. index, middle, ring) achieved lower mean error and RMSE than others. Hence, best regions can be combined and used to predict the final bone age.

### 5.5.2 Selection of number of clusters for BoF method

The results of BoF method presented in Tables 5.2-5.4 are found to be better with a value of  $k = 150$  (i.e. 150 clusters), but the number of clusters is taken without any analysis. Therefore, for the selection of an appropriate value of a number of clusters, an analysis with a number of clusters versus error is performed. In Figure 5.4, the number of clusters is increased from 150 to 1500 and the change in error is plotted. Figure 5.4 clearly shows that there is a minimum change in error after  $k=500$ . Hence, the appropriate value of a number of clusters,  $k=500$  is selected for further experimental analysis.



**Figure 5.4:** Graph of error values versus number of clusters in bag of features

A bag of features is constructed and results are computed which are presented in Table 5.5. The results presented in Table 5.5 show that they are better than the previous two methods of texture analysis and HOG features. To compare the results with existing BAA method presented in Thodberg *et al.* (2009), a reduced dataset for ages between 2-17 years is created. The results of BoF method for the reduced dataset(RD) is presented in Table 5.5 with k=500 using random forest classifier.

**Table 5.5:** Random Forest classifier results for BoF with k=500 and with reduced dataset (2-17 years)

Segmented PROI	Combined dataset			Male dataset			Female dataset		
	Merr	RMSE	Sdev	Merr	RMSE	Sdev	Merr	RMSE	Sdev
BoF-500 (Avg5)	0.616	0.786	0.488	0.527	0.691	0.446	0.633	0.839	0.550
BoF-500 (Avg3)	<b>0.581</b>	<b>0.744</b>	<b>0.464</b>	<b>0.484</b>	<b>0.646</b>	<b>0.425</b>	<b>0.588</b>	<b>0.777</b>	<b>0.506</b>
BoF(RD) (Avg5)	0.584	0.757	0.481	0.505	0.677	0.451	0.530	0.667	0.406
BoF(RD) (Avg3)	<b>0.557</b>	<b>0.721</b>	<b>0.458</b>	<b>0.466</b>	<b>0.617</b>	<b>0.405</b>	<b>0.501</b>	<b>0.637</b>	<b>0.394</b>

### 5.5.3 Result comparison with other existing BAA methods

To prove robustness of improved ABAA system with BoF method using random forest classifier, the results are compared with existing BAA methods presented in the literature (Thodberg *et al.* (2009), Kashif *et al.* (2016), Harmsen *et al.* (2013), and Spampinato *et al.* (2017)). Classification results of improved ABAA system and other existing BAA methods for combined and reduced datasets are presented in Table 5.6.

**Table 5.6:** Comparison between our results and various other existing methods from literature

BA range	Used Gender	Metric	All PROI	Best PROI	Thodberg <i>et al.</i> (2009)	Kashif <i>et al.</i> (2016)	Harmsen <i>et al.</i> (2013)	Spampinato <i>et al.</i> (2017)
0-18	Yes	Merr RMSE	<b>0.5801</b> 0.7650	<b>0.4622</b> 0.6085	- -	0.6172 -	0.832 -	0.79 -
0-18	No	Merr RMSE	<b>0.6156</b> 0.7856	<b>0.5662</b> 0.7135	- -	0.7509 -	0.9637 -	- -
2-17	Yes	Merr RMSE	<b>0.5177</b> 0.6720	<b>0.4525</b> <b>0.5926</b>	- <b>0.61</b>	0.6082 -	0.8265 -	- -
2-17	No	Merr RMSE	<b>0.5837</b> 0.7565	<b>0.5446</b> 0.7203	- -	0.856 -	0.985 -	- -

Table 5.6 clearly shows that BoF method with random forest classifier outperforms all the methods present in the literature except for Bonexpert method (Thodberg *et al.*

(2009)). The best PROI results presented are from the index finger. As mentioned earlier, 3 PROI's among all 5 give best results. So, taking the average of results obtained for reduced dataset, RMSE value of 0.62 is obtained which is comparable to Bonexpert method (Thodberg *et al.* (2009)) which gives RMSE as 0.61.

## 5.6 Summary

- Experimental results of three different feature extraction methods are compared namely texture feature analysis, histogram of oriented gradients and bag of features method.
- The Bag of Features method gave the best result among all three with number of clusters set to 500.
- Three different classifiers are implemented for calculating the results which are ANN, SVM and Random Forest.
- BoF method with random forest classifier provides lowest values of Merr, RMSE and Sdev as compared to the other existing BAA methods.



## Chapter 6

# CONCLUSION AND FUTURE WORK

This thesis investigated and analyzed design and development of a fully automated system for bone age assessment of a person from the left-hand radiograph. Two automatic ROI extraction methods are designed which are independent of hand placement and orientation. It involves simple morphological operations and basic mathematical functions. Hence, the extraction of PROI and RUROI images from hand radiographs is simple, accurate and fast because the proposed automatic ROI extraction techniques took a negligible amount of time. A hierarchical bone localization technique is followed to make it easier for segmentation stage of ABAA system wherein the boundary of hand is found at first and then regions are identified.

The proposed segmentation techniques are extremely robust for segmentation of bones in extracted regions. The proposed segmentation techniques and other existing techniques are validated on the left hand radiograph database with an age group of 0-18 years. The proposed techniques along with previously investigated techniques are successfully implemented on under-exposed as well as over-exposed radiographic images. A close look at quantitative performance measures indicate that the simulation results obtained using proposed segmentation techniques are better than that achieved from previously reported techniques. The visual information obtained from figures in chapter 4 indicate that the proposed segmentation techniques yield good results as compared to other existing segmentation techniques as the bones can be clearly delineated. Further, the proposed segmentation techniques deliver an approx-

imate segmentation accuracy of 94 percent for PROI and 97 percent for RUROI. Finally, experimental results demonstrated that the proposed segmentation techniques offer better quantitative and qualitative results as compared to other tested techniques reported in the literature.

The segmentation results are also verified by different medical experts. Mean of ratings given by all four medical experts for segmentation results are above the average value i.e 3. The advantages of the proposed technique are that it is very effective and robust and disadvantage of the proposed technique is that it is a complex mathematical process and consumes more processing time.

Further, in this thesis, a fully ABAA system is designed and developed by integrating ROI extraction stage, segmentation stage, and feature extraction with classification stage. In this context, 3 different feature extraction methods namely, texture feature analysis, Histogram of Oriented Gradients (HOG), and Bag of Features (BoF) methods are implemented on segmented PROI images. These feature extraction methods are integrated with most popular and widely used classification techniques like ANN, SVM, and random forest classifiers. It is found that BoF method with a number of clusters set to 500 performed better than other two feature extraction methods. Results are compared with other existing BAA methods and analysis showed that the obtained results are fairly satisfactory. The usage of gender bias results also indicated improvement of bone age prediction, hence it can be used during practical implementation. Further, the classification results also demonstrated that a fairly good performance is obtained from ring, middle and index regions of hand radiograph. Therefore, proposed fully automatic system can be used for BAA of a person with enhanced accuracy.

The future work in automated bone age assessment procedure is designing an effective feature extraction for radius and ulna bones (Simu *et al.* (2017b)) and try to incorporate it in the analysis of bone age estimation. A robust classification technique which takes suitable features and improves the results further can be designed. The estimation of age can be further improved by adding proper weights to ROI's and designing a complete automated BAA system.

# Bibliography

- Aja-Fernández, S., R. de Luis-Garcia, M. A. Martín-Fernandez, and C. Alberola-López** (2004). A computational tw3 classifier for skeletal maturity assessment. a computing with words approach. *Journal of Biomedical Informatics*, **37**(2), 99–107.
- Bay, H., T. Tuytelaars, and L. Van Gool**, *SURF: Speeded Up Robust Features*. Springer Berlin Heidelberg, Berlin, Heidelberg, 2006. ISBN 978-3-540-33833-8, 404–417. URL [https://doi.org/10.1007/11744023\\_32](https://doi.org/10.1007/11744023_32).
- Behiels, G., F. Maes, D. Vandermeulen, and P. Suetens** (2002). Retrospective correction of the heel effect in hand radiographs. *Medical image analysis*, **6**(3), 183–190.
- Breiman, L.** (2001). Random forests. *Machine learning*, **45**(1), 5–32.
- Census of India** (2011). New Delhi: Registrar General and Census Commissioner of India. <http://censusindia.gov.in/>.
- Chai, H. Y., T. T. Swee, G. H. Seng, and L. K. Wee** (2013). Multipurpose contrast enhancement on epiphyseal plates and ossification centers for Bone Age Assessment. *Biomedical engineering online*, **12**(1), 1–19.
- Chai, H. Y., L. K. Wee, T. T. Swee, and S. Hussain** (2011). GLCM based adaptive crossed reconstructed (ACR) k-mean clustering hand bone segmentation. *Book GLCM based adaptive crossed reconstructed (ACR) k-mean clustering hand bone segmentation*, 192–197.
- Chan, T. F., L. Vese, et al.** (2001). Active contours without edges. *Image processing, IEEE transactions on*, **10**(2), 266–277.

- Chang, C.-C.** and **C.-J. Lin** (2011). Libsvm: A library for support vector machines. *ACM transactions on intelligent systems and technology (TIST)*, **2**(3), 27.
- Cortes, C.** and **V. Vapnik** (1995). Support-vector networks. *Machine Learning*, **20**(3), 273–297. ISSN 1573-0565. URL <https://doi.org/10.1007/BF00994018>.
- Csurka, G., C. Dance, L. Fan, J. Willamowski,** and **C. Bray**, Visual categorization with bags of keypoints. *In Workshop on statistical learning in computer vision, ECCV*, volume 1. Prague, 2004.
- Dalal, N.** and **B. Triggs**, Histograms of oriented gradients for human detection. *In Computer Vision and Pattern Recognition, 2005. CVPR 2005. IEEE Computer Society Conference on*, volume 1. IEEE, 2005.
- Dougherty, E. R.** and **R. A. Lotufo**, *Hands-on morphological image processing*, volume 71. SPIE Optical Engineering Press Washington, 2003.
- Eberhart, R. C.** and **J. Kennedy**, A new optimizer using particle swarm theory. *In Proceedings of the sixth international symposium on micro machine and human science*, volume 1. New York, NY, 1995.
- Elazab, A., C. Wang, F. Jia, J. Wu, G. Li,** and **Q. Hu** (2015). Segmentation of brain tissues from magnetic resonance images using adaptively regularized kernel-based fuzzy-means clustering. *Computational and Mathematical Methods in Medicine*, **2015**.
- Gertych, A., A. Zhang, J. Sayre, S. Pospiech-Kurkowska,** and **H. Huang** (2007). Bone age assessment of children using a digital hand atlas. *Computerized Medical Imaging and Graphics*, **31**(4), 322–331.
- Gilsanz, V.** and **O. Ratib**, *Hand bone age: A digital atlas of skeletal maturity*. Springer Science & Business Media, 2005.
- Giordano, D., I. Kavasidis,** and **C. Spampinato** (2016). Modeling skeletal bone development with hidden markov models. *Computer methods and programs in biomedicine*, **124**, 138–147.
- Giordano, D., R. Leonardi, F. Maiorana, G. Scarciofalo,** and **C. Spampinato**, Epiphysis and metaphysis extraction and classification by adaptive thresholding and

- DoG filtering for automated skeletal bone age analysis. *In Engineering in Medicine and Biology Society, 2007. EMBS 2007. 29th Annual International Conference of the IEEE*. IEEE, 2007.
- Giordano, D., C. Spampinato, G. Scarciofalo, and R. Leonardi** (2010). An automatic system for skeletal bone age measurement by robust processing of carpal and epiphysial/metaphysial bones. *Instrumentation and Measurement, IEEE Transactions on*, **59**(10), 2539–2553.
- Gong, M., D. Tian, L. Su, and L. Jiao** (2015). An efficient bi-convex fuzzy variational image segmentation method. *Information Sciences*, **293**, 351–369.
- Gonzalez, R. C., R. E. Woods, and S. L. Eddins**, *Digital image processing using MATLAB*. Pearson Education India, 2004.
- Gonzalez, W. and R. E. Woods** (2004). Eddins, *Digital Image Processing Using MATLAB. Third Edition: Prentice Hall*.
- Greulich, W. W. and S. I. Pyle** (1959). Radiographic atlas of skeletal development of the hand and wrist. *The American Journal of the Medical Sciences*,, **238**,(3).
- Gross, G. W., J. M. Boone, and D. M. Bishop** (1995). Pediatric skeletal age: determination with neural networks. *Radiology*, **195**(3), 689–695.
- Gupta, D., R. Anand, and B. Tyagi** (2015). A hybrid segmentation method based on gaussian kernel fuzzy clustering and region based active contour model for ultrasound medical images. *Biomedical Signal Processing and Control*, **16**, 98–112.
- Guraksin, G. E., H. Uguz, and O. K. Bayakan** (2016). Bone age determination in young children (newborn to 6 years old) using support vector machines. *Turkish Journal of Electrical Engineering & Computer Sciences*,, **24**(3), 1693–1708.
- Han, C.-C., C.-H. Lee, and W.-L. Peng** (2007). Hand radiograph image segmentation using a coarse-to-fine strategy. *Pattern Recognition*, **40**(11), 2994–3004.
- Harmsen, M., B. Fischer, H. Schramm, T. Seidl, and T. M. Deserno** (2013). Support vector machine classification based on correlation prototypes applied to bone age assessment. *IEEE journal of biomedical and health informatics*, **17**(1), 190–197.

- Hartigan, J. A.** and **M. A. Wong** (1979). Algorithm as 136: A k-means clustering algorithm. *Journal of the Royal Statistical Society. Series C (Applied Statistics)*, **28**(1), 100–108.
- Haykin, S.**, *Neural Networks: A Comprehensive Foundation*. Prentice Hall PTR, Upper Saddle River, NJ, USA, 1998, 2nd edition. ISBN 0132733501.
- Hsieh, C., C. Chen, T. Jong, T. Liu, and C. Chiu** (2012). Automatic segmentation of phalanx and epiphyseal/metaphyseal region by gamma parameter enhancement algorithm. *Measurement Science Review*, **12**(1), 21–27.
- Hsieh, C.-W., T.-L. Jong, and C.-M. Tiu** (2007). Bone age estimation based on phalanx information with fuzzy constrain of carpals. *Medical & biological engineering & computing*, **45**(3), 283–295.
- Hsieh, C.-W., T.-C. Liu, T.-L. Jong, and C.-M. Tiu** (2010). A fuzzy-based growth model with principle component analysis selection for carpal bone-age assessment. *Medical & biological engineering & computing*, **48**(6), 579–588.
- Hum, Y. C.**, *Segmentation of hand bone for bone age assessment*. Springer, 2013.
- Kashif, M., T. M. Deserno, D. Haak, and S. Jonas** (2016). Feature description with SIFT, SURF, BRIEF, BRISK, or FREAK? A general question answered for bone age assessment. *Computers in biology and medicine*, **68**, 67–75.
- Kashif, M., S. Jonas, D. Haak, and T. M. Deserno**, Bone age assessment meets SIFT. *In SPIE Medical Imaging*. International Society for Optics and Photonics, 2015.
- Lee, H., S. Tajmir, J. Lee, M. Zissen, B. A. Yeshiwas, T. K. Alkasab, G. Choy, and S. Do** (2017). Fully automated deep learning system for bone age assessment. *Journal of Digital Imaging*, 1–15.
- Lee, J.-M. and W.-Y. Kim**, Epiphyses extraction method using shape information for left hand radiography. *In International Conference on Convergence and Hybrid Information Technology, 2008. ICHIT'08.. IEEE*, 2008.
- Li, C., R. Huang, Z. Ding, J. C. Gatenby, D. N. Metaxas, and J. C. Gore** (2011). A level set method for image segmentation in the presence of intensity

- inhomogeneities with application to MRI. *Image Processing, IEEE Transactions on*, **20**(7), 2007–2016.
- Liu, J., J. Qi, Z. Liu, Q. Ning, and X. Luo** (2008). Automatic bone age assessment based on intelligent algorithms and comparison with TW3 method. *Computerized Medical Imaging and Graphics*, **32**(8), 678–684.
- Liu, Z., J. Chen, J. Liu, and L. Yang**, Automatic Bone Age Assessment based on PSO. *In 2007 1st International Conference on Bioinformatics and Biomedical Engineering*. 2007.
- Loizou, C. P., C. Theofanous, M. Pantziaris, and T. Kasparis** (2014). Despeckle filtering software toolbox for ultrasound imaging of the common carotid artery. *Computer methods and programs in biomedicine*, **114**(1), 109–124.
- Luis-Garcia, D., M. Martin-Fernández, J. I. Arribas, C. Alberola-López, et al.**, A fully automatic algorithm for contour detection of bones in hand radiographs using active contours. *In Image Processing, 2003. ICIP 2003. Proceedings. 2003 International Conference on*, volume 3. IEEE, 2003.
- Mahmoodi, S., B. Sharif, E. Chester, J. Owen, and R. Lee** (1997). Automated vision system for skeletal age assessment using knowledge based techniques.
- Manos, G., A. Cairns, I. Ricketts, and D. Sinclair** (1994). Segmenting radiographs of the hand and wrist. *Computer Methods and Programs in Biomedicine*, **43**(3), 227–237.
- Michael, D. J. and A. C. Nelson** (1989). Handx: a model-based system for automatic segmentation of bones from digital hand radiographs. *IEEE Transactions on Medical Imaging*, **8**(1), 64–69. ISSN 0278-0062.
- Niemeijer, M., B. van Ginneken, C. A. Maas, F. J. Beek, and M. A. Viergever**, Assessing the skeletal age from a hand radiograph: automating the tanner-whitehouse method. *In Medical Imaging 2003*. International Society for Optics and Photonics, 2003.
- Orlando, J. I., E. Prokofyeva, and M. B. Blaschko** (2017). A discriminatively trained fully connected conditional random field model for blood vessel segmentation

in fundus images. *IEEE Transactions on Biomedical Engineering*, **64**(1), 16–27. ISSN 0018-9294.

**Osher, S.** and **J. A. Sethian** (1988). Fronts propagating with curvature-dependent speed: algorithms based on hamilton-jacobi formulations. *Journal of computational physics*, **79**(1), 12–49.

**Otsu, N.** (1975). A threshold selection method from gray-level histograms. *Automatica*, **11**(285-296), 23–27.

**Pappas, T. N.** (1992). An adaptive clustering algorithm for image segmentation. *Signal Processing, IEEE Transactions on*, **40**(4), 901–914.

**Park, K.-H., J.-M. Lee,** and **W.-Y. Kim**, Robust epiphyseal extraction method based on horizontal profile analysis of finger images. *In International Symposium on Information Technology Convergence, 2007. ISITC 2007.* IEEE, 2007.

**Perona, P.** and **J. Malik** (1990). Scale-space and edge detection using anisotropic diffusion. *IEEE Transactions on Pattern Analysis and Machine Intelligence*, **12**(7), 629–639.

**Pietka, E., A. Gertych, S. Pospiech, F. Cao, H. Huang,** and **V. Gilsanz** (2001). Computer-assisted bone age assessment: Image preprocessing and epiphyseal/metaphyseal ROI extraction. *Medical Imaging, IEEE Transactions on*, **20**(8), 715–729.

**Pietka, E., L. Kaabi, M. Kuo,** and **H. Huang** (1993). Feature extraction in carpal-bone analysis. *Medical Imaging, IEEE Transactions on*, **12**(1), 44–49.

**Pietka, E., M. F. McNitt-Gray, M. Kuo,** and **H. Huang** (1991). Computer-assisted phalangeal analysis in skeletal age assessment. *Medical Imaging, IEEE Transactions on*, **10**(4), 616–620.

**Pietka, E., S. Pospiech-Kurkowska, A. Gertych,** and **F. Cao** (2003). Integration of computer assisted bone age assessment with clinical PACS. *Computerized medical imaging and graphics*, **27**(2), 217–228.

**Rucci, M., G. Coppini, I. Nicoletti, D. Cheli,** and **G. Valli** (1995). Automatic analysis of hand radiographs for the assessment of skeletal age: a subsymbolic approach. *Computers and Biomedical Research*, **28**(3), 239–256.



- Seok, J., J. Kasa-Vubu, M. DiPietro, and A. Girard** (2016). Expert system for automated bone age determination. *Expert Systems with Applications*, **50**, 75–88.
- Sethian, J. A.**, Numerical methods for propagating fronts. In *Variational methods for free surface interfaces*. Springer, 1987, 155–164.
- Sharif, B., S. Zaroug, E. Chester, J. Owen, and E. Lee**, Bone edge detection in hand radiographic images. In *Engineering in Medicine and Biology Society, 1994. Engineering Advances: New Opportunities for Biomedical Engineers. Proceedings of the 16th Annual International Conference of the IEEE*. IEEE, 1994.
- Simu, S., S. Lal, K. Fadte, and A. Harlapur** (2017a). Fully automatic segmentation of phalanges from hand radiographs for bone age assessment. *Computer Methods in Biomechanics and Biomedical Engineering: Imaging & Visualization*, **0**(0), 1–26. URL <https://doi.org/10.1080/21681163.2017.1416491>.
- Simu, S., S. Lal, P. Nagarsekar, and A. Naik** (2017b). Fully automatic roi extraction and edge-based segmentation of radius and ulna bones from hand radiographs. *Biocybernetics and Biomedical Engineering*, **37**(4), 718 – 732. ISSN 0208-5216. URL <http://www.sciencedirect.com/science/article/pii/S0208521617300918>.
- Spampinato, C., S. Palazzo, D. Giordano, M. Aldinucci, and R. Leonardi** (2017). Deep learning for automated skeletal bone age assessment in x-ray images. *Medical image analysis*, **36**, 41–51.
- Tanner, J. and R. Gibbons** (1994). Automatic bone age measurement using computerized image analysis. *Journal of Pediatric Endocrinology and Metabolism*, **7**(2), 141–146.
- Tanner, J., M. Healy, H. Goldstein, and N. Cameron** (2001). Assessment of skeletal maturity and prediction of adult height: Tw3 method saunders.
- Tanner, J. M., R. Whitehouse, W. Marshall, M. Healty, and H. Goldstein** (1975). Assessment of skeleton maturity and maturity and prediction of adult height (tw2 method).
- Thangam, P., K. Thanushkodi, and T. Mahendiran** (2012). PSO for graph-based segmentation of wrist bones in bone age assessment. *International Journal of Computers Communications & Control*, **8**(1), 153–160.

- Theodoridis, S., A. Pikrakis, K. Koutroumbas, and D. Cavouras**, *Introduction to pattern recognition: a matlab approach*. Academic Press, 2010.
- Thodberg, H. H., S. Kreiborg, A. Juul, and K. D. Pedersen** (2009). The bon-expert method for automated determination of skeletal maturity. *Medical Imaging, IEEE Transactions on*, **28**(1), 52–66.
- Tillett, J., T. Rao, F. Sahin, and R. Rao** (2005). Darwinian particle swarm optimization.
- Tristán, A. and J. I. Arribas**, A radius and ulna skeletal age assessment system. *In Machine Learning for Signal Processing, 2005 IEEE Workshop on*. IEEE, 2005.
- Tristan-Vega, A. and J. I. Arribas** (2008). A radius and ulna TW3 bone age assessment system. *Biomedical Engineering, IEEE Transactions on*, **55**(5), 1463–1476.
- UNICEF** (2011). The Situation of Children in India: A profile. New Delhi: United Nations Childrens Fund/India.
- Van Lenthe, F., H. Kemper, and W. Van Mechelen** (1998). Skeletal maturation in adolescence: a comparison between the tanner-whitehouse ii and the fels method. *European journal of pediatrics*, **157**(10), 798–801.

# PUBLICATIONS

## *Refereed International Journals:*

1. **Simu, S.** and Lal, S., (2017), “A study about evolutionary and non-evolutionary segmentation techniques on hand radiographs for bone age assessment ”, *Biomedical Signal Processing and Control*, 33, pp.220-235, **Elsevier Publisher. (SCI Indexed)**.  
doi: <https://doi.org/10.1016/j.bspc.2016.11.016>.
2. **Simu, S.**, Lal, S., Nagarsekar, P. and Naik, A., (2017), “Fully automatic ROI extraction and edge-based segmentation of radius and ulna bones from hand radiographs ”, *Biocybernetics and Biomedical Engineering*, 37(4), pp.718-732, **Elsevier Publisher. (SCI Indexed)**.  
doi: <https://doi.org/10.1016/j.bbe.2017.07.004>.
3. **Simu, S.**, Lal, S., Fadte, K. and Harlapur, A., (2017), “Fully automatic segmentation of phalanges from hand radiographs for bone age assessment ”, *Computer Methods in Biomechanics and Biomedical Engineering: Imaging & Visualization*, **Taylor and Francis Publisher. (ESCI and SCOPUS Indexed)**.  
doi: <https://doi.org/10.1080/21681163.2017.1416491>.
4. **Simu, S.**, Lal, S., (2018), “Feature Extraction and Classification Techniques for Bone Age Assessment from Hand Radiographs ”, *The Imaging Science Journal*, **Taylor and Francis Publisher. (SCI Indexed). (Under Review)**.

## *International Conference Proceedings:*

1. **Simu, S.** and Lal, S., (2017). “Automated Bone Age Assessment using Bag of Features and Random Forests ”. *IEEE International conference on Intelligent Sustainable Systems - ICISS 2017*, Coimbatore, India, December 7-8, 2017. **(Best Paper Award)**

# CURRICULUM VITAE

## **Shreyas Ajitkumar Simu**

F7, 2nd Floor, Saidatta Apts.

Joefilnagar, Ponda, Goa - 403401

**Email:** shreyas.simu@gmail.com

### **Education:**

1. M.tech, Digital Electronics and Advance Communication,  
Manipal Institute of Technology, Manipal, Karnataka, India. (June 2012)  
CGPA: 8.39/10
2. B.E, Electronics and Telecommunication,  
Goa College of Engineering, Farmagudi, Goa, India. (June 2009)  
Aggregate: 65.13

### **Teaching Experience:** 2 years

Assistant Professor, Department of Electronics and Telecommunication  
Engineering, Goa College of Engineering, Farmagudi, Goa.

### **Industry Experience:** 1 year

Intern, Technology Research and Development (TR&D) Dept.  
ST Microelectronics, Greater Noida, Uttar Pradesh, India.